Multimodal Functional Neuroimaging of Epilepsy and Pain

A DISSERTATION SUMITTED TO THEFACULTY OF THE GRADUATE SCHOOL

OF THE UNIVERSITY OF MINNESOTA

BY

HUISHI ZHANG

IN PARTIAL FULFILLMENT OF THE REQUIREMENTS

FOR THE DEGREE OF

DOCTOR OF PHILOSOPHY

Name of Advisor

BIN HE

Professor of biomedical engineering

Expected Month and year of Degree clearance

June 2015

Acknowledgements

I would like to express my sincere gratitude to my mentor and advisor, Dr. Bin He, without whose guidance and support, none of the work presented in this thesis would have been possible. I would also like to acknowledge the members of my thesis committee: Dr. Wei Chen, Dr. Kalpna Gupta, Dr. Theoden Neoff and Dr. Zhiyi Sha for their continued support during my doctoral training.

Special thanks are owed to our collaborators: Dr. Zhiyi Sha, Dr. Tomas R. Henry, at the University of Minnesota and for patient recruitments and clinical input of the EEG-fMRI epilepsy work; Dr. Gregory Worrell, Dr. Benjamin Brinkmann and Dr. Kirk Welker at the Mayo Clinic (Rochester, MN) for providing the clinical data used in the fMRI of epilepsy work; Dr. Yvonne Datta and Dr. Kalpna Gupta at the University of Minnesota Dr. Stephen Nelson at Minnesota Children's Hospital for patient recruitment of the sickle cell disease work. In addition, I am grateful for the valuable contributions of Dr. Yunfeng Lu, Dr. Mr. John Mundahl and Ms. Michel Case to the research presented in this dissertation as well as technical discussions with Mr. Keith Jamison, Dr. Lin Yang, Mr. Abbas Sohrabpour, Ms. Nessa Johnson and Mr. Abhrajeet Roy.

Finally, I would like to thank my parents, Mrs. Yinshu Wang and Mr. Yonggang Zhang, my husband and best friend Mr. Jacob Mohs and other family and friends for their continued love, support and patience during my doctoral training.

This thesis work was supported in part by NIH HL117664, EB007920, and EB006433.

Dedication

This dissertation is dedicated to my parents.

Abstract

The overall goal of this thesis work is to use advanced noninvasive neuroimaging modalities and techniques to study the underlying neurological mechanisms of both diseased and healthy brains. The two main applications of this work are for the diagnosis of epilepsy and management of pain.

Epilepsy is one of the most prevalent neurological disorders. It affects an estimated 2.7 million Americans. There are two broad types of epilepsy: partial and generalized epilepsy. For patients with drug resistant focal epilepsy, which account for one third of the patient population, surgical resection may provide the opportunity of seizure control. Existing presurgical planning methods are not only invasive in nature, they may also fail to provide additional information needed for surgery due to the relatively limited spatial coverage. On the other hand, idiopathic generalized epilepsy (IGE), unlike focal or partial epilepsy, often affects the whole or a larger portion of the brain without obvious, known cause. Treatment options are more restricted as resection is not a choice. Therefore, it is important to understand the underlying network which generates epileptic activity and through which epileptic activity propagates. One aim of the present thesis was to use noninvasive imaging techniques including fMRI and EEG to localize epileptogenic zone for the purpose of assisting surgical planning in the focal epilepsy cases; and to improve our understanding the underlying mechanisms of generalized epilepsy, thalamocortical relationship in the IGE cases.

Chronic pain is one of the biggest medical burdens in developed countries, affecting 20% of adult population with estimated economic cost in the United States alone over $500 billion annually (Gaskin and Richard 2012). Functional imaging of brain networks associated with pain processing is of vital importance to aid developing new pain-relief therapies and to better understand the mechanisms of pain perception. The long-term goal of this project is to study the neurological mechanisms of subjective perception of pain using non-invasive neuroimaging methods. In this thesis study, changed in brain activities in healthy subjects experiencing sustained external painful stimuli were first studied. Neural activities in patient with sickle cell disease (SCD), who often surfer spontaneous acute or chronic pain as one of the comorbidities of the disease, were contrasted with healthy controls to study changes in neural network as a result of prolonged exposure to internal pain.

In summary, the present dissertation research developed and evaluated the spatiotemporal imaging approaches for the non-invasive mapping of network activities in the diseased and normal brain. Evaluations were conducted in epilepsy patient and healthy control groups in order to test the clinical applicability of pre-surgical noninvasive imaging. An investigation has been conducted to study the widespread generalized spike and wave discharges (GSWDs) of generalized epilepsy patients. The spatial resolution has been further improved by adding the component of fMRI through an EEG-fMRI integrated imaging framework. For the application in pain study, two investigations were conducted to study changes in network level activity due to external pain in healthy subjects and spontaneous pain in patients with SCD. All of the results that were obtained suggest the importance of noninvasive spatiotemporal neuroimaging

approaches for solving clinical problems and for investigating neuroscience questions. Furthermore, an improved understanding of neurological diseases and their mechanisms would help us to develop and deliver curative treatments of neurological diseases.

Table of Contents

List of Tables

List of Figures

Chapter 1 Introduction and Motivation

1.1 Scope

The overall goal of this thesis work is to use advanced noninvasive neuroimaging modalities and techniques to study the underlying neurological mechanisms of both diseased and healthy brains. The two main applications of this work are for the diagnosis of epilepsy and management of pain.

The organization of this thesis is such that Chapter One covers a brief introduction of the key imaging modalities of electroencephalography (EEG) and functional MRI (fMRI), main computational algorithms of independent component analysis (ICA) and Granger causality analysis, and two areas of applications for these imaging techniques in epilepsy and pain. In Chapter Two, a novel fMRI based technique is presented for lateralization and localization of epileptic zone in focal epilepsy. In Chapter Three, a study using both EEG and fMRI is reported to investigate the network dynamic of generalized spike and wave discharges in generalized epilepsy patients. In Chapter Four, an experiment using EEG is described to study how healthy brains respond to tonic thermal pain. In Chapter Five, findings are presented on the differences in resting state neural networks between patients with sickle cell disease (SCD) as a result of chronic pain and healthy controls.

1.2 EEG

EEG (electroencephalogram) signals are primarily generated by cortical pyramidal cells from net synaptic activities (Hämäläinen et al. 1993; Baillet et al. 2001; Engel et al. 2008; He and Liu 2008). Pyramidal cells reside in deep layers with dendrites

reaching out to the surrounding neurons in the top layers of cortex. The organization of the pyramidal cells is such that they are perpendicular to the local cortical surface. The total number of neurons in the human brain can amount to 10^{11}. In one mm^3 alone, there can be 30,000~40,000 pyramidal cells, but the density of cells varies across different parts of the brain (Ramon y Cajal 1928; Cullen et al. 2006; Engel et al. 2008). The signal measured by each EEG electrode is the synchronized activities of many neurons summed at the scalp through volume conduction. A dipole is a mathematical approximation of a net synchronized activity in the grey matter viewed from scalp electrodes. Since a dipole represents the underlying pyramidal activities, its direction is also perpendicular to the local cortical surface. Since EEG measures relatively large-scale brain activity, it is more suitable for studying system level behaviors and network activities.

EEG imaging is a noninvasive neuroimaging method to estimate the locations, magnitudes and distributions of underlying sources that produce the scalp EEG. This information is achieved by solving both a 'forward' and an 'inverse' problem.

In the EEG forward model, the spatiotemporal EEG/MEG recording **x** can be related with underlying brain activity **S** through a linear system:

$$x = LS + B \tag{1.1}$$

where **x** is a $\boldsymbol{n}$ by $\boldsymbol{t}$ signal matrix ($\boldsymbol{n}$ is the number of electrodes and $\boldsymbol{t}$ is the number of time points), **S** is a $\boldsymbol{m}$*$\boldsymbol{t}$ source matrix ($\boldsymbol{m}$ is the dimension of source space) and B is a $\boldsymbol{n}$*$\boldsymbol{t}$ noise matrix. **L** is a $\boldsymbol{n}$*$\boldsymbol{m}$ lead field matrix that can be calculated based on the boundary element method (BEM) (He et al. 1987; Hamalainen and Sarvas 1989; Fuchs et al. 1998) or the finite element method, the finite difference method, or another numerical method.

In the BEM model, the head volume conductor can be separated into three conductive layers, the brain, the skull and the skin with conductivity of 0.33 S/m, 0.0165 S/m and 0.33 S/m, respectively (Oostenveld and Oostendorp 2002; Lai et al. 2005). Alternatively, the BEM model can be separated into four conductive layers, the brain, the skull, the skin and the CSF. A 3D distributed source model can be used to model the brain source distribution that includes around ten thousand equivalent current dipoles with unconstrained orientations evenly positioned within the 3D brain volume.

Given the forward modeling of lead field matrix, spatiotemporal brain sources can be estimated from the EEG measurements by solving an inverse problem as follows

$$S = L^{-1}x \tag{1.2}$$

where $\mathbf{L}^{-1}$ is the inverse of lead field matrix.

Existing algorithms such as Low Resolution Electromagnetic Tomography (LORETA) (Pascual-Marqui et al., 1994), minimum norm estimate (MNE), variants of MNE (e.g. weighted MNE, L-p norm algorithms (e.g., L-1 norm), sub-space scanning algorithms such as MUSIC, RAP-MUSIC, FINE algorithms (Ding et al. 2007; Lu et al. 2012b; He and Ding 2013), or dipole source localization algorithms, can be incorporated into this method to estimate the source activity S.

1.3 FMRI

Since its introduction in the clinic in the 1980s, MRI has seen unparalleled importance in diagnostic medicine, and has superseded X-ray in many ways. In neurology, MRI is primarily used to produce structural images of the brain to detect any anatomical abnormalities. Following the success of MRI, the emergence of functional

MRI (fMRI) in the early 1990s had a revolutionary impact on basic cognitive neuroscience research (Logothetis 2008). Functional MRI is a functional neuroimaging technique that detects hemodynamic changes associated with brain activity. Blood oxygen level dependent (BOLD) contrast is the most common form of fMRI that measures changes in metabolic changes. BOLD signal changes are contributed by the variation of cerebral blood flow, cerebral blood volume and the cerebral metabolic rate of oxygen (Ogawa and Lee 1990; Ogawa et al. 1992; Logothetis 2008). It is believed that increased local neural activity, as a response to external stimuli or internal processes, will lead to increased metabolic demand to the local areas. Blood flow to the said area will be detected as a BOLD signal by the MRI scanner.

Based on the modern MRI technique, fMRI is a non-invasive procedure, which requires no surgical intervention or injection of agents. Since the early effort in 1990s (Bandettini et al. 1992; Kwong et al. 1992; Ogawa et al. 1992), this relatively young imaging technique has become one of the major functional neuroimaging tools, especially in neuroscience research. Similar to other MRI techniques, the fMRI measure of neural activity is characterized by high spatial resolution, which can distinguish functional changes on a millimeter scale. Recent development of high-field MRI has further improved our ability to visualize functional changes in deep and fine structures.

1.4 Concurrent EEG-fMRI

Although vascular signals as measured by BOLD are tightly correlated with the neural activity, these signals reflect neural activity in an indirect manner. Understanding the neurovascular coupling relationship that underlies the generation of fMRI signals, therefore, is crucial for the interpretation of fMRI data. Recent studies have investigated

the relationship between BOLD signals and electrophysiological signals through invasive methods (in animals or in epileptic patients). The BOLD signal change is better explained by the local field potential (LFP) of many synchronized neurons rather than the neuronal firing by individual or multiple neurons (Logothetis 2008). In line with the invasive investigations, non-invasive EEG-fMRI studies have also revealed a tight correlation between BOLD and EEG signals (Goldman et al. 2002; Debener et al. 2005; Feige et al. 2005).

However, unlike the high resolution in the spatial domain, the fMRI signal has temporal resolution much lower than the time scale of neuronal activity. The nature of the blood flow signals highly restricts the BOLD-fMRI's capability to track the rapid changes of neurons. It has been widely recognized that EEG and fMRI are featured with complementary advantages and limitations: high temporal resolution but low spatial resolution of EEG, in contrast to high spatial resolution but low temporal resolution of fMRI. The complementary features of the two imaging methods have motivated the development of multimodal integration of EEG and fMRI, in a hope to obtain a neuroimaging approach with high resolution in both the spatial and temporal domains. Most commonly, EEG and fMRI signals are combined through an EEG-informed fMRI analysis or an fMRI-weighted EEG source imaging. The first strategy of EEG-informed fMRI analysis (Goldman et al. 2002; Debener et al. 2005; Feige et al. 2005; Gotman et al. 2005) uses EEG signals to form a temporal regressor, and then scans the brain to find activated/deactivated fMRI signals that can be explained by the electrophysiological signatures. This strategy is based on the assumption that neuronal signals measured by EEG and the vascular signals measured by fMRI are correlated in the time domain. The

second strategy of the fMRI-weighted EEG source imaging (Liu et al. 1998; Liu and He 2008) uses fMRI map as a spatial weighting or mask for solving EEG source imaging problems. This strategy is based on the assumption that the neuronal signals measured by EEG and the vascular signals measured by fMRI are overlapped in the spatial domain. The integrated EEG-fMRI imaging incorporates the information from both EEG and fMRI, and is designed to provide high resolution in time and space simultaneously.

1.5 ICA

Independent component analysis (ICA) is a data-driven technique to separate spatio-temporal signals into components with temporal independence. An ICA algorithm such as the infomax ICA algorithm (Bell and Sejnowski, 1995; Delorme and Makeig, 2004) can be used to decompose the spatio-temporal electrophysiological data into a time-by-space formulation:

$$x = QWT \tag{1.3}$$

where x is electrophysiological recording data, Q is an N×N matrix, W is an N×N diagonal scaling matrix, and T is an N×M matrix. The equation (1) can be expanded as:

$$x = \sum_{i=1}^{N} Q_i w_i T_i \tag{1.4}$$

where Q_i is the *i*th column of Q, T_i is the *i*th row of T and w_i is the *i*th diagonal element of W. This equation suggests that the electrophysiological data x can be expressed as a weighted superposition of a series of spatial distributions Q_i multiplied by associated time courses T_i, where each T_i is statistically independent among each other. The temporal, spectral and spatial characteristics of the components can be used to identify and remove

artifacts in the electrophysiological recordings due to eye, muscle movements etc. (McKeown et al. 1998; Makeig et al. 2002; Debener et al. 2005, 2006; Yang et al. 2011a).

1.6 Granger Causality

Granger causality was first developed by Granger in 1960 (Granger 1969) to depict the interactions between a pair of time series based on their temporal relation. It was initially applied in the broad field of econometrics and later adapted in a wide range of other fields including neuroscience to study the network activities in diseased and normal brains. Mathematically, a univaratie time series, x(t)=[x(1),x(2),…,x(n)], can be written as a linear combination of the historic values of x(t) using an autoregressive (AR) model such that:

$$x(t) = a_1 x(t-1) + a_2 x(t-2) + \cdots + a_p x(t-p) + e_x x(t) \quad (1.5)$$

Or equivalently,

$$x(t) = \sum_{i=1}^{p} a_i x(t-i) + e_x(t) \quad (1.6)$$

Where $a_{i=1,2,\ldots p}$ are the weighting coefficients corresponding to the previous values of x(t), p is the order of the system and $e_x(t)$ is the residual noise which cannot be described by the linear combination of the prior values of x(t).

If a second time series y(t) is to be incorporated into the previous equation to reflect the contribution of y(t)'s previous values to x(t), x(t) can be rewritten as,

$$x(t) = \sum_{i=1}^{p} a_i x(t-i) + \sum_{k=1}^{h} b_i y(t-k) + e_{xy}(t) \quad (1.7)$$

Where $b_{k=1,2,...h}$ are the weighting coefficients corresponding to the previous values of y(t), h is the AR model order for the y terms and $e_{xy}(t)$ is the residual noise.

In the expression of x(t) as shown in (1.7), Granger defined the direction of the information flow between x and y time series as: if inclusion of the previous values of y(t) helps improve the residual error of the AR modeling of x(t), then y(t) had a predictive or causal influence on x(t) (Granger 1969).

The functional connectivity analysis utilizing DTF (Kaminski and Blinowska 1991) is an extension of Granger causality theory. Instead of being only suitable for pair-wise directional causality as in Granger theory, the DTF can be applied to analyze connectivity among multi-channel signals (Babiloni et al. 2005; Wilke et al. 2010, 2011a; He et al. 2011a).

1.7 Epilepsy

Epilepsy is one of the most prevalent neurological diseases. According to the World Health Organization (WHO), it affects approximately 3 million Americans in the US and 50 million worldwide (http://www.who.int/mediacentre/factsheets/fs999). Its impact is greater than Parkinson's and multiple sclerosis combined. An annual increase of new cases is around 40 – 70 per 100,000 people in developed countries and twice as high in developing countries. Epilepsy causes disease burden not only because of early death but also because of life-long disability and illness. The burden of epilepsy accounts for around 0.5% of the burden of all the diseases in the world, and contributes even more significantly to the burden caused by disability (Leonardi and Ustun 2002). In addition to the measurable burdens, epileptic patients suffer more social and economic impacts. The discrimination, misunderstanding and social stigma can be worse than the disease itself.

Electroencephalography (EEG) is one of the most used and earliest epilepsy diagnostic tools. On the EEG reading, epilepsy can be characterized by highly synchronous, large amplitude fluctuations during seizures that may be accompanied by other symptoms including sensory and motor activities as well as a loss of consciousness. The precise mechanism that underlies seizure initiation and propagation is still unclear. Experimental evidence has shown that decreases in hippocampal bursting synchrony as well as imbalances between excitatory and inhibitory neurotransmitters may contribute to the seizure initiation.

1.8 Pain

Pain represents the most important cause of physician consultation in the United States, and more than 30 million people are suffering from chronic or recurrent pain (Turk and Dworkin, 2004). Patients who suffer from chronic pain or recurrent pain usually take mediations such as analgesic to reduce or eliminate their pain. However the drug therapy is highly influenced by the subjective pain ratings of the patients. There is a clinical need to develop noninvasive approaches to quantitatively assess the pain severity levels. The availability of quantitative pain severity assessment technology will have a significant impact to clinical management of pain, will objectively guide and optimize drug therapy.

1.9 Motivation

Epilepsy and pain are two critical problems that have huge social economic burdens. Therefore, these two present as uniquely fitting areas for the applications of the imaging techniques we developed. The motivation of this dissertation is to develop noninvasive functional neuroimaging approaches to image the epileptic sources in order

to help the pre-surgical planning of epilepsy treatment and to study the network activity as a response to pain to develop a potential biomarker for the measurements of pain.

The history of using EEG to diagnose epilepsy is almost as long as the discovery of EEG itself by Hans Berger in 1929 (Berger 1929). EEG has since been used in the clinical practice for its portability, noninvasiveness and direct measurements of neurophysiological events. Both focal and generalized epilepsy have very distinctive waveforms that are different from a healthy brain during and between seizures. EEG based electrical source imaging (ESI) has been studied extensively to show its effectiveness in determining the epileptogenic foci (Lantz et al. 2003; Michel et al. 2004; Holmes et al. 2010; Brodbeck et al. 2011; He and Ding 2013), including source localization during inter-ictal spikes (Sohrabpour et al. 2015; Plummer et al. 2010; Wang et al. 2011; Kaiboriboon et al. 2012) and seizures (Assaf and Ebersole 1997; Boon et al. 2002; Ding et al. 2007; Holmes et al. 2010; Koessler et al. 2010; Yang et al. 2011b; Lu et al. 2012b). However, scalp EEG has relatively low resolution and sensitivity to the underlying brain activity because of the distance between the sources and the sensors and the volume conduction effect through all the barriers (skin, skull and the cortex).

The invasive form of EEG – intracranial EEG (iEEG) was developed to achieve more direct and precise mapping of the epileptic activities in patients in the 1950s (Ajmone-Marsan and Van Buren, 1958; Rosenow and Luders, 2001). Electrodes of iEEG can be implanted over the cortical surface (electrocorticography - ECoG) or inserted into the deep structures as depth electrodes to render direct recordings of local activities without the barriers of the skull and skin (Engel et al. 1990). However, because of the risks and expenses associated with invasive procedures, iEEG is always considered as the

last choice if all the other non-invasive measurements or tests cannot converge to a conclusive diagnosis. Furthermore, due to physical constraints of the placements of the iEEG electrodes, it cannot achieve full brain coverage.

Recently, functional neuroimaging techniques with minimum or noninvasiveness such as SPECT, PET and fMRI have been explored in a hope that the hemodynamic signal changes can reflect the neural activity in the epileptogenic zone. These techniques identified epileptic networks showing positive or negative responses to the epileptic activity (Laufs and Duncan 2007; Blumenfeld et al. 2009; Grouiller et al. 2011; Zhang et al. 2015). Although these techniques can offer full brain coverage with excellent spatial resolution, the temporal sampling is often sparse with significant lag. In the case of fMRI, the most widely used sequences take up to 2 to 3 seconds to scan through the whole brain. Furthermore, it has been disputed as whether metabolic changes can always reflect the underlying epileptic activities. Given the complementary strengths and weaknesses of EEG and fMRI, the two have been combined to offer unique insights to epileptic networks (Lemieux et al. 2001; Gotman et al. 2005, 2006; Bénar et al. 2006).

In the context of pain management, functional imaging of brain networks associated with pain processing is of vital importance to better understand the mechanisms of brain function in addition to aid the development of new pain-relief therapy. The pain response in the brain is a complex process, which involves multiple cortical brain regions, such as primary and secondary somatosensory cortices, anterior cingulated cortex, and insular cortex (Bromm 2001). Recent advancement in neuroimaging techniques suggests the possibility to map the brain structure and networks that involve pain processing (Chen 2001; Stern et al. 2006; Roberts et al. 2008). Few

attempts have been made to use EEG to map the active brain regions in pain patients (Bromm 2001, 2004; Stern et al. 2006). Studies have shown that fMRI is a useful tool to delineate the brain regions associated with pain processing (Davis et al. 1995; deCharms et al. 2005). Recent studies from simultaneous EEG and fMRI recording have suggested that the EEG response to the pain may be correlated with the fMRI response, and both EEG and fMRI could be used to image the brain pain processing regions, such as the primary somatosensory cortex and anterior cingulated cortex (Christmann et al. 2007; Roberts et al. 2008). However, the EEG analysis and fMRI analysis in the studies were performed separately and only the induced pain in healthy subjects was investigated.

Most current studies about brain pain processing were targeted at the induced pain. Only a few studies about brain pain processing were related to the more clinically-relevant spontaneous pain due to the difficulties in comparing the painful and pain-free conditions of spontaneous pain. The MEG sources of spontaneous pain were previously studied in a patient with phantom limb pain (Kringelbach et al. 2007). The EEG sources of spontaneous pain were studied in neurogenic pain patients at the group-level analysis (Stern et al., 2006). The spontaneous pain in patients with chronic back pain was also studied using fMRI (Baliki et al., 2006). However, it remains important to noninvasively quantify and image the brain processing in clinically-relevant spontaneous pain of chronic pain patients.

As discussed above, the scalp EEG provides a non-invasive approach to measure the neural electrophysiological activity with a high temporal resolution. Although many other neuroimaging techniques have emerged, the advantages of EEG, including noninvasiveness, direct measurement of electrophysiology, and high temporal resolution,

make EEG an important neuroimaging tool for neuroscience research and clinical diagnosis. The application of EEG, however, is highly restricted by its relatively far distance from the underlying brain sources. On the other hand, functional MRI has excellent spatial resolution and coverage but suffer from low temporal resolution. Therefore, imaging techniques, which leverage on the benefits for both modalities can significantly improve our ability to noninvasively image and understand the functions of the brain and address urgent unmet clinical needs. Epilepsy and pain are two critical problems that can cause huge social economic burdens. Therefore, these two present as uniquely fitting areas for the applications of the imaging techniques we developed. This thesis is consisted of the work I did on these two areas of applications.

Chapter 2 FMRI in Focal Epilepsy

2.1 Introduction

For patients with drug resistant epilepsy, surgical resection is among the well-established methods for seizure control. During presurgical planning, if non-invasive methods such as structural MRI, semiology, single photon emission computed tomography (SPECT) and positron emission tomography (PET) etc. are not adequate in localizing the epileptic foci, invasive procedures including electrocorticography (ECoG) and depth electrodes are currently employed to define the seizure onset zone. However these methods are not only invasive in nature, they may also fail to provide additional information needed for surgery due to the relatively limited spatial coverage (Rodionov et al. 2007).

EEG/ MEG source imaging approaches (Fukushima et al. 2012; Wang et al. 2012; Wu et al. 2012) have also been investigated from noninvasive measurements during interictal (He et al. 1987, 2011a; Hamalainen and Sarvas 1989; Baillet et al. 2001; Lantz et al. 2003; Baumgartner and Pataraia 2006; Holmes et al. 2010; Koessler et al. 2010; Wang et al. 2010a; Lai et al. 2011) and ictal stages (Ding et al. 2007; Yang et al. 2011b; Lu et al. 2012a, 2012b) by solving the EEG/MEG inverse source imaging problem. While such noninvasive imaging techniques have improved substantially over the past decades, source imaging approaches in general are still relatively insensitive toward deep brain structures.

As a noninvasive imaging method, functional MRI (fMRI) has shown promises in the evaluation of epileptic foci. FMRI is currently used in presurgical assessment to

identify eloquent cortex that affect visual, language, motor functions to be spared during surgery (Thornton et al. 2010). In addition, fMRI may also offer values as a useful tool to localize epileptic foci. It is commonly used in combination with simultaneously collected scalp EEG (Liu et al. 2006; He and Liu 2008; Liu and He 2008). Temporal information of epileptic events identified from EEG can be used to correlate with hemodynamic changes in blood oxygen level dependent (BOLD) signal, to study the areas in the brain with epileptic activities(Hamandi et al. 2004; Gotman et al. 2006; Laufs and Duncan 2007; Lopes et al. 2012). In standard EEG-fMRI analysis, timing of interictal epileptiform discharges (IED) on scalp EEG is first identified. Each occurrence is treated as an impulse function which is then convolved with the hemodynamic response function (HRF) to obtain a general linear model (GLM). The model is then statistically fitted to the fMRI data, with appropriate thresholding to arrive at an activation map (Lemieux et al. 2001; Bénar et al. 2002; Hamandi et al. 2004). However, EEG recorded in the scanner is often heavily contaminated with artifacts that are difficult to remove completely. EEG is also known for its limited sensitivity towards deep brain structures. Another challenge in using the GLM approach is that an accurate model of the HRF is often needed, as it serves as the linkage that represents the neurovascular coupling. A standard canonical shaped HRF has been widely used but there is a growing consensus about the variability among subjects, or within the same individual but among different brain areas (Jacobs et al. 2009; Bai et al. 2010; LeVan et al. 2010). Additionally, recording EEG and fMRI simultaneously requires a complicated setup system that is not easy to use in a clinical setting. Moreover, some researchers using EEG informed fMRI have demonstrated the

value of fMRI in epilepsy, as it may be able to identify patients with widespread epileptic networks (Zijlmans et al. 2007).

Several previous studies have described the possibility of utilizing model-free, data driven methods on the BOLD signal alone to delineate epileptic activities (Rodionov et al. 2007; LeVan et al. 2010; Moeller et al. 2011; Lopes et al. 2012). Such approaches may offer an alternative to circumvent some of the aforementioned challenges associated with simultaneous EEG and fMRI. Independent component analysis (ICA) is a widely used blind source separation method. In the context of fMRI signals, it extracts regions of activities with corresponding time course based on spatial independence, which does not impose any constraint on the prior knowledge of HRF or the timing of interictal epileptiform discharges (IED) on EEG (Rodionov et al. 2007; LeVan and Gotman 2009). However, the process to select the independent components (ICs) that are related to epileptic activity often requires human supervision to a large extent. Therefore, we sought to develop an easy to implement framework that requires minimal subjective input to extract clinically relevant components.

Normally, focal epilepsy is highly treatable by surgery due to the focality of isolated epileptogenic zone. On the other hand, patients with diffused or distributed epileptogenic zones may not be suitable for surgical consideration. We intended to develop a tool to aid surgical planning for surgical candidates. Therefore, in the present study, we focused on the focal epilepsy population. To assess the sensitivity of the method, we simulated focal cortical activity in healthy subjects performing a lateralized motor task. We then evaluated the results of the proposed method by comparing selected components to expected motor activation area in healthy subjects and to surgical

resection in patients respectively. To assess the specificity of the method of component selection, we also included a study of healthy volunteers during resting state.

This chapter has been published in Clinical Neurophysiology (Zhang et al, 2015).

2.2 Methods

2.2.1 Data Acquisition

2.2.1.1 Patients

Data were collected from 10 consecutive patients (ages 20-58 years, 35.3±15.9 years, 5 males) with intractable epilepsy who underwent presurgical evaluation at Mayo Clinic (Rochester, MN). Clinical information was listed in Table 1. Resting state functional images were acquired using a General Electric 3T Signa HDx (Waukesha, Wisconsin) scanner. Each set of data was 20 min using a T2*-weighted EPI sequence. TR=3000 ms, flip angle =90, 3 mm isotropic voxel, 30±2 slices. A spoiled gradient recalled T_1-weighted anatomical image before and after operation was acquired for coregistration with functional data (1 mm isotropic voxel, 120 or 190 slices). The study was conducted according to a protocol approved by the Institutional Review Boards (IRB) of Mayo Clinic and the University of Minnesota respectively.

2.2.1.2 Healthy subjects with motor tasks

In order to evaluate the application of our method in localizing lateralized focal activity with known activity pattern, we performed an experiment where subjects performed hand movement tasks. Ten healthy volunteers (ages 20-36 years, 27.5±5.6 years, 5 males) participated in this study with written consent according to a protocol

approved by the Institutional Review Board of the University of Minnesota. The experiment followed a block design where task blocks were interleaved with resting blocks. Each block lasted for 20 s. Within a task block, subjects performed randomized left and right hand movement tasks. The tasks included either finger tapping or hand clenching of a given hand for one hand at a time. Each task block included only one type of task. Each individual anatomical MRI data set consisted of 176 contiguous sagittal slices with 1 mm slice thickness (matrix size: 256 * 256; FOV: 256 mm * 256 mm; TR/TE=20 ms/3.3 ms) on a 3T MRI system (Siemens Skyra, Siemens, Erlangen, Germany). Whole-brain functional images with BOLD contrast were acquired using gradient echo planar imaging sequence (32 axial 3-mm thick interleaved slices with 0.3-mm gap; TR/TE = 2000 ms/30 ms; flip angle = 90°; matrix size: 64 * 64; FOV: 192 mm * 192 mm). Each functional run started with a rest block and contained 160 volumes.

2.2.1.3 Healthy subjects during Resting State

In order to test the specificity of the algorithm, we also recruited a group of healthy subjects for resting state recording. Seven healthy volunteers (ages 24-31 years, 26±2.4 years, 5 males) participated in this study with written consent according to a protocol approved by the Institutional Review Board of the University of Minnesota. Each subject was instructed to lie quietly in the scanner for two scans, each lasting for six minutes. Additionally, individual anatomical MRI data were collected which were consisted of 176 contiguous sagittal slices with 1 mm slice thickness (matrix size: 256 * 256; FOV: 256 mm * 256 mm; TR/TE=20 ms/3.3 ms) on a 3T MRI system (Siemens Trio, Siemens, Erlangen, Germany). Whole-brain functional images with BOLD contrast were acquired using gradient echo planar imaging sequence (32 axial 3-mm thick

interleaved slices with 0.3-mm gap; TR/TE = 2000 ms/30 ms; flip angle = 90°; matrix size: 64 * 64; FOV: 192 mm * 192 mm).

2.2.2 Data processing

2.2.2.1 MRI data preprocessing

First, the pre-surgical structural MRI was segmented into two parts: regions within the boundary of the brain volume and those outside of the boundary. FMRI data were then spatially coregistered to the structural MRI. The boundary of the brain from the segmented structural MRI was used as a marker to distinguish voxels from the fMRI that corresponded to areas inside *vs.* outside of the brain in a later step after ICA decomposition. All fMRI data were pre-processed for slice scan time correction, 3-D motion correction and temporal filtering using BrainVoyager QX software (Brain Innovation, Maastricht, Netherlands).

2.2.2.2. Independent Component Analysis of fMRI data

Independent component analysis (ICA) in the spatial domain was performed using Brain Voyager QX. Detailed methodological principles of ICA decomposition implemented in Brain Voyager QX were previously described (Formisano et al. 2004; De Martino et al. 2007). Briefly, ICA decomposition of fMRI signal can be written as:

$$Y=TS \quad (2.1)$$

where *Y* is the fMRI signal, S is the spatial maps of the components and T is the time course defining the weights of the spatial maps in the time domain. S and T were obtained using the hierarchical (deflation) mode of the FastICA algorithm (Hyvarinen

1999; Calhoun et al. 2001, 2005). Thirty components were computed and the voxel intensities of each IC maps were converted to z-scores. The spatial maps were color coded to reflect the absolute value and sign. It should be noted that the sign of each voxel value does not correspond to BOLD activation or deactivation. A positive value represents that the time course of the particular voxel is positively correlated with the time course of the IC. A higher z-score represents a higher correlation coefficient. As pointed out previously, the z-values have no statistical significance, as no hypothesis was tested (McKeown and Sejnowski 1998; De Martino et al. 2007).

2.2.3 Classification of components

We proposed a set of data driven criteria to identify epilepsy related independent components (ICs). The criteria and rationales are described as following:

Criterion 1: Biophysical constraints of neurological sources. The BOLD signal of our interest indirectly measures neurological activity in the brain (Arthurs and Boniface 2002). Neurological activities are known to be generated by neurons residing in the grey matter of the cortex. However the BOLD signal measured is often confounded with other sources caused by physiological activities such as breathing, pulsation, or abrupt motion artifacts (Mitra et al. 1997; McKeown et al. 1998; Jiang et al. 2002). Some of these noisy components tend to have majority of the activity outside of the cortex in areas such as brainstem, eyes or the periphery of the cortex, which is usually due to residual motion artifacts (Mitra et al. 1997; De Martino et al. 2007). As described in the pre-processing section, the boundary of the brain obtained from segmenting the structural MRI was used to mark fMRI voxels as inside vs. outside of the brain. FMRI voxels outside of the brain,

which are clearly caused by noise, were not excluded before performing ICA. ICA was performed before exclusion of any voxels because we aimed to find and reject noisy activities within the brain that have statistical dependence with the noisy voxels outside of the brain. Therefore, by retaining obviously noisy voxels outside of the brain, it can help identify noisy activities that are within the brain in subsequent processing steps. To quantify this feature, we used the index $R_{i/o}$, where

$$R_{i/o}=N_i/N_o, \quad (2.2)$$

N_i denotes the number of voxels inside the brain, and N_o is the number of voxels outside of the brain. Components with $R_{i/o}$ value below a cut-off value will be excluded from further analysis (Fig. 2.1, Step 2, Criterion 1). This was to separate cortical components from noisy components with signals concentrated predominantly outside of the brain volume. The default cut-off value was set to be the median of $R_{i/o}$ values of all thirty components. This particular cut-off value was adopted to be inclusive rather exclusive. In this way, half of all the components will remain to be considered based on the next

criterion.

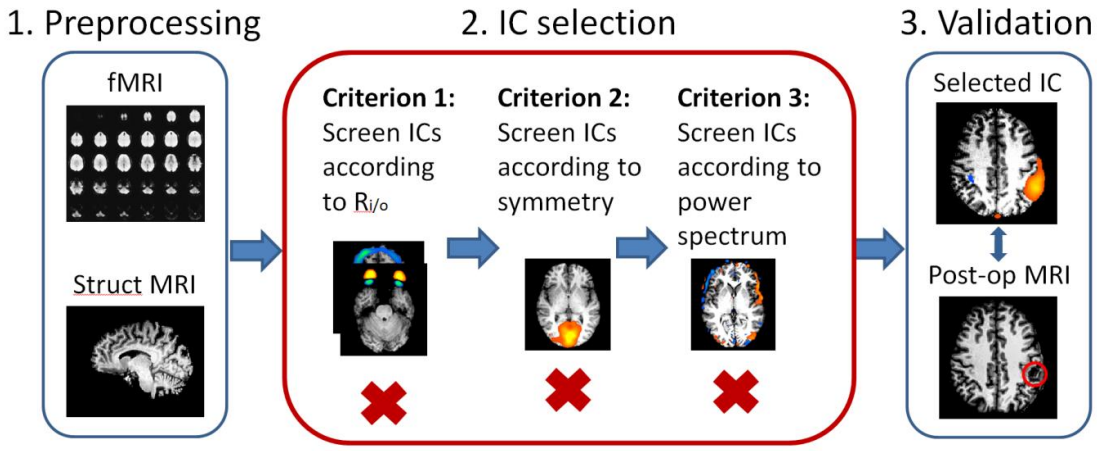

Figure 2.1 Data analysis procedures.

Step 1. Preprocessing of fMRI and MRI images. Step 2. Selection of the components basing on proposed three criteria. Step 3. Evaluation of the method. In the patient group, selected component was compared with post-surgical MRI.

Criterion 2: Spatial lateralization of the epilepsy related components in suitable surgical candidates. The concept of lateralization has traditionally been used in EEG to initially lateralize epileptogenic zone and to guide placement of intracranial recording. We now applied a similar concept in fMRI data analysis. As mentioned earlier, the patient population is surgical candidates with focal epilepsy. We assumed the epileptic activity is lateralized to one hemisphere. On the other hand, other common resting state activities in the brain are usually symmetrical. Such components include signals arising from major blood vessels, auditory activities, or default mode network (Raichle et al. 2001; Seifritz et al. 2002; Beckmann et al. 2005; Fox et al. 2005; Fransson 2005; Aragri et al. 2006; De Martino et al. 2007; Rodionov et al. 2007; Greicius et al. 2009). To quantify the symmetricity of the signal distribution of each component, we used the index Corr to denote the correlation of activities among mirroring voxels about the anterior

commissure – posterior commissure (ACPC) plane. The three-dimensional (3D) distribution of voxel intensity about on either side of the ACPC plane was first reduced to a one-dimensional series. It was arranged so that the i^{th} entry of both series corresponds to the mirroring voxels in the 3D space. The correlation value was calculated using Pearson's correlation coefficient.

$$\mathrm{Corr} = \frac{\mathrm{cov}(L, R)}{\sigma_L \sigma_R} = \frac{E[(L - \mu_L)(R - \mu_R)]}{\sigma_L \sigma_R} = \frac{\sum_{i=1}^{n}(L_i - \underline{L})(R_i - \underline{R})}{\sqrt{\sum_{i=1}^{n}(L_i - \underline{L})^2}\sqrt{\sum_{i=1}^{n}(R_i - \underline{R})^2}} \quad (2.3)$$

where L(i) denotes the i^{th} entry of the activity of the i^{th} voxel in the left half of the brain and R(i) denote the mirroring i^{th} voxel on the right side. Then the components were ranked according to their Corr values, from the smallest to the largest. Asymmetrical components are thus the ones with low Corr values. A cut-off threshold was set as one standard deviation smaller than the mean of the remaining components which passed the first level screening. This cutoff was used to identify components which would be considered for subsequent Criterion 3.

Criterion 3: Temporal features of the components. Components that passed the two aforementioned spatially based criteria were subjected to a third temporally based criterion to remove any additional noise. Components with dominant power outside of the range of 0.01 to 0.1 Hz were excluded. As described by De Martino et al (De Martino et al. 2007), neurophysiologically meaningful components are expected to have certain temporal structure, which often fall within the range of 0.01 to 0.1 Hz (Cordes et al. 2001; van de Ven et al. 2005). Components with dominant frequency outside of this range are often a reflection of aliasing of cardiac and respiration artifacts (>0.1 Hz) or scanner

susceptibility artifacts (<0.01 Hz). Power contribution of each component at each frequency band was computed as part of the BrainVoyager QX ICA 'Fingerprint' function. Briefly, the power spectrum density of each IC was first computed. Relative contribution of each frequency band ([0, 0.008 Hz], [0.008, 0.02 Hz], [0.02, 0.05 Hz], [0.05, 0.1 Hz] and [0.1, 0.25 Hz]) was captured by calculating the weight of each frequency bands over the entire spectrum. The metric of each component at any given frequency was normalized first within the component then cross all components to arrange from 0 to 1(De Martino et al. 2007). If a component has a metric of 1 for a specific frequency band, that frequency band is considered as a dominant frequency of the component. Components with dominant frequency above 0.1 Hz or below 0.008 Hz were removed.

2.2.3 Evaluation

In the patient study, the spatial patterns of identified components were compared to the co-registered postoperative MRI. If the area of activity in the identified component falls within or well overlaps with the resected area, the component was considered as concordant. In the motor task experiment, the accuracy of identified components was evaluated both temporally and spatially. Temporally, the expected time course of motor response was obtained by convolving the block design time and the canonical HRF. The time course of identified components was then compared with the expected time course to compute the correlation coefficient. Spatially, a general linear model was used with expected time course as a regressor to obtain the activation maps corresponds to the motor tasks. The activation maps were compared to maps of identified components. Group averages of the maps from both GLM and ICA were computed and compared in

the Talairach space. In the resting state experiment with healthy subjects, the specificity of the algorithm was assessed by examining if there were any components that passed the three-criterion algorithm.

2.3 Results

2.3.1 General component screening

Fig. 2.2 shows representative components taken from a subject in the motor-task simulation, where the subjects were asked to perform hand movement tasks to simulate a unilateral focal neural activity. Components removed by Criterion 1 included a pattern that is consistent with activity in eye areas (Fig. 2.2A). This eye component has low in-brain *vs.* out-brain ratio, $R_{i/o}$, of 0.02, which is significantly lower than the average of all the 30 ICs (1.60±0.9). The second criterion of lateralization rejected a component consistent with fMRI activity in visual cortex (Fig. 2.2B). This component has $R_{i/o}$ =1.6 and Corr= 0.4. It survived Criterion 1 but rejected by Criterion 2 due to high symmetry between left and right visual cortex. The component shown in Fig. 2.2C passed both Criterion 1 and 2 but was rejected by Criterion 3 as this component has dominant frequency in the >0.1 Hz range. The spatial pattern of this component matches the pattern of typical residual motion artifacts as reported in previous studies (Mitra et al. 1997; McKeown et al. 1998; Thomas et al. 2002). The only component which passed all three criteria showed activity in left motor cortex (Fig. 2.2D). It is consistent with the right finger tapping activity of the subject during the fMRI recording.

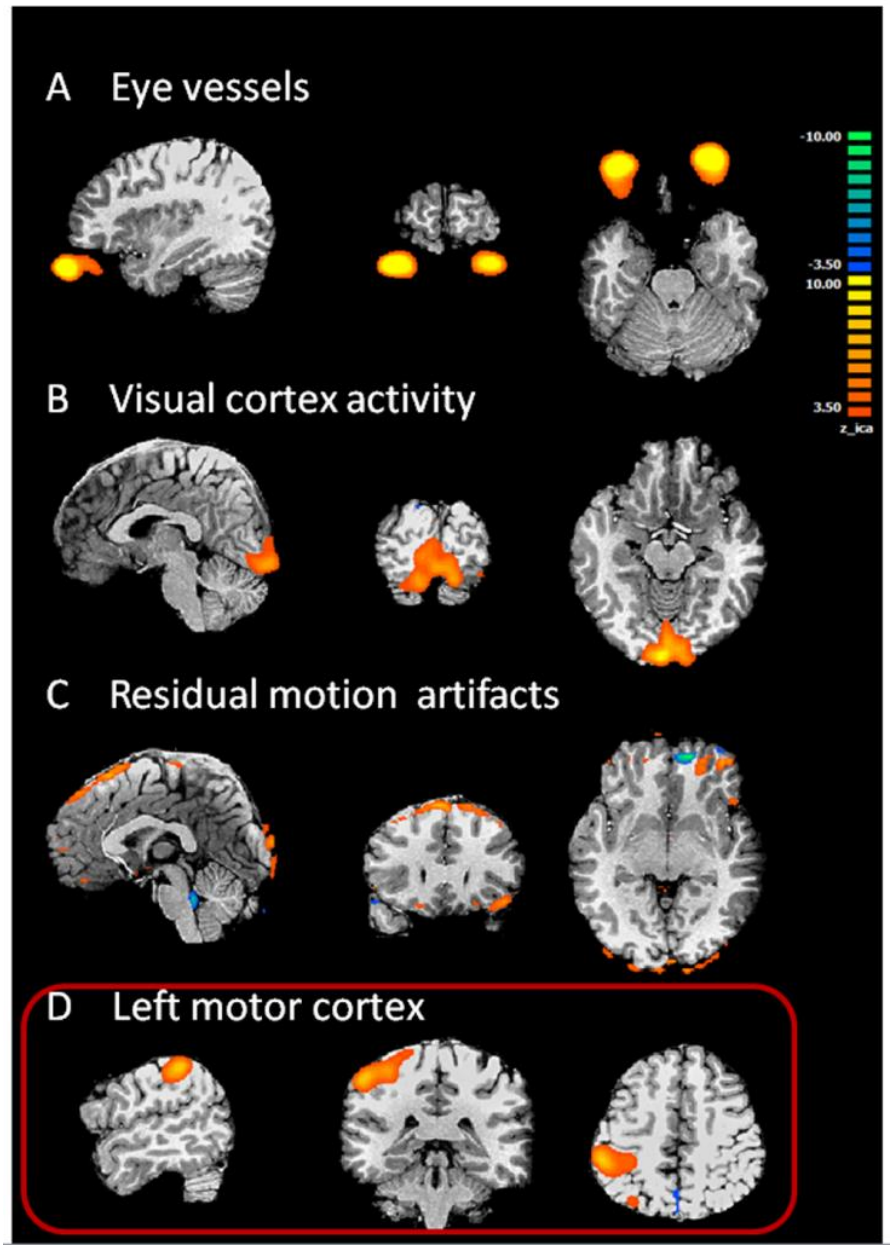

Figure. 2.2 Illustration of different components from motor simulation in a healthy subject

A. Eye movements. The BOLD activities are located outside of the brain volume. This component has a low $R_{i/o}$ value and was screened out by Criterion 1. B. Visual activity. This BOLD pattern is highly symmetrical and was rejected based on Criterion 2 because of the high symmetry between left and right mirroring voxels. C. Residual motion artifacts, located at the periphery of the brain. This component was rejected by Criterion 3. D. Selected component that passed all 3 screening criteria. The spatial distribution of this component is concentrated in the left motor cortex. This is an example of contralateral activation, as expected from right hand movement. In the patient group, components rejected by Criterion 1-3 have similar patterns as shown in A-C.

2.3.2 Patients with focal epilepsy

Patient 1 was diagnosed with frontal lobe epilepsy and underwent left frontal craniotomy. In our component selection algorithm, the cut-off value of $R_{i/o}$ used in Criterion 1 is 0.9 and the cut-off value of Corr used in Criterion 2 is 0.16. Three out of fifteen components passed Criterion 2.The first component (Fig. 2.3A, $R_{i/o}$=2.62, Corr = 0.12) shows activity in left frontopolar cortex, which falls within the surgical resected zone as indicated by the red arrow in postoperative MRI (Fig. 2.3B). Component 2 ($R_{i/o}$=0.90, Corr = 0.16) has two areas of activities (Fig. 2.3C). One is located in the midline along the longitudinal fissure, and another near to the left middle frontal gyrus, which coincides with another region of resection as shown in Fig. 2.3D. The third component (Fig. 2.3E) survived the screening process but was not considered epilepsy-related by visual evaluation. This is because it has a ring shaped distribution of activity around the peripheral of the cortex, which is a typical pattern for residual movement artifact.

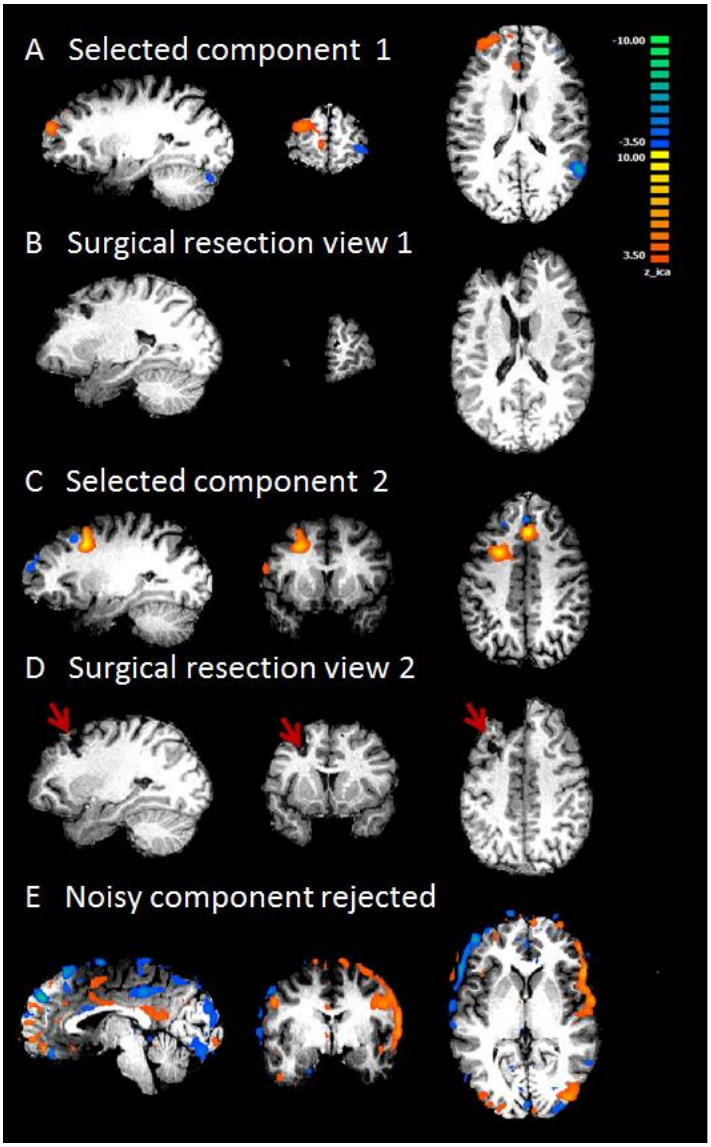

Figure. 2.3 Results from Patient #1

A and C are the two components selected by the proposed algorithm. They both have high lateralization values. This patient had left frontal lobe epilepsy and received surgical resection in left frontal lobe. B and D are post-operation MRI, showing two different surgical locations corresponding to the two identified components. E shows a typical noisy component that survived the three criteria but was rejected by visual insepection. This component has voxels within the brain volume and is highly asymmetrical. But the spatial pattern of this component is of a typical residual movement artifact.

Patient 2 had left parietal epilepsy. Presurgical EEG showed frequent epileptogenic abnormalities over the left central region, which was consistent with a

partial seizure disorder. In this patient, the cut-off value of $R_{i/o}$ in Criterion 1 is 1.2 and the mean of $R_{i/o}$ and cut-off value of Corr used in Criterion 2 is 0.29. Two out of the fifteen components passed Criterion 3 and were examined by visual inspection. One first component (Fig. 2.4A, $R_{i/o}$= 2.2, Corr=0.27) localized in the close vicinity of the surgical resected parietal cortex (Fig. 2.4B). This patient received intra-cranial recording and left parietal cortical resection. The largest cluster with the highest z-sore of the selected component falls in the right parietal cortex, which is in concordance with the resected region. The other component was considered not epilepsy-related by visual evaluation because it has a similar ring-shaped pattern as shown in Fig. 2.3E in Patient 1.

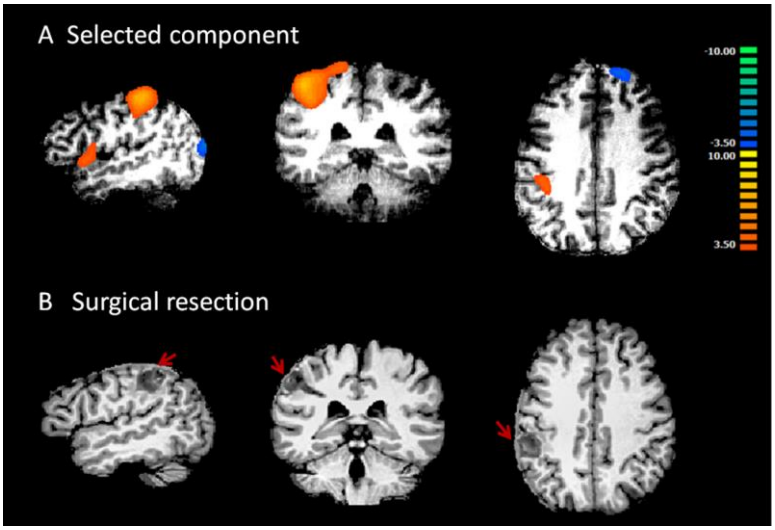

Figure. 2.4 Results from patient #2

A shows the only component selected by the algorithm and accepted by visual inspection. This component has high lateralization value and is localized in the left parietal lobe. This patient had left parietal lobe epilepsy. B shows surgical resection in left parietal lobe, indicated by red arrows. The orange cluster in left parietal region shown in A agrees well with the surgical resection in B.

Patient 3 was diagnosed with left temporal epilepsy and underwent left temporal lobectomy. In this patient, the cut-off value of $R_{i/o}$ in Criterion 1 is 0.50 and the cut-off

value of Corr used in Criterion 2 is 0.12. Only one component was identified by our first two criteria (Fig. 2.5A). This component also passed the additional Criterion 3. It has activity in left anterior temporal area, which agrees with spikes and sharp waves observed from anterior temporal electrodes on ECoG. It also co-localizes to the surgical resected zone as indicated by the red arrow in postoperative MRI (Fig. 2.5B). The $R_{i/o}$ and Corr of this component are 0.54 and 0.01 respectively.

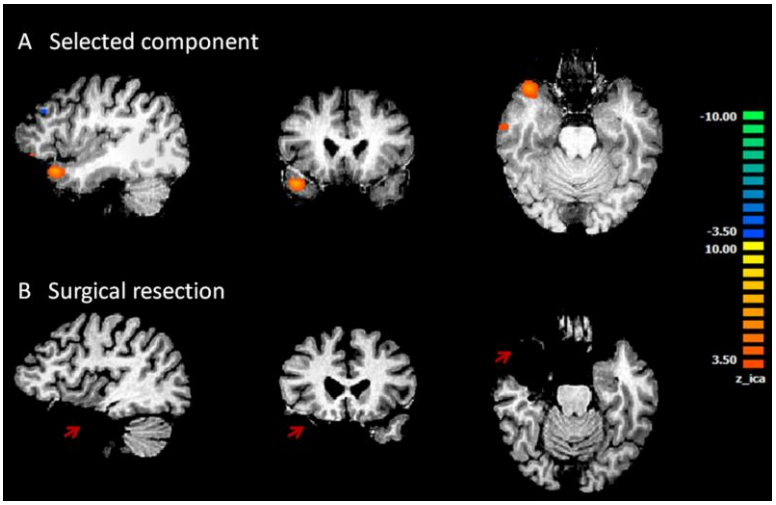

Figure. 2.5 Results from Patient #3

A shows the only component selected by the algorithm and accepted by visual inspection. This component is located at the anterior portion of the left temporal lobe. This patient had left temporal lobe epilepsy. B shows surgical resection in left temporal lobe. Orange cluster in left temporal lobe in A falls well within the surgical resection indicated in B.

Patient 8 was diagnosed with right parietal epilepsy. However, no component was identified from the fMRI basing our 3-criterion algorithm. We carefully examined all the components from the patient, and noticed that two components had abnormal spatial distributions (Fig. 2.6A and 2.6B). Both components show distributed activity in the bilateral inferior parietal lobules and posterior cingulate cortex, which resemble typical 'default-mode-network' pattern. Additionally, as shown in Fig. 2.6B, this component

also has a dorsal/ventral medial prefrontal cortex node which is typical in default mode network. However, several extra-network clusters in the right frontal and parietal regions were found to be temporally correlated with the default mode network. These clusters occur unilaterally in the right hemisphere. According to the clinical report of video EEG, ECoG and SPECT, this patient had diffuse seizure onset in frontal central as well as right central head regions. The observations of the altered network property and diffuse epileptogenesis may suggest the interplay between the two phenomena. Consistent with our inconclusive findings, presurgical evaluation of the patient conducted independently in the hospital resulted in a conclusion that the patient was not a good surgical candidate.

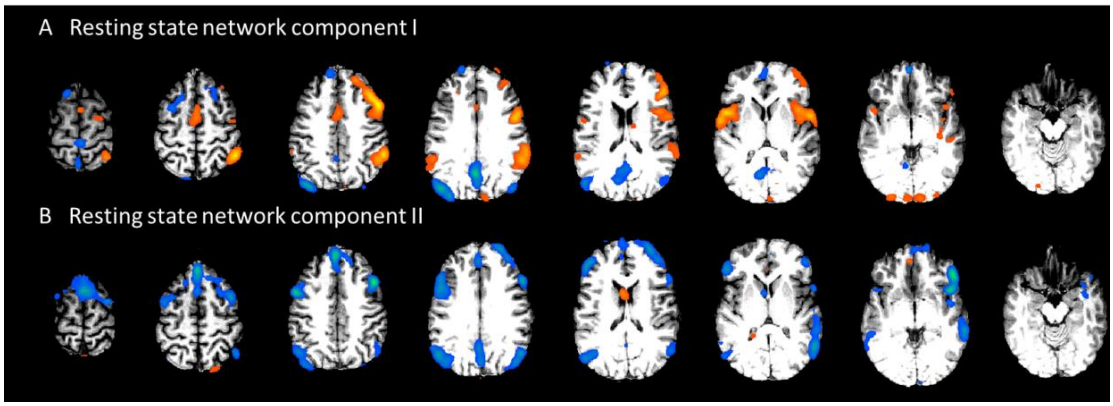

Figure. 2.6 Results from Patient #8

A shows one component associated with the bilateral fronto-parietal association cortex, which represents a typical resting state network. Additionally, there are also clusters on the right lateral frontal and parietal regions. B shows another component associated with the bilateral network, with an additional cluster on the right fronto-parietal region. This patient was initially diagnosed with right parietal epilepsy. Presurgical ECoG revealed diffuse seizure onset involving a large region simultaneously. This patient was not selected to receive surgical resection.

Information and results of all patients were summarized in Table 2.1 with additional information provided in Table 2.2. Out of ten patients studied, nine received surgery. Epilepsy related components found in seven patients were highly concordant

with surgical resection. For the patient who did not receive surgery, our analysis showed activity lateralized to right parietal lobe, however, overlapping with widespread resting state network in bilateral parietal and frontal areas. Diffused epileptic activity is not suitable for surgical resection treatment. This finding is consistent with the surgeon's decision not to operate on this particular patient. The algorithm did not identify any epilepsy related components in two other patients.

Patient	Age	Gender	Clinical diagnosis	Resection	Results
1	27	Male	Left frontal	Left frontal craniotomy	++
2	25	Female	Left parietal	Left frontoparietal craniotomy	++
3	58	Female	Left temporal	Left temporal lobectomy	++
4	29	Male	Right temporal	Right temporal lobectomy	++
5	20	Female	Left temporal	Left temporal lobectomy	++
6	20	Male	Left temporal	Left temporal lobectomy	++
7	47	Female	Left temporal	Left temporal lobectomy	++
8	20	Female	Right parietal	N. A.	+
9	58	Male	Right temporal	Optic laser ablation of hippocampus	*
10	49	Male	Left temporal	Left temporal lobectomy	-

Table 2.1
++ : Identified components in agreement with surgical resection
+ : Altered resting state network found consistent with presurgical evaluation
* : A component was found in close vicinity to ablation after adjusting the screening threshold
- : No epilepsy related component found

Patient	# ICs passed Criterion 2	# ICs passed Criterion 3	# ICs concordant	Concordant cluster w. max z-score?	# clusters in concordant ICs
1	3	3	2	yes	6
				no	7
2	3	2	1	yes	7
3	1	1	1	yes	3
4	3	1	1	yes	7
5	3	1	0	--	--
6	2	2	2	yes	4
				yes	3
7	2	1	1	yes	5
8	3	0	--	--	--
9	3	3	1	no	4
10	2	0	0	--	--

Table 2.2

ICA classification results # clusters in concordant ICs: the total number of distinct clusters that are present in each ICs with one cluster that is in concordance with surgical resection. If the concordant cluster has the highest z-score, it is indicated as yes in the second-to-last column.

2.3.3 Healthy subjects with motor tasks

Results from healthy subjects performing motor tasks served as a preliminary evaluation of the sensitivity of the proposed algorithm. The method detected lateralized motor-task-related components from ICA with minimal supervision and high accuracy across all subjects. We examined the spatial and temporal features of the selected

components to the timing of the task design. The temporal feature of the selected component has time course that correlated with the expected time course based on the known stimulus onset convolved with canonical hemodynamic function (HRF). The identified components have BOLD activities in the sensorimotor areas correspond to the left or right hand. Fig. 2.7 shows group-level average activation maps in the left motor area that corresponds to right hand movement across all healthy subjects. Fig. 2.7A shows the averaged map obtained from maps of identified motor task related ICs. Fig. 2.7B shows the averaged map obtained from GLM using expected time course derived from experiment design as the main regressor. Temporally, the Pearson's correlation coefficient between the identified IC time course and the expected time course specified by the experiment is 0.72 ±0.08.

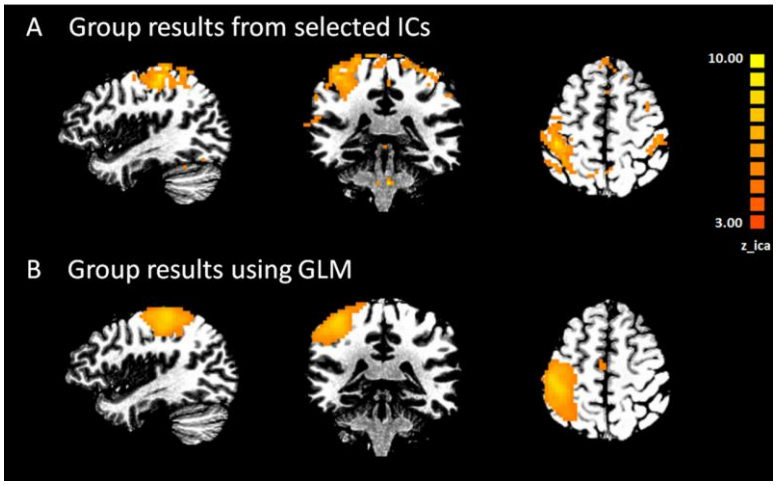

Figure. 2.7 Group results in healthy subjects performing right hand motor tasks

A) Averaged map of selected independent components(IC) from all subjects. B) Group averaged activation map obtained from GLM analysis. Expected time course derived from experiment design was used as the main regressor.

2.3.4 Healthy subjects during Resting State

Results from seven healthy subjects during resting state served as a preliminary evaluation of the specificity of the proposed algorithm. Identical parameters were applied to this data set, and the data was processed to examine whether there were any components selected by the algorithm as epilepsy related. In four out of the seven subjects, the three objective criteria ruled out all the components, which reflected true negative results as expected. In the other three subjects, between one to three components were identified by the algorithm as potentially epilepsy related. They represented either additional noisy component (Fig. 2.8A), similar to that seen in Fig. 2.3E, that the algorithm was not able to screen out or lateralized physiological activities, for example in sensorimotor area (Fig. 2.8B). In one out of the three false positive cases, the only component identified was associated with noise. In two other cases, both a noisy component and a lateralized physiological component were identified. The nature and frequency of occurrence of such non-epilepsy component identified by the method is similar to what we observed in the patient group. Findings from this study can be used to guide further refinement of the algorithm in the future.

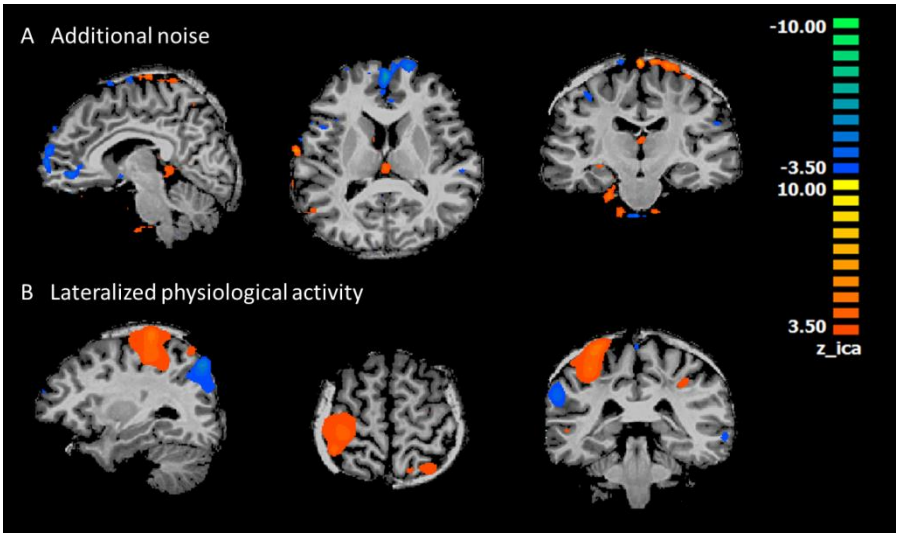

Figure. 2.8 Examples of spurious components in resting state healthy subjects

A) Typical noisy component with distributed pattern in small clusters through the brain but mostly near to the peripheral or along the midline. B) Unilateral physiological activity in sensorimotor area.

2.4 Discussion

For the purpose of both lateralizing and localizing hemodynamic foci in focal epilepsy patients, we proposed an automated algorithm that detects epilepsy related components from ICA with minimal supervision and high accuracy. Our algorithm was evaluated by comparing the identified components to surgical resection. In the current patient group we were able to lateralize and localize hemodynamic foci using proposed method reasonably well. We also tested the algorithm in healthy subjects with and without tasks and the results showed reasonable sensitivity and specificity of the method.

This proposed method can be easily implemented in the current presurgical workup to provide additional information for guiding the surgical resection. The benefits are two folds. Firstly of all, the data currently used were collected as part of clinical

routine for mapping of eloquent brain to preserve during the surgery. Therefore, to implement this method, no additional scans need to be prescribed. Secondly, the algorithm is automated and does not require subjective input or excessive training from the clinicians. However, at this stage, it is not meant to replace any aspect of the presurgical planning process, but rather to further inform each step of presurgical planning.

2.4.1 Method Applications

The spatial ICA algorithm allows for the computation of as many components as the number of time points. We explored a range of different numbers of components from twenty to forty five. The overall patterns of the components remained similar to the case of thirty components. But when a larger number of components were used, there were occasional splits of components in a few subjects. This will result in false positives by using the symmetry measure, as split components can be asymmetrical but symmetrical when combined. Therefore, the number of components used in the ICA decomposition was set to thirty, as it represented a good tradeoff between computation efficiency and separation of components in our data set. The optimal number may vary among subjects and different groups, but we used thirty for all the subjects studied.

In the patients we studied, the surgical resection sizes are typically large, except in the case of one patient, #9, who received focal ablation. In the six patients where we found ‘overlapping’ clusters with surgical resection, four had temporal lobectomy, where the resection size is approximately 3.5 cm in length. The identified clusters in the four temporal cases are much smaller and fall within the surgical resection area. In patient#1,

the clusters identified are comparable in size with the two separate resection areas. The degree of overlap is about 80%. In the case of patient#2, the identified cluster is roughly two times greater than the actual resection but covers the resection completely.

2.4.2 Method Assumptions

In this study, we aimed to identify epilepsy related components from components produced by spatial ICA of resting state fMRI. Characteristics of task related fMRI independent components (ICs) of healthy subjects were previously discussed by De Martino *et al*. (De Martino et al. 2007) and applied in the context of focal epilepsy (Rodionov et al. 2007). In our approach, instead of comprehensively studying all different types of ICs, we focused mainly on extracting epilepsy related components by applying three basic assumptions.

The first assumption is that neurological activity dominant components should locate mainly inside the brain volume. This was assessed by calculating the ratio between the numbers of voxels with activity inside *vs.* outside of the brain volume. Secondly, we focused on focal epilepsy patients and assumed that this group of patients have unilateral, epilepsy related BOLD foci. Most successful surgeries in epilepsy often involve patients with focal epilepsy because of the isolated epileptogenic zone. Therefore, it is clinically important to noninvasively identify suitable candidates as well as to localize epilepsy foci for resection. We thus targeted this group of patients with unilateral, instead of bilateral epilepsy related BOLD activities. With this condition, we could easily separate epilepsy related components from other neurophysiological components associated with auditory or occipital activation, resting-state networks, and major endovascular activities. These

non-epilepsy components often have a symmetrical spatial distribution, which will lead to a high correlation score, Corr, when the signals between mirroring voxels of the left and right hemispheres were compared. The third assumption is that BOLD fluctuations due to neurological activity have a frequency range near to 0.01 to 0.1 Hz. Some noisy components may fall within the perimeter of the brain and have asymmetrical distribution, but these components often have dominant frequency fall below 0.01 Hz or above 0.1 Hz due to artifacts from aliasing of cardiac and respiration activity or scanner susceptibility.

In the first noise reduction step we used median $R_{i/o}$ as cut-off, which represents thresholding at 50%. This may appear to be too aggressive. At this cut-off, the actual cut-off value of $R_{i/o}$ was 0.74±0.28 among all patients. This means there are still a relatively large number of voxels outside of the brain comparing to inside of the brain at the cut-off level. Such a component may still be relatively noise dominant. Certainly an even more stringent cut-off value may further control the specificity of the algorithm, but it may also result in less sensitivity in detecting actual epilepsy related components. The current cut-off level, therefore, seems to be appropriate for this group studied.

The concept of lateralization has traditionally been used in epilepsy diagnosis. For example, scalp EEG is often used in clinic to initially lateralize epileptogenic zone and to guide placement of intracranial electrodes. In the application of fMRI, Negishi and colleagues (Negishi et al. 2011) found lateralized fMRI connectivity could serve as a predictor of the surgical outcome. When a patient has lateralized connectivity pattern, they found their surgical outcome is likely to be seizure free. In this study, we applied the same concept to the fMRI data analysis. By taking advantage of the spatial resolution of

fMRI, we aimed to not only lateralize but also to localize epileptic activities in patients with focal epilepsy.

2.4.3 Model-free approach

A number of previous studies have explored the utility of fMRI alone, both ictal and interictal, using data driven approaches. Ictal fMRI studies reported have shown concordance between identified IC and seizure onset (LeVan et al. 2010; Thornton et al. 2010), but ictal events are hard to capture in a limited time window of the scanning time. Several other studies have reported using interictal resting state fMRI and compared the accuracy using simultaneously acquired EEG-fMRI in a general linear model (GLM) (Rodionov et al. 2007; LeVan and Gotman 2009; LeVan et al. 2010; Lopes et al. 2012). Unlike the aforementioned studies, we focused on the localization value of interictal fMRI without simultaneously acquired EEG in focal epilepsy. We compared our results with surgical resection and follow-up. Resection with seizure free outcome is considered as the ground truth for evaluation of the localization accuracy.

This data-driven, exploratory approach using ICA has several advantages. First of all, knowledge of the precise timing of interictal epileptic discharges (IEDs) is not required. Scalp EEG has a long history in the diagnosis of epilepsy. Abnormalities observed on EEG can be used to classify epilepsy types and lateralize epileptic area. However, in cases when EEG is absent, or when clear epileptiform discharges are not well formed, our results suggested that it is still possible to extract epilepsy related activities using fMRI analysis alone. Secondly, motion residual artifacts or various physiological noises do not need to be modeled explicitly. In conventional GLM-based

fMRI analysis, movement parameters and other physiological noises need to be accounted for to improve the effects caused by epileptic activity. However, using ICA analysis, these noisy components are often well separated automatically. Thirdly, the complexity and variability of HRF can be circumvented. The HRF is the link between electrophysiological events and hemodynamic responses in the brain. There has been growing evidence suggesting variability of the HRF in different areas of the brain and among individuals. Simultaneously acquired EEG and fMRI can provide insight into the nature of the HRF, but for our specific purpose of assessing the localization value of fMRI-alone recording without EEG, the knowledge of HRF is not required. Furthermore, if simultaneously acquired EEG is available, this method can offer a way to study epilepsy specific HRF characteristics.

2.4.4 Resting-state network

Components representing the resting-state networks including default mode network (DMN) were found in all patients. Previous studies also showed that networks including the default mode network are involved in epileptic activity (Archer et al. 2003; Laufs and Duncan 2007; Zijlmans et al. 2007; Blumenfeld et al. 2009; Bai et al. 2010) and other pathological brain diseases such as Alzheimer's (Greicius et al. 2004; Buckner et al. 2005). However, the primary goal of our proposed method is to lateralize and localize the hemodynamic foci for presurgical evaluation purpose. Regions in the resting state network are hypothesized to be involved in multiple cognitive functions (Raichle and Snyder 2007) and are rarely the target for surgical removal. Therefore, we design the algorithm to detect areas that can be surgical targets instead of other brain networks that are not suitable for current surgical treatment, although those regions might also be

impacted or involved in complicated epileptic activities. Our method identified the DMN components as neurological sources with high spatial signal to noise ratio, i.e. high $R_{i/o}$ values. But the correlation coefficient indices of the DMN components are much higher than the selected component due to the symmetric nature, Corr=0.51± 0.10 for DMN components *vs.* 0.18 ± 0.09 for epilepsy foci components. As reported previously, DMN may be altered by epileptic events in both focal as well as generalized epilepsy (Laufs and Duncan 2007; Blumenfeld et al. 2009; LeVan and Gotman 2009; Zhang et al. 2010, 2011; Voets et al. 2012). Interestingly, in the case of Patient 8 we also found two components representing altered DMN or resting-state networks. In addition to activities in the typical bilateral fronto-parietal association cortex, there were also unilateral clusters in the right frontal and central parietal regions (Fig. 2.6A and 2.6B). This statistical dependency between the right central parietal and frontal clusters with the resting state network may shed some light in explaining this patient's seizure characteristics. In the surgical report of this patient, it was mentioned that she had diffuse onset involving a large region simultaneously on ECoG and was therefore not suitable for operation. No abnormal pattern was found in other patients DMN components. The spatial and temporal features of DMN in focal and generalized epilepsy will be examined more thoroughly in future studies.

2.4.5 Method limitations

Although the proposed method worked reasonably well in the current patient group, where patients only had unilateral focal epilepsy, this method was not intended to be an all-encompassing approach that will detect all epilepsy foci in all focal epilepsy cases. The current method was designed to detect epileptic activities with unilateral

origin. If we know ahead of time that the epileptic activities originate bilaterally, the method will not provide additional insight. Fortunately in partial epilepsy, there are a good portion of surgical patients with epileptogenic foci located unilaterally. It may also be able to detect bilateral multifocal epileptic activity if the distribution of the foci is not symmetrical. However, it may not be suitable for detecting epileptogenic foci located near to the midline or symmetrically in both hemispheres. Sometimes, the BOLD response of unilateral spike activity may appear to be bilateral. In these cases, our method will not capture such a component, which may explain why we did not detect an epilepsy related unilateral component in patient #5 and #10.

This method is also not perfect in rejecting all non-epilepsy components. As seen in both patient and healthy subject resting state results, there are a small number of non-epilepsy related components selected by the algorithm. These components can be largely summarized into two categories: 1) Additional noise that was not captured by the noise-reduction procedure. Such components often have distributed small clusters (Fig. 2.8A) often near to the peripheral of the brain boundary (Fig. 2.3E). A further improvement in the algorithm could potentially exclude such components. For example, the brain boundary can be slightly shrunk so that activities of the voxels in close vicinity of the boundary can be disregarded from evaluation, since they are often prone to residual movement artifacts. 2) Unilateral physiological activities that are mislabeled as epilepsy related (Fig. 2.8B). Such components may be resulted from unilateral activation in eloquent cortex. In patient #2 for example (Fig. 2.4A), the identified epilepsy component was in close vicinity to the left sensorimotor area. Fortunately in this case, additional evidence from ECoG, surgical resection and the seizure free outcome indicated the

accuracy of the selection. But for future application, if the algorithm identifies an area overlapping with eloquent cortex, as we saw in two of the healthy subjects, additional care should be given to exclude false detection of other physiological activities that are not related to epilepsy.

One additional implicit assumption of this method is the symmetry of the anatomical structure. Because the symmetricity calculation was based on the relative location to the ACPC plane specified on the anatomical MRI. The current method may not be sensitive to slight contoured ACPC plane or small imbalance of anatomical sizes between the left and right hemispheres. But if the brain is largely asymmetrical due to prior surgery, a large lesion or congenital distortions, this method will not be applicable.

In the present study we proposed an ICA-based automated method to lateralize and localize hemodynamic foci in focal epilepsy patients for presurgical evaluation. Focal activities identified by our method were in concordant with surgical resection in majority cases studied. Our findings suggest the possibility of noninvasively and accurately localizing hemodynamic epileptic foci using fMRI alone in presurgical planning. Overall, this is a feasibility study to demonstrate the value of the proposed method. Additional features can be incorporated in the algorithm to improve reliability and performance. A larger patient population needs to be studied to test the broad applicability of this method. This proposed method can be easily implemented in the current presurgical workup to provide additional information for guiding the surgical resection.

Chapter 3 Multimodal Imaging of Generalized Epilepsy

3.1 Introduction

Idiopathic generalized epilepsy (IGE) is characterized by various combinations of generalized tonic-clonic seizures, absence seizures, myoclonus (Blumenfeld 2005; Zhang et al. 2011), and generalized spike-and-wave discharges (GSWD) observed during interictal periods on electroencephalography (EEG) recordings (Hamandi et al. 2006; Moeller et al. 2011; Zhang et al. 2011). Focal spike-wave complexes occasionally are observed interictally in patients with IGE, although ictal EEG recordings show only generalized-onset seizures and no focal-onset seizures in IGE (Drury and Henry 1993; Seneviratne et al. 2012). Unlike focal or partial epilepsy, which has a confined range of influence, IGE affects the whole or a larger portion of the brain often without obvious, known cause (Engel 2001). Among drug-resistant epilepsy, patients with focal epilepsy may receive surgical resection to become seizure free. On the other hand, patients with generalized epilepsy do not have such a treatment option. Recently deep brain stimulation (Johnson et al. 2013) has been hypothesized as a way to treat epilepsy patients (Fisher et al. 2010). Therefore, it is important to distinguish the driver (or source) versus recipient (or sink) to understand how the epileptic activities propagate to the entire brain.

In the recent decades, it has been generally agreed that the highly interconnected circuitry of the cortex and thalamus plays a crucial role for generalized epilepsy (Blumenfeld 2005). There is general agreement that both cortex and thalamus participate in the generation of typical spike-wave seizures, but their relative importance is still unclear. Previous works using EEG-functional magnetic resonance imaging (fMRI) and

anatomical MR-based study (Bernhardt et al. 2009) indicated the involvements of thalamus, default mode network (Raichle et al. 2001; Fox et al. 2005), cerebellum, caudate nuclei and corticocortical networks in the generations of GSWDs (Blumenfeld 2003, 2005; Gotman et al. 2005; Hamandi et al. 2006; Bernhardt et al. 2009; Blumenfeld et al. 2009). However, the exact interplay between the cortical and sub-cortical structures remains to be further explored.

The goal of the present study is to use noninvasive, multimodal imaging techniques to elucidate the underlying mechanisms that generate GSWDs in IGE patients. Specifically, we aim to map the cortical networks associated with GSWDs and investigate the causality between cortex and thalamus during GSWDs. We first performed EEG-informed fMRI analysis and identified regions of interest (ROI). We then tested the specific connectivity patterns by seed-based connectivity analysis in fMRI data. The seeds include both regions determined by the EEG-informed fMRI analysis and additional ones identified by EEG waveforms. ROIs that exhibited network properties, i.e. the ones that share temporal profile with remote regions, were further subjected to the Granger Causality analysis to identify sources and sinks within the networks.

EEG and fMRI are two noninvasive neuroimaging tools used in epilepsy research and clinical applications. EEG has a long history being used as an important diagnostic tool for epilepsy. EEG has the benefit of having high temporal resolution but often suffers from limited spatial resolution. With the advancement of source imaging techniques (Lantz et al. 2003; Holmes et al. 2010; Koessler et al. 2010), successfully localizing epileptic activity in focal epilepsy is possible (Sohrabpour et al Epub.; Lantz et al. 2003; Michel et al. 2004; Ding et al. 2007; Lai et al. 2011; Yang et al. 2011; Lu et al.

2012a; He and Ding 2013). However, very few studies have looked into using dense-array EEG to study the temporal dynamics of the sources in IGE (Jung et al. 2005). With complementary high spatial and temporal resolution, simultaneous fMRI and EEG (Liu and He 2008) has been shown to provided valuable information in diagnosis of epilepsy (Pittau et al. 2012; Zhang et al. 2015).

Seed-based connectivity analysis using resting state fMRI is another common technique in studying of both healthy and diseased neurological networks (Greicius et al. 2009; Moeller et al. 2011; O'Muircheartaigh et al. 2012). Using this technique, remote areas that share the same temporal characteristics can be identified. Compared with EEG-informed fMRI, seed-based connectivity analysis does not rely on precise knowledge of the EEG event timing, which can be difficult to obtain given the noisy signal collected concurrently with fMRI. However, it requires prior knowledge in determining the ROIs as seeds. In our study, we used regions identified by the EEG-informed fMRI result as seed in conjunction with other areas that may potentially be involved in the network activities in generating GSWDs. By using seed-based analysis, we can obtain a more specific network level activity than using EEG-informed fMRI alone.

Once we establish a network that is involved in generating GSWDs, the next question is which node in the network is driving the others. Directed connectivity measures based on the concept of Granger causality (Granger 1969) has been proposed (Kaminski and Blinowska 1991; Goebel et al. 2003; Babiloni et al. 2005) to discern the causal relationship among different temporal series. The direction can be estimated with the following rationale: the driver is earlier than the recipient implying that the driver contains information about the future of the recipient not contained in the past of the

recipient while the reverse is not the case. The directed transfer function (DTF) has been used to quantify the directionality and strength of the connectivity profile among different brain regions (Kaminski and Blinowska, 1991). DTF has been successfully applied in the field of epilepsy research, to identify sources (active or efferent sources) and sinks (passive or afferent sources) that may play important roles in generating seizures and interictal activities (Babiloni et al. 2005; Ding et al. 2007; Wilke et al. 2010; Lu et al. 2012b). Built upon the DTF method, which computes the overall connectivity strength in a given time window, an adaptive DTF (ADTF) method was developed to study the time-variant propagation of interictal spike (Wilke et al. 2008, 2011a). The ADTF method may be able to captures the temporal dynamics of the propagation and shed light in the inter-play among the networks in the genesis and propagation of GSWDs.

3.2 Methods

3.2.1 Subjects

3.2.1.1 Patients

Ten patients (mean age 33+/- 14, three female) with idiopathic generalized epilepsy syndromes were recruited from the Department of Neurology of the University of Minnesota, USA. The patients included in this study were selected based on the criteria that there were visible interictal GSWDs recorded from clinical EEG (with rare focal spikes only if GSWDs were frequent interictally), normal brain MRI (or normal brain CT in subjects 5 and 10), and a clinical diagnosis of IGE. All the patients were evaluated by board certified epileptologists. The patients' data are summarized in Table 1.

Written informed consent was obtained from all patients. The study has been approved by the Institutional Review Board of the University of Minnesota.

3.2.1.2 Healthy controls

Ten healthy volunteers (ages 21-31 years, 26±2.4 years, 6 males) participated in this study. All subjects had written consent according to a protocol approved by the Institutional Review Board of the University of Minnesota. A total of two functional MRI scans, each lasting for six minutes, were recorded from each subject while lying in the MR scanner quietly. Individual structural MRI was also collected.

3.2.2 Data recording and preprocessing

3.2.2.1 EEG recording

64-channel EEG caps were placed on patients' scalp. One electrode was placed on patients' back to record cardiac activity for noise removal purpose. Electrode impedances were brought below 20 kΩ. The EEG was amplified using MR-compatible amplifiers (BrainAmp MR 64 plus, BrainProducts, Germany) and recorded at 1000 Hz. Two sessions of EEG were recorded both inside and outside of the scanner experiment. During outside scanner recording, each patient was instructed to sit still and rest with eyes open. Outside-scanner recording lasted about 30 minutes. During inside scanner recording, each patient was asked to lie still and relax. Each recording lasted for 6 to 20 minutes. We recorded simultaneous EEG and fMRI for at least a total of 40 minutes for each patient. Experiment setup is illustrated in Fig. 3.1.

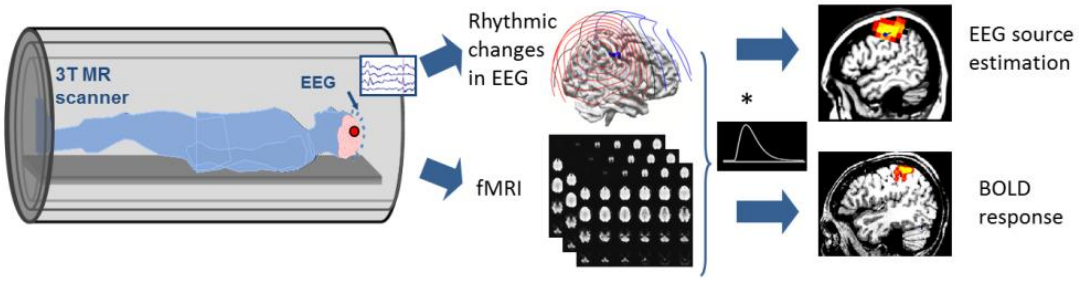

Figure. 3.1 Experiment setup for simultaneous EEG-fMRI

3.2.2.2 In-scanner EEG preprocessing

The MR gradient artifact was removed using a principal component analysis (PCA)-based optimal basis set (OBS) algorithm (Niazy et al. 2005). When detecting and removing the cardioballistic artifact (CBA), ECG signal from a single electrode on the subject's back, was used. The timing of each heartbeat artifact in this channel was determined using an R-peak detection algorithm adapted from Liu et al (Liu and He 2008; Liu et al. 2012). The final artifact correction procedure is based on a combination of ICA, OBS, and an information-theoretic rejection criterion (Liu et al. 2012). Briefly, the signal is decomposed into independent components, which are rejected if the mutual information between the component's time course and the CBA artifact is sufficiently high. The remaining components are then divided into epochs around each heartbeat and an optimal basis set is obtained across all epochs to fit and remove the artifacts. Detection of bad electrodes and data epochs was performed before CBA detection, and again after CBA correction. Electrodes were first re-referenced to a common average of electrodes connected to the same amplifier, and then to the combined average. Together with EEG data obtained from outside of MR scanner, the EEG signal was filtered and down-sampled to 256 Hz.

3.2.2.3 MRI recording and preprocessing

We used 3 T Siemens Magnetom Trio and Skyra MR scanners (Germany) with 16 channel head coil. The echo planar imaging (EPI) volumes underwent several preprocessing steps including three-dimensional (3-D) motion correction, slice scan time correction and linear trend removal. Then, the fMRI data were aligned with the anatomical MR images. All fMRI data were pre-processed for slice scan time correction, 3-D motion correction and temporal filtering. Matlab based toolbox SPM8 (Ashburner et al. 2010) was used for EEG-informed fMRI analysis. BrainVoyager QX software (Brain Innovation, Maastricht, Netherlands) was used for the seed-based connectivity analysis. Similar preprocessing steps were implemented in both software. All subject had individual structural MRI. In each set of structural MRI, there were 176 contiguous sagittal slices with 1 mm slice thickness (matrix size: 256 * 256; FOV: 256 mm * 256 mm; TR/TE=20 ms/3.3 ms). Whole-brain functional images with BOLD contrast were acquired using gradient echo planar imaging sequence (32 axial 3-mm thick interleaved slices with 0.3-mm gap; TR/TE = 2000 ms/30 ms; flip angle = 90°; matrix size: 64 * 64; FOV: 192 mm * 192 mm). Structural MRIs were normalized via alignment to the anterior-posterior commissural line and then transformation into Talairach space. FMRI data were spatially coregistered to the anatomical MRI.

3.2.3 ICA analysis of EEG

Independent Component Analysis (ICA) is a widely used data-driven technique to separate spatio-temporal signals into spatial components that are independent from each other through the selected time segment. Infomax ICA algorithm (Bell and Sejnowski

1995; Delorme and Makeig 2004) was used to decompose the spatio-temporal electrophysiological data into multiple independent components (ICs) using a time-by-space formulation. ICA was performed on EEG obtained both in- and out- of the scanner to identify GSWD related components for the subsequent EEG-informed fMRI analysis.

3.2.4 EEG-informed fMRI analysis

In the EEG-informed fMRI analysis, the important issue is the identification of GSWD timing based on EEG collected in the scanner. Although the artifact removal algorithm used was adequate in removing the majority of noise, it is still possible that some GSWDs were distorted by the residual noise and were rendered difficult to identify using visual inspection. Comparing to baseline activity, GSWDs are characterized by synchronized large amplitude discharges that present in multiple channels. Such large changes in activities are visible in both raw EEG and independent components related to the GSWD activities. Therefore, the temporal correlation between the two signals can be used in this study for the selection of GSWD components. This method is similar to what was previously described in seizure imaging (Yang et al. 2011b). Once an IC of interest was identified from out-scanner EEG, it can be used as a benchmark for the IC selection from in-scanner EEG. The detailed steps are as following.

For EEG obtained outside of the scanner, timing of each GSWD was marked by two trained epileptologists. Each ten second time window containing one or multiple GSWD(s) was selected and concatenated to form a GSWD-dense EEG. The cross correlation between the time course of each IC and the averaged time course of all of the EEG channels was computed (Yang et al. 2011b). The IC with the maximum absolute

cross correlation valued was selected as most representative of the GSWD activity. ICA was also performed on in-scanner EEG after artifact removal. The same IC selection method was applied to ICs from in-scanner EEG. The correlation between the spatial map of the selected IC from in-scanner EEG and that from out-scanner EEG was computed to ensure accuracy. Since both spatial maps from in- and out- of the scanner represent the same GSWD activities, the two should share similar spatial pattern. The timings of GSWD were then identified basing on the time course of the selected IC.

The regressor of the general linear model (GLM) was constructed using identified time points convolving with the canonical hemodynamic response function (HRF) (Jann et al. 2008; Marques et al. 2009). The final design matrix was composed of the regressor that represents GSWD activity and the 6 movement parameters as previously described (Marques et al. 2009). The group level analysis was performed using SPM8 (Ashburner et al. 2010). Individual T-statistic images were averaged using random-filed theory to correct for multiple comparison errors.

3.2.5 Seed-based ROI analysis

Seed-based ROI analysis was performed in BrainVoyager QX. FMRI data was filtered using a band-pass filter (0.009Hz~0.15 Hz) to reduce low frequency drift and high-frequency noise (Lowe et al. 1998; Seeley et al. 2007). The ROIs used in this study were informed by the EEG-informed fMRI results, with additional seeds added based on EEG waveform where the regions with the strongest GSWD discharges. Such areas include the left and right superior gyri and the middle frontal superior gyrus. A seed in the anterior nucleus of the thalamus was also included, as it was the stimulation target of

the SANTE trial (Fisher et al. 2010). Seeds were selected in the Brainvoyager software by referencing Talairach Client's (Lancaster et al. 1997, 2000) archive of Talairach labels and selecting a central coordinate for each seed. The time courses of both seed coordinates was regressed against all brain voxel time courses to create two brain maps of r-values for each fMRI scan. A p-value threshold less than 0.05 with correction via Bonferroni multiple comparisons was used to identify which voxels were significantly correlated with the seed location. All images were smoothed using a 2.0 mm full width at half maximum (FWHM) Gaussian kernel within BrainVoyager. The resulting voxels were clustered and counted to record a total volume of significantly correlated connectivity for each fMRI scan. At the group level, a second-level, random-effects analysis was performed. Connectivity maps were created with the same threshold levels and smoothing parameters described above. Only voxels with correlation less than the p-value of 0.05 corrected using the Bonferroni method, are reported as significant across subjects.

3.2.6 EEG source imaging

Generalized spike-and-wave discharges (GSWD) were selected from the interictal EEG of each patient via visual inspection. Source reconstruction was performed at the peak of each individual spike using three different inverse methods: dipole fitting (He et al. 1987; Homma et al. 1987) low resolution electromagnetic tomography (LORETA, Worrell et al., 2000; Pascual-Marqui et al., 1994) and standardized LORETA (sLORETA, Pascual-Marqui, R. D., 2004). CURRY7 software was used to perform the analysis. A 3-D source space within the brain volume was considered for the solution space of the inverse problem. A pre-defined fixed mesh was set within the brain volume to serve this

end. We employed the realistic geometry boundary element model (BEM) (He et al. 1987; Hamalainen and Sarvas 1989) head model with four surfaces (skin, outer skull, inner skull and cortex), separating three compartments, scalp, skull, and brain (Fuchs et al. 1998). Homogeneous electrical conductivity within each layer was assumed, with conductivity ratio between the skull and brain as 1:20. (Lai et al. 2005; Zhang et al. 2006b). To make results more accurate, we built subject-specific BEM models by segmenting the MR images from individual patients using CURRY7 software. In order to study the propagation pattern of the GSWD, source localization was performed at every 15 ms window for a representative GSWD.

3.2.7 Granger causality analysis

In each of the selected well-formed GSWDs, an epoch of approximately 400 ms before and 600 ms after the peak of the spike was extracted for the subsequent continuous source localization as described above. The distributed current density of the underlying neuronal activity was estimated to obtain the source waveform at each voxel. Time series of the source waveforms corresponding to three ROIs, i.e. left mediodorsal nucleus of the thalamus, right mediodorsal nucleus of the thalamus and the medial frontal cortex, were selected. These anatomical locations were chosen based on analysis previously described in the seed-based connectivity analysis. The three source waveforms were subjected to the DTF computation, similar to the procedure previously described (Ding et al. 2007; Lu et al. 2012b) Nonparametric permutation tests were conducted to test the significance of the obtained directional DTF values. 5000 times of phase shuffling of the original input signal were performed. The threshold was set at $p< 0.01$ to consider a DTF value as significant. As a step towards computing the overall DTF value between two time series,

the contribution of each frequency point, at 1 Hz increment, was computed automatically. Since different frequencies might carry information differently, DTF output at each frequency point was averaged across all spikes spanning form 1 to 125 Hz to show the contributions of different frequency bands. Additionally, adaptive DTF (ADTF, Wilke et al., 2011, 2008) was performed on individual spikes to study the time varying feature of the information flow at different time points of the spike-slow wave complex. This measure will aid in delineating the temporal changes of the connectivity strength and determining the dynamics in initiation and propagation of the GSWDs.

3.3 Results

Patient information is summarized in Table 3.1.

Pt ID	Sex	Age	Onset	Intericatal activities	Seizure types	AED
1	M	58	54	3 hz centrally predominant generalized spike and wave	Aphasia, SPS? GTC	Levetiracetam
2	M	28	15	Generalized spike and waves and poly spikes	GTC (IGE)	Lamotrigene
3	F	45	16	Generalized spike and waves, Left frontal temporal focal spikes.	GTC	Levetiracetam, Zonesamide, Lamotrigene
4	M	20	20	Generalized spike and wave, occasional left temporal spike and wave	GTC	Valproic acid
5	M	40	20	Generalized atypical spike-wave and polyspike-wave discharges with suggestion of left temporal onset and secondary synchrony.	GTC	Levetiracetam, Carbamazepine
6	F	21	15	Generalized anteriorly predominant 4-5 Hz spike wave discharges	GTC, Myoclonic seizures	Levetiracetam
7	M	62	12	Generalized spike and wave activities 2-4 hz	GTC, Myoclonic seizures	Carbamazepine, Valproic acid
8	M	21	19	Generalized spike and wave activities and polyspikes at 1-4 Hz	GTC	Valproic acid, Lamotrigene
9	M	24	15	Generalized atypical spike-wave activity at 4-5 hz	GTC	Levetiracetam, Lamotrigene, Felbamate
10	F	20	13	Generalized spike and waves	GTC, Myoclonic seizures	Levetiracetam

Table 3.1
PT, patient; GTC, generalized tonic-clonic seizure; IGE, idiopathic generalized epilepsy; AED, anti-epileptic drug

3.3.1 EEG-informed fMRI

Figure 3.1A shows in one patient, a segment of the EEG waveforms. Five out of fifty corresponding IC time courses are shown in Fig. 3.2B. Fig. 3.2C shows the histogram of the temporal cross-correlation coefficients between each IC and the global field potential. The red rectangle indicates the correlation coefficient of the selected IC. Spatial weight distribution of the selected components is shown in Fig. 3.2D. The cross correlation between the spatial weight of this IC and that of out-scanner EEG is 0.99. The cross correlation between the time course of the selected IC and the averaged time course

of all the EEG is 0.73. On a group level, the correlation between the spatial weight of the selected IC and that of out-scanner EEG is 0.99±0.01. The cross correlation between the time course of the selected IC and the mean global field potential is 0.71±0.05. Group-level EEG informed fMRI results are shown in Fig. 3.3 The highest activations were observed in anterior cingulate cortex, bilateral mediodorsal nuclei, left caudate nucleus, bilateral insula and bilateral sensorimotor areas.

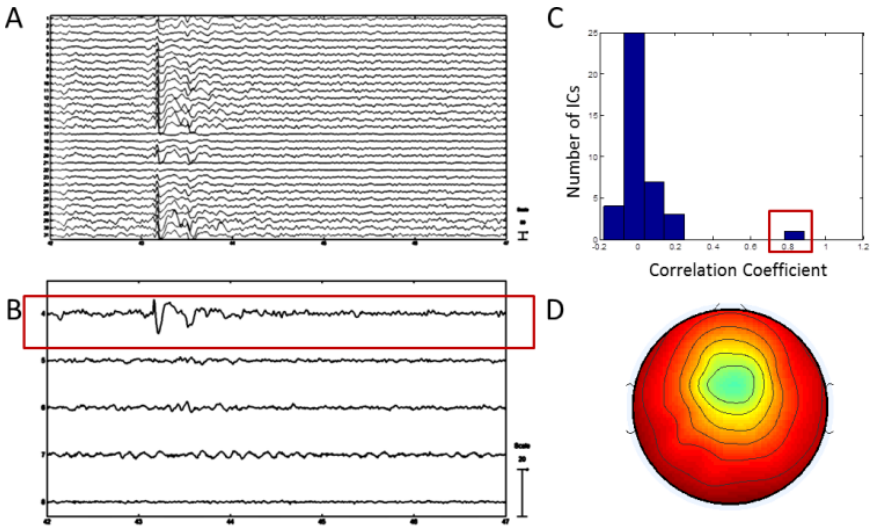

Figure. 3.2 Characteristics of the selected independent component (IC) to represent GSWDs

A. Waveform of an example segment of the EEG spike. B. Time courses of five ICs. Red rectangle indicates the time course of the selected IC. C. Distribution of the temporal correlation coefficients between all ICs and the global field potential. The red rectangle indicates the correlation coefficient of the selected IC. D. Topological map of the selected IC. The activity is centered at the medial frontal area.

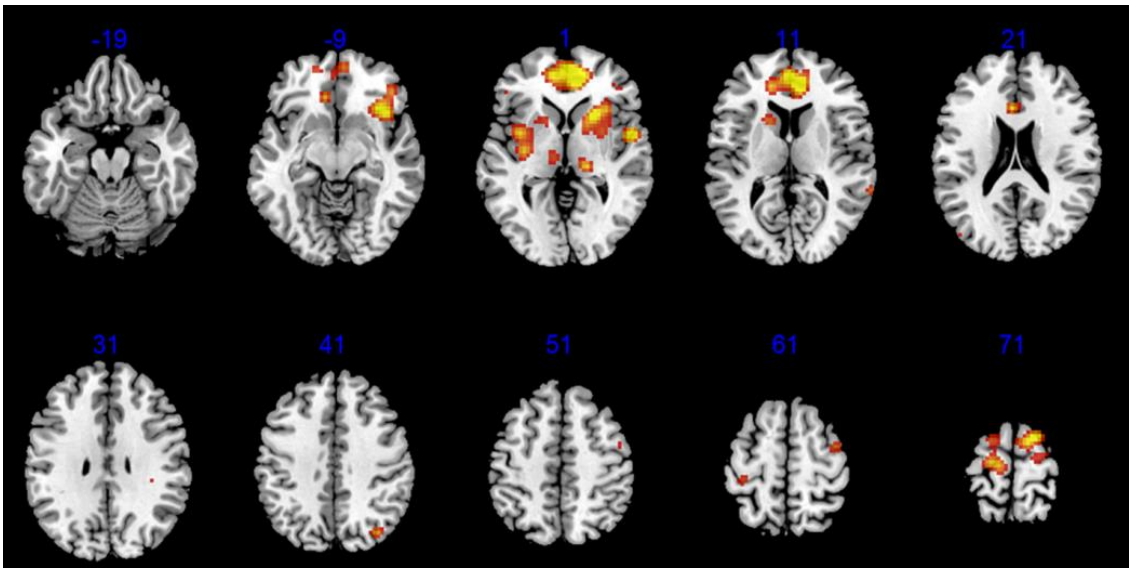

Figure. 3.3 Group results from EEG-informed fMRI using GLM

Z-axis is indicated in blue. Activities are found in medial frontal cortex, bilateral mediodorsal nuclei, caudate nuclei, bilateral insula and sensorimotor cortex.

3.3.2 Seed-based connectivity study

Seed-based connectivity analysis with seed in left, right superior gyrus, and the insula showed these regions are connected bilaterally (Fig. 3.4 A, B and E). But seeds in middle frontal superior gyrus, caudate nucleus and sensorimotor cortex are only temporally correlated to the close vicinities (Fig. 3.4 C, D and F).

Group average of seed-based analysis in ACC in both patients with IGE and healthy controls are shown in Fig. 3.5A. The total voxel counts among all activities that are correlated to the ACC were significantly different between patients with IGE and healthy controls ($p<0.05$ by nonparametric Wilcoxon Test, Fig. 3.5B). There was a linear positive trend between the degree of connectivity between ACC and the thalami, reflected by the number of voxels in the thalami that are correlated with the ACC time

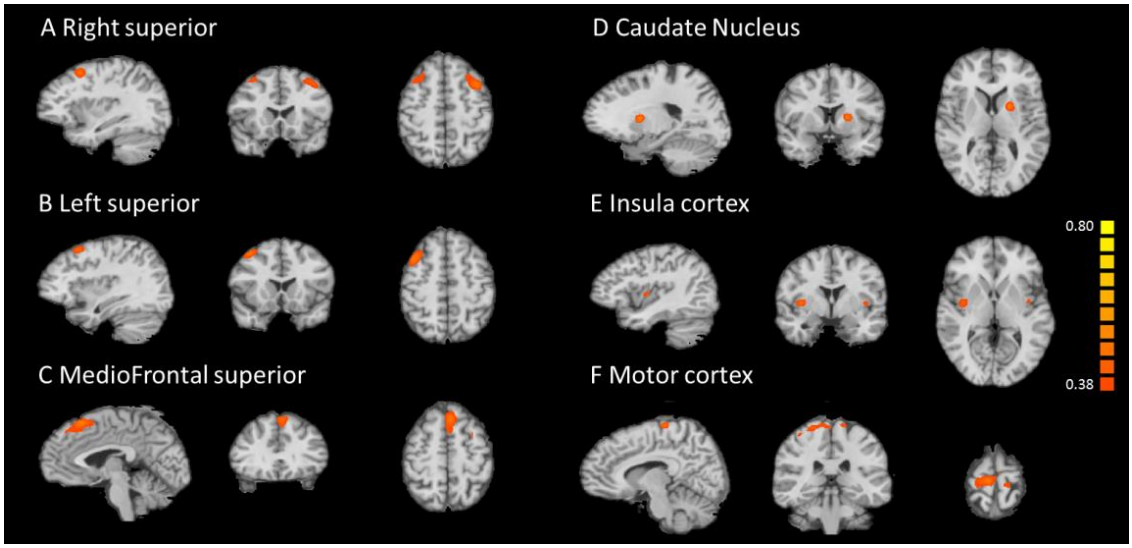

Figure. 3.4 Seed based analysis in the patient group

A. Seed in the right superior gyrus. B. Seed in the left superior gyrus. C. Seed in the mediofrontal superior gyrus. D. Seed in the right caudate nucleus. E. Seed in the left insula cortex. F. Seed in the left sensorimotor cortex.

course, and the frequency of GSWDs (Fig. 3.5C). Activities in the thalami that are correlated with ACC are located in the bilateral mediodorsal nuclei.

Group comparison of seed-based analysis in mediodorsal nuclei of the thalamus between patients with IGE and healthy controls are shown in Fig. 3.6A. The total voxel counts among all activities that are correlated to the mediodorsal nuclei were significantly different between patients with IGE and healthy controls ($p<0.05$, Fig. 3.6B). There was a similar linear trend between the degree of connectivity and the frequency of GSWDs (Fig. 3.6C) as seen previously in Fig. 3.5C.

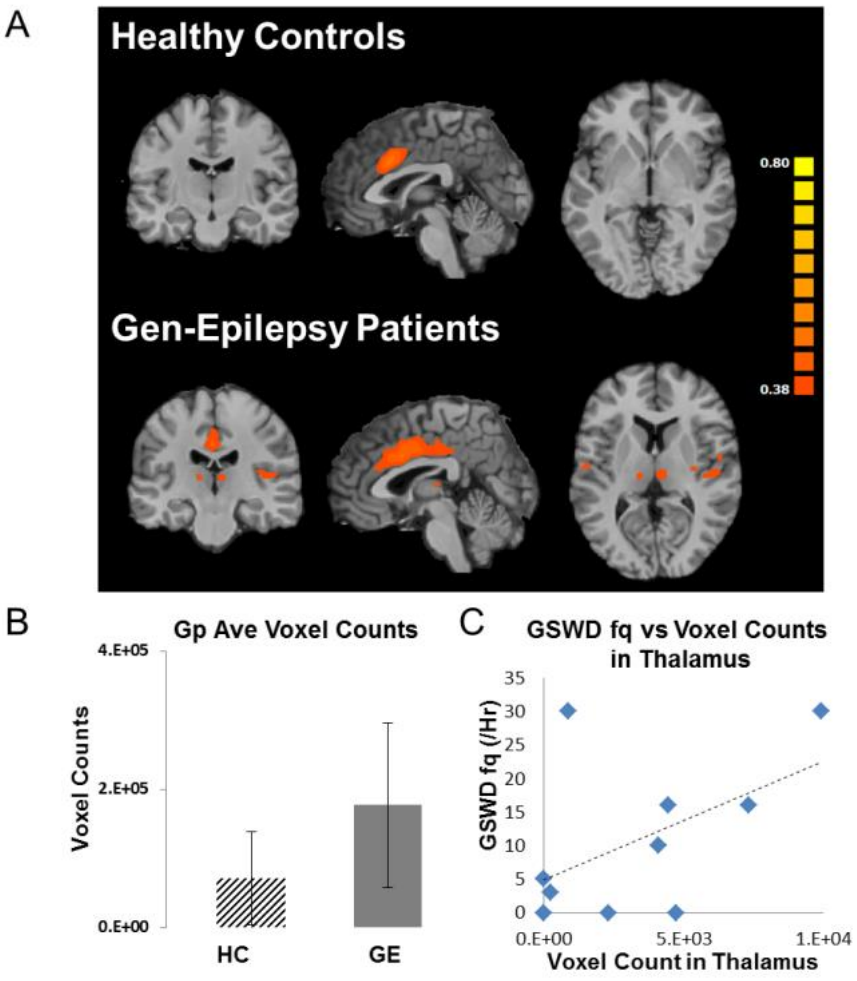

Figure. 3.5 Seed based analysis at medial frontal cortex

A. Seed-based connectivity analysis between healthy controls and patients with generalized epilepsy. Within the thalamus, voxels in the mediodorsal nuclei are related to the seed in the patients but not in controls. Seed location: medial frontal lobe. B. Voxel counts of the total number of voxels in the two groups that are correlated to the seed activity in medial frontal lobe. C. Scatter plot of voxel counts in the thalamus and the occurrence rate of GSWDs. Gp: group; HC: healthy control; GE: generalized epilepsy

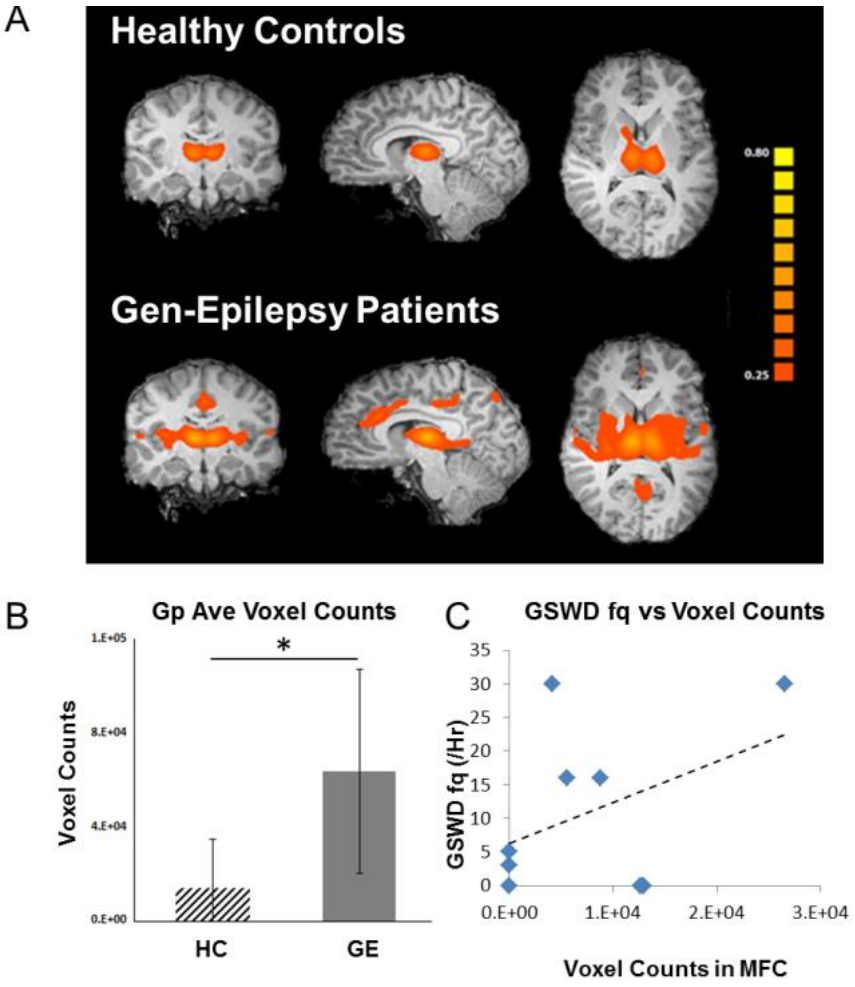

Figure. 3.6 Seed based analysis at dorsal medial thalamus

A. Seed-based connectivity analysis between healthy controls and patients with generalized epilepsy. Voxels in the medial frontal cortex are related to the seed in the patients but not in controls. Seed location: mediodorsal nuclei of the thalami. B. Voxel count of the total number of voxels in the two groups that are correlated to the seed activity in medial frontal lobe. C. Scatter plot of voxel counts in the medial frontal cortex and the rate of GSWDs.

3.3.3 Granger causality analysis

The connectivity patterns among the ROIs as measured by DTF are depicted in Figure 3.7A. The blue and two red dots represent the ACC area in the medial frontal cortex and the two mediodorsal nuclei respectively. The arrows between the dots indicate

the directionality of the flow, where the arrows are pointing from one area, the "source" toward another, the "sink". The strengths of the information flowing from the medial frontal cortex is only about half in strength as the reverse direction. Figure 3.7B quantitatively illustrates this difference in strengths in the two directions. The difference in strength between the two directions is statistically significant ($p<0.05$). The time varying feature of the causality as results of the ADTF analysis is shown in Fig. 3.7C. The blue and red traces show the group averaged temporal changes of the connectivity during GWSD. The black trace shows an averaged EEG waveform. The most significant exchange seems to occur as early as 50 ms before the peak of the spike, initiated by the thalamus. The averaged information flow spanning the entire frequency range (1-125Hz) is plotted in Fig. 3.6D by averaging over all spikes. There is a considerable variability but alpha and low gamma bands appear to have the most contribution.

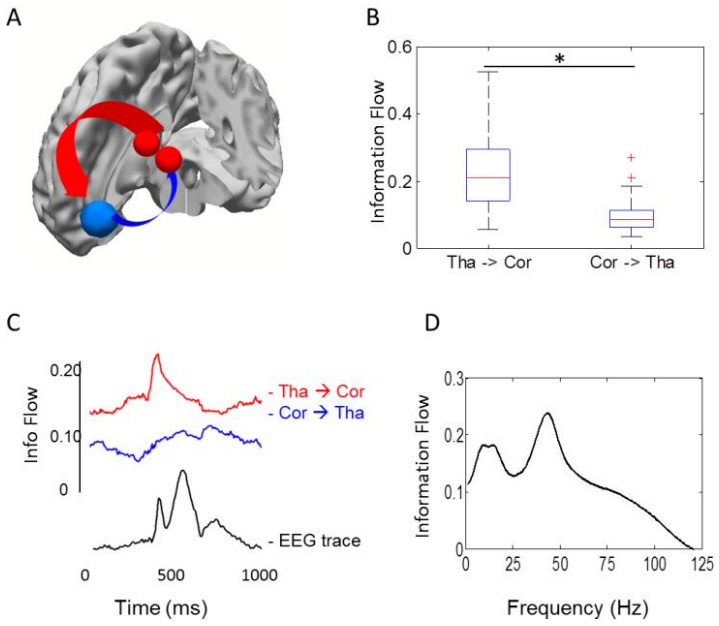

Figure. 3.7 Granger Causality Analysis

A. Illustration of the connectivity patterns among different ROIs. The arrows indicate the directions and relative strengths of information flows. Red: ACC; Blue: Mediodorsal Nuclei of Thalamus. B. Averaged information flow between thalamus nuclei and medial frontal cortex. Labels on the x-axis indicate the direction of flow. Cor: medial frontal cortex, Tha: mediodorsal nuclei. $p<0.05$. C. Results of ADTF analysis of one spike with the accompanying EEG waveform. D. Averaged frequency contribution in information flow (y-axis).

3.3.4 EEG source imaging

Group averaged EEG source localization results from seven patients are shown in Fig. 3.8. Five to thirty five spikes were collected and analyzed for EEG source localization in each patient. Current density distributions from all spikes of each patient were averaged to obtain the group averaged current density map. Group average results with the highest current density value located in the medial frontal region as shown in Fig. 3.8 A. Group ICA with concatenated spikes from all patients were also performed. The one component with the highest temporal correlation (0.89±0.03) with the global average time course was selected. Source localization on the selected IC spatial map was

performed to yield the current density distribution and dipole localization as shown in Fig. 3.8 B.

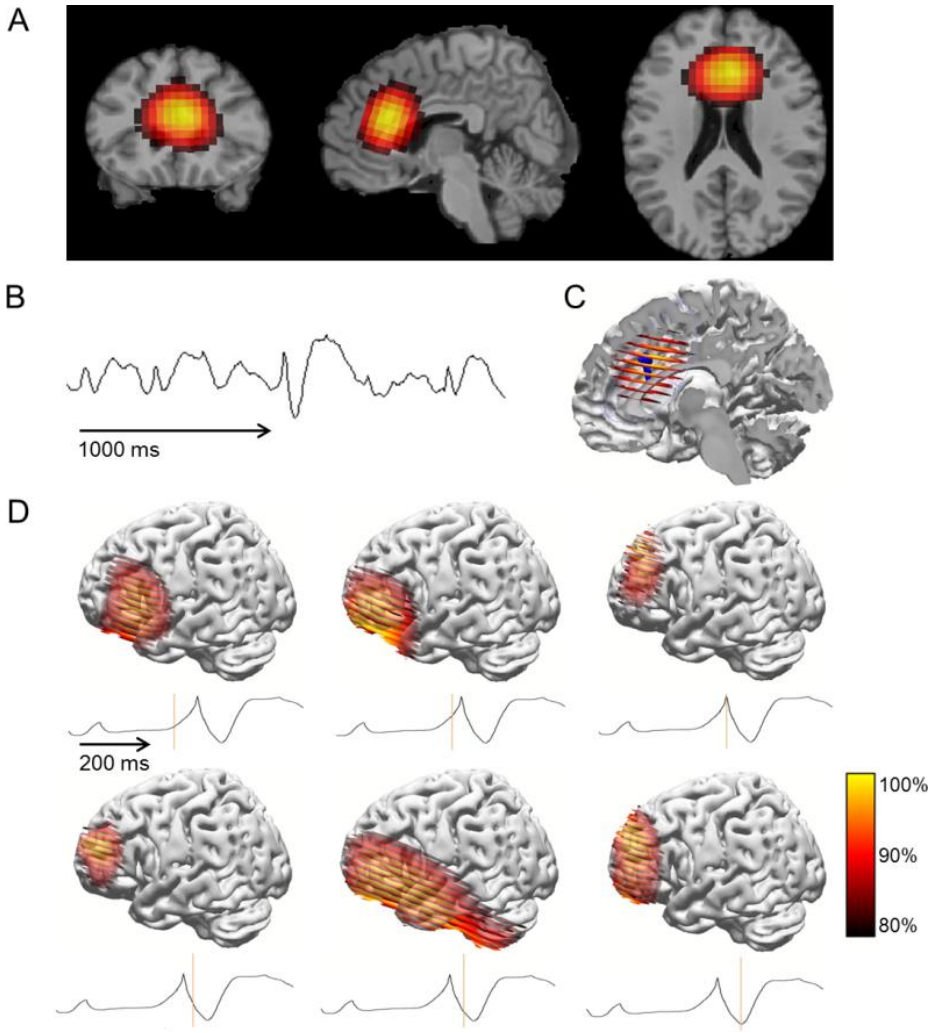

Figure. 3.8 EEG source localization results

A. Group average source localization results of all spikes. B. Time course of an example of independent component that has the highest correlation with the GSWD activity. C. Source localization using the spatial map of the independent component in B. D. Source localization at different time points of the GSWDs. Cortex was set at 50% transparency.

In order to study the propagation pattern of the GSWD, source localization was performed at every 15 ms window for one representative GSWD. Five intervals are

shown in Fig. 3.8 C. All the current density distributions were displayed at 80% of maximal intensity.

3.4 Discussion

3.4.1 Seed-based connectivity

Seed-based connectivity analysis was performed with a focus on two specific structures: anterior cingulate cortex in the medial frontal lobe and the mediodorsal nuclei in the thalamus. These two structures have been previously mentioned in works of IGE but not been specifically studied. Medial frontal cortex has been known to generate GSWDs on EEG. However it was also thought that the sources can be much more distributed only with center of gravity located near to the midline instead of having the actual focus in the medial frontal cortex. Using the seed-based connectivity analysis, we were able to specifically target this region and find its remote connections in the thalamus. This connection in IGE patients was more prominent compared with healthy controls.

Surprisingly, activity of just the mediodorsal nuclei, not the entire thalamus, is significantly correlated to the medial frontal lobe. Activation in mediodorsal nuclei has been previously seen anecdotally in a patient with history of generalized tonic-clonic seizure (Aghakhani 2004). In agreement with this finding, all ten patients in the present group have generalized tonic-clonic seizure. Another previous study by Moeller and colleague found that in 6 children patients with IGE (Moeller et al. 2008). They saw symmetrical medial thalamic activation, which is also in agreement with our observation. When we put the seed in the mediodorsal nuclei, its connectivity with the medial frontal cortex was replicated as expected in the IGE patients and again absent in healthy controls.

In fact, the specific cortical projections of mediodorsal nucleus to the frontal cortex has long been reported in rodents and monkeys (Leonard 1969; Krettek and Price 1977; Price and Drevets 2009). However, the different degree of connection between IGE patient group and the control group is unexpected. It may be explained that a strengthened connection between the two structures in each patient can make the spread of GSWDs and seizure activity progress quickly. Furthermore, the degrees of connectivity between these two structures also seem to be positively correlated, albeit not statistically significant, with the discharge rate of GSWDs. Interestingly, a similar fMRI connectivity study (Moeller et al. 2011) on IGE patients showed slight difference in connectivity for seed in the left mediodorsal nucleus of the thalamus compared with control. This is in partial agreement with our findings. The reason they did not see bithalamic correlation, or the connection between the thalamus and the cingulate cortex could be due to the fact that Moeller and colleagues selected the GSWD-free periods for their analysis, where we did not make such selection. Therefore, the effect they observed is weaker compared with ours.

However, bilateral superior gyri and the middle frontal superior gyrus, where strong GSWDs are observed from raw EEG, do not seem to be involved in a thalamocortical level network activity. Left and right superior gyri did show temporal correlation between the two. And bilateral insula showed such correlation as well.

Despite the preprocessing steps taken in reducing the effect of noise, the periphery of the cortex is still prone to movement artifacts in the fMRI recording. Therefore, seeds-based analysis in close vicinity of the periphery may contain erroneous

connection caused by noise rather than neurophysiological activities, as seen in Fig. 3.3E, coronal view.

3.4.2 Functions of ACC in GSWD

Devinsky et al. (Devinsky et al. 1995) reported that the anterior executive region formed by ACC around the rostrum of the corpus callosum has numerous projections into motor systems, which can be linked to the motor response such as uncontrolled jerking movement in tonic-clonic seizure. There is also evidence indicating correlation between the neural activity in the ACC and the degree of consciousness in patients with disorders of consciousness (DOC) (Qin et al. 2010). It was shown that slow delta wave activity was generated in the frontal area accompanying loss of consciousness post secondarily generalized partial seizures and complex partial seizures (Blumenfeld et al. 2009; Yang et al. 2012). This may partially explain another significant symptom of generalized epilepsy, such as the momentary loss of awareness during or post seizures.

3.4.3 Functions of mediodorsal nuclei

The central role of mediodorsal nuclei has been shown in the interconnected medial frontal cortico-striato-pallido-thalamic and amygdalo-striato-pallido-thalmic networks in multiple animal models ranging from rats to monkeys (Russchen et al. 1987; Ray and Price 1992, 1993; Price and Drevets 2009). The projections from mediodorsal nuclei to the amygdala and hippocampus form important circuitries that regulate emotions and memory (Price and Drevets 2009). Not surprisingly, depression and memory loss are some of the prominent comorbidities in patients with epilepsy (Nilsson et al. 1997; Hesdorffer et al. 2000). However, we did not see explicit change in the seed-

based functional connectivity between mediodorsal nuclei and amygdala or hippocampus. These changes may be too subtle or not time linked to GSWDs.

3.4.4 Predictive value of connectivity and epileptic activity

We initially hypothesized that the degree of global connectivity to the thalamus, which is defined as the total voxel counts within the brain that are correlated to the seed in the thalamus, may be indicative of the rate of occurrence of GSWDs. However, it appeared not to be the case. Instead, the number of voxels in the thalamus that are connected with the ACC alone appears to be positively correlated to the rate of GSWDs. Since ACC is probably where most of the GSWD signals are produced, the degree of connection between thalamus and ACC may be able to serve as a predictor of the level of activity observed on scalp. However, because of the limited recording period (up to 2.5 hours total) of EEG in each patient, the actual GSWD rate may deviate from the value we obtained. This limitation could influence the strength of the correlation between the connectivity and discharge rate.

3.4.5 Hemodynamic Response Function

In this study, we used canonical HRF to convolve with spike timing to construct regressor in the EEG-informed fMRI step. Canonical HRF is the most widely used function to represent the link between electrophysiological activity and the corresponding hemodynamic activity. However, there have been several recent studies pointing out that a canonical HRF may not be the best in presenting the actual function, as it may vary from person to person or may even change from location to location (Bai et al. 2010; LeVan et al. 2010). To mitigate this issue, we opted for canonical HRF basis functions

with time and dispersion derivatives which can model small differences in the latency and the duration of the peak response (Ashburner et al. 2010).

3.4.6 EEG source estimation

Additionally, we performed source reconstruction using sLORETA (Fig. 3.9). The source of GSWD is located in the medial frontal lobe, more specifically, at the anterior cingulate cortex (ACC). Consistent with our results, Rodin *et al.* (1994) used regional dipoles to localize source of generalized epilepsy activities, and the location of equivalent dipole was around the midline of baso-frontal area. This location suggested by EEG source localization appeared to be plausible, given the general predominance of EEG in fronto-central region (Montalenti et al. 2001; Aghakhani 2004). However a few recently published works suggested that potential spurious results may be yielded when applying source estimation methods to wide spread spike and wave discharges (Kobayashi et al. 2005; Daunizeau et al. 2010; Wennberg and Cheyne 2013). Wennberg and Cheyne (2013) reported that despite intracranial evidence of cortical origins, the scalp EEG during K-complex was localized to deep brain regions using either dipole localization or distributed current density source imaging. While this finding was based on a low-density scalp electrode configuration (27 electrodes), Wennberg and Cheyne's results suggested the possibility of mislocalization of widespread bi-hemispheric activities to mid-deep brain. In our study, since there were no intracranial recordings in the patients studied, we cannot preclude the possibility of mislocalization of EEG sources due to technical limitations in solving the EEG inverse problem. However, our high-density EEG recording- (64-channel) based source analysis did return source locations that are in agreement with the EEG-informed fMRI results, a technique (Gotman et al,

2005) that is not based on inverse solutions. The middle frontal region was implicated by both approaches in the group of patients we studied. Further investigations are needed with regard to source localizations of GSWD. One possible approach is to validate using intracranial recordings. Another approach is to integrate BOLD fMRI to improve the EEG source localization accuracy (Dale and Sereno 1993; Liu and He 2008; Daunizeau et al. 2009, 2010; Pittau et al. 2012).

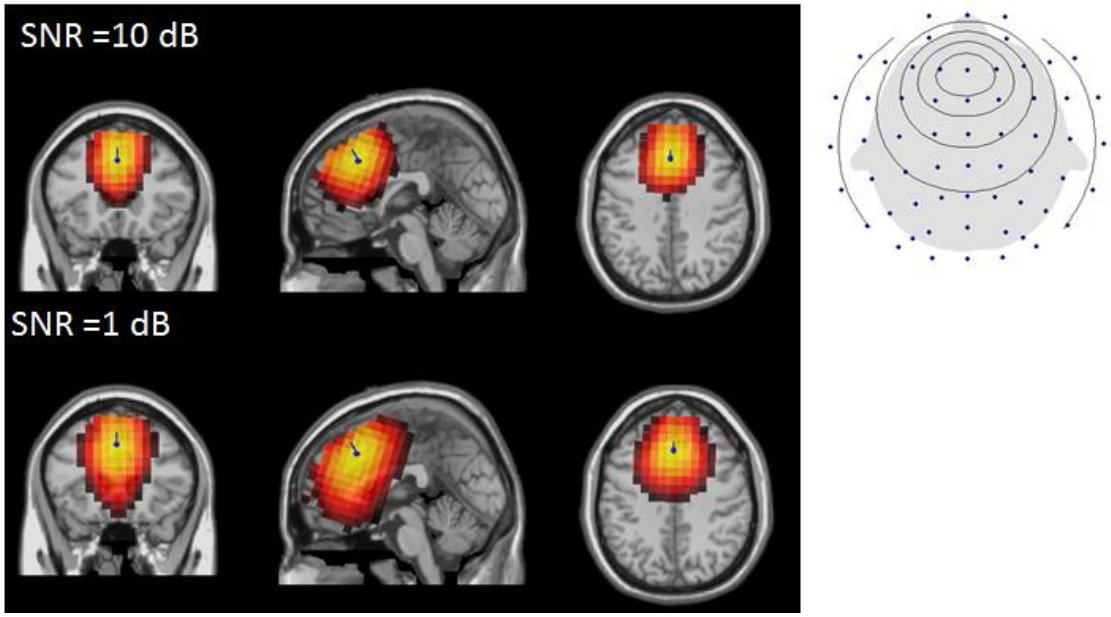

Figure. 3.9 Simulation of a single dipole deep on the midline

Blue Pin: location of simulated dipole; Orange-Red: Distributed source localization results using sLORETA; Right: scalp topography. Left: scalp topography

To test the validity of the EEG source localization result and rule out the possibility that the GSWDs are formed by a group of distributed sources near to the surface of the cortex, we conducted a simulation study. A single deep dipole and two surface dipoles were simulated separately. The arrangement of the dipoles were such that the resultant surface topography is similar to what we observed in the patient data.

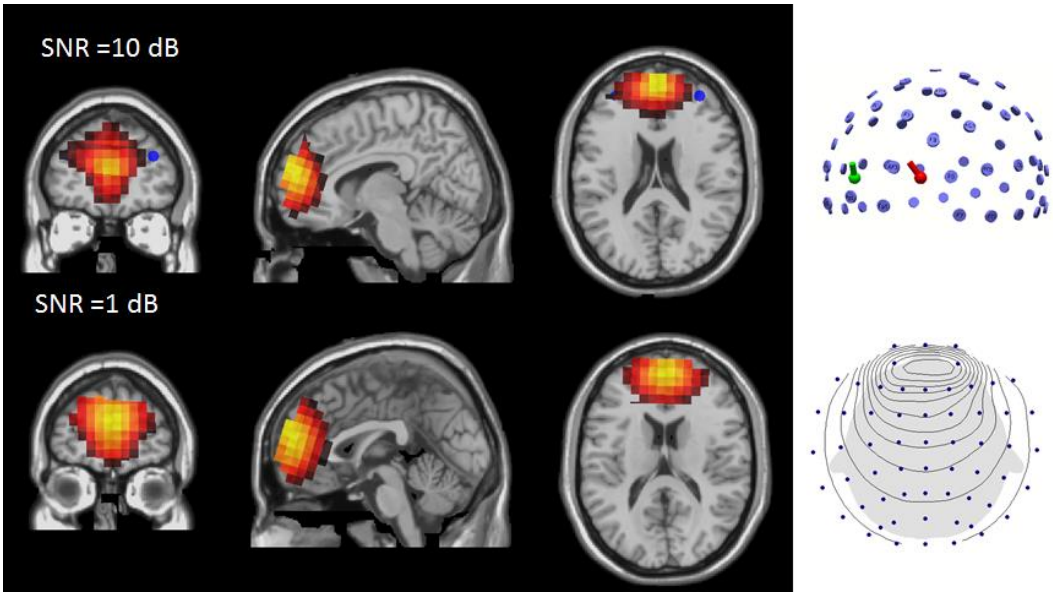

Figure. 3.10 Simulation of two superficial dipoles

A. Orange-Red: sLORETA source localization results, SNR=10 dB; B. Orange-Red: sLORETA source localization results, SNR=1 dB; C. Green and red pins: locations and orientations of the simulated dipoles; D. Simulated scalp topography

A deeper source near the thalamus was occasionally observed in some patients when performing source localization for several spikes. But such spikes occurred much less frequently compared to spikes in the medial frontal region. One possible explanation is that volume conduction can render deep brain sources hard to detect, even using LORETA, which is considered to have the least bias in the ability of correct localization in 3-D space (Pascual-Marqui et al. 1994; Worrell et al. 2000; Wang et al. 2011). Also, in order to acquire the highest signal-noise ratio (SNR), we only chose the peak of the spike to localize the source. During the onset-to-peak interval, the propagation of electrical activity from the original source may already be in progress.

3.4.7 Causality measures

DTF and ADTF of EEG activity have been previously applied in finding driving sources in epileptic activities (Ding et al., 2007; He et al., 2011b; Lin et al., 2009; Lu et al., 2012b). Our DTF findings showed a reciprocal causal relationship between the frontal cortex and the thalamus, where thalamus serves more as a driver. Specifically, mediodorsal nuclei of the thalamus have strong projection to the medial frontal cortex in the ACC area. The reverse projection is much weaker in comparison, approximately at half of the strength. The reciprocal directionality of Granger Causality is generally accepted (Ding and He 2013). This particular thalamocortical reciprocal relationship is also in agreement with the understanding of the interconnected thalamocortical circuitry in generating spontaneous spike-waves in IGE (Blumenfeld 2005). The crucial role of thalamus as part of the cortico-thalamo-cortical network, in sustaining seizures has been shown recently by Paz et al. in a rat model with optogenetics (Paz et al. 2013). Based on our ADTF finding (Fig. 4.6C), which shows the temporal evolution of the connectivity strength, thalamus seems to play the main role from the initiation to the propagation of the GSWDs. The main changes in the connectivity strength from the thalamus to the cortex occur as early as 50 ms before the start of the spike. It drops after the end of the slow wave discharge. This is in agreement with previously reported by Moeller et al (Moeller et al. 2008) using EEG-fMRI, information exchange among the thalamocortical precedes the peak of the spike GSWD, though the changes we observes occur only 50 milliseconds prior to the GSWD events, as opposed to the seconds level window observed by Moeller et al.

There are a few considerations regarding our approach that are worth noting. First, due to volume conduction effect, the time courses extracted using weighted

minimum norm type of inverse source estimation algorithms might be smeared. It could result in cross-talk and false interactions. Other source localization approaches, such as nulling, where nulling constraints are used to cancel signals from specific cortical locations beamforming (Cheung et al. 2010; Hui et al. 2010), might be able to decrease such effects. However, these methods are not without their own limitations. For example, nulling beamformer requires that we know the locations and extent of the sources to be canceled. Such information is often not available in practical applications. Another potential issue with our model is that we only studied the relationships between the medial frontal cortex and the mediodorsal nuclei of the thalamus. This is because these structures were implicated by our EEG informed fMRI and fMRI connectivity analysis. Other anatomical entities, such as other nuclei in the thalamus that were not included in the present study, or hippocampus, may potentially play a role in the network of generating GSWDs as well. Although seed-based connectivity analysis was performed on anterior nucleus and caudate nucleus of the thalamus (Supplement Fig. ure S1) (Fig. 4.3D), we did not see they were involved in network level activity. Clusters that are temporally correlated to the seeds were confined to the close vicinity of each seed itself. It is possible but unlikely, that the network activity was not in the form of temporal correlation and thus was not detected by our analysis method. Lastly, other causality measures, such as phase slope index (PSI) (Marzetti et al. 2008; Nolte et al. 2008), effective connectivity methods (DCM) (Friston 2009; Murta et al. 2012) and structural equation models (SEM) may provide additional insight. Since such methods all require prior anatomically motivated assumptions, this ACC-mediodorsal nuclei network may serve as a model framework.

A few other approaches using different recording systems may also help circumvent the volume conduction issue. For example, functional MRI, has excellent spatial resolution. But fMRI has limited temporal resolution due to hemodynamic effects. It was disputed whether fMRI can be a viable tool to study causal relationships, especially in the context of epilepsy research (David et al. 2008). It has been shown recently that by using a faster sampling rate, at the order of 250- 500ms repetition time (TR) it was possible to detect a multivariate network using Granger causality in several simulation studies (Deshpande et al. 2010a, 2010b; Rogers et al. 2010). Unfortunately, the TR used in our study ranged from 2000 ms to 2500 ms. It may be too slow to delineate meaningful causal information at a scale of milliseconds or lower. With advancement in MRI acquisition techniques using multiband approaches, TR can be shortened to 400ms (Feinberg et al. 2010; Uğurbil et al. 2013). At this rate, we may be able to extract causal information using fMRI time courses in future studies. Invasive recording using intracranial electrodes planted in the thalamus and cortex may provide the most direct measures of the neurophysiological activity and dynamic changes of GSWDs. Similar approach using Granger Causality and electrocorticalgraphy (ECoG) have been previously applied in seizure imaging with success (Wilke et al. 2008, 2010, 2011a).

By combining the complementary strengths of EEG and fMRI, we showed consistent results concerning the originating and propagation of GSWDs. EEG-informed fMRI revealed multiple brain regions that may be involved in GSWDs. By means of seed-based fMRI, we tested the specific network level activity and found temporal correlation between cortical and bithalamic BOLD activities. According to the Granger

Causality analysis the mediodorsal nuclei of the thalamus serve as the main driver from the initiation and throughout the propagation of the GSWDs. Once validated, this work may provide insight in understanding the enigmatic etiology of generalized epilepsy and offer guidance in treatments. Thalamus, especially the mediodorsal nuclei, may serve as potential targets for deep brain stimulation to treat patients with drug-resistant generalized epilepsy.

Chapter 4 Functional Neuroimaging of Thermal Pain Stimulation

4.1 Introduction

Chronic pain is one of the biggest medical burdens to our society, affecting 20% of the adult population (Breivik et al. 2006). The costs associated with management and treatment of chronic pain is estimated to be over $260 billion each year in the United States alone (Tracey and Mantyh 2007; Gaskin and Richard 2012). Functional imaging of neurological responses associated with pain processing is of vital importance to better understand the mechanisms of pain perception. The establishment of an objective way for measuring and quantifying pain is in great need for better pain management in patients suffering from chronic pain.

Electroencephalography (EEG) is a noninvasive monitoring technique, which is widely used to probe neurological disorders with high temporal resolution. Few attempts have been made to use EEG to map the active brain regions in pain patients (Bromm 2004; Stern et al. 2006). Myriad studies have been published on the correlation between evoked potential and transient painful stimuli using EEG. The strong relationship reported by these studies is promising in terms of the possibility of using objective measures to quantify acutely elicited pain (Bromm and Chen 1995; Chang et al. 2002b; Valeriani et al. 2002; Arendt-Nielsen and Chen 2003). There is a growing number of studies on the cortical responses to sustained painful stimulations that last several seconds or longer (Backonja et al. 1991; Chen and Rappelsberger 1994; Ferracuti et al. 1994; Chang et al. 2002b; Nir et al. 2012; Wager et al. 2013). As opposed to transient pain produced by laser evoked potential, contact heat evoked potential (CHEP) can

produce longer lasting pain sensation (Chen et al. 2001). Although tonic stimulation at the order of several seconds or minutes may not involve the same neurological responses as clinical chronic pain, it may trigger coping strategies (Huber et al. 2006; Nir et al. 2012), which can be different than that evoked by transient stimuli. Therefore, we chose to focus on subject's neural response to tonic painful stimulation in the present study.

Alpha rhythm has been reported extensively as being correlated to both transient and tonic noxious painful experiences (Chen and Rappelsberger 1994; Huber et al. 2006; Domnick et al. 2009; Nir et al. 2010). Other frequency bands including theta, beta and gamma activities have also been reported to be related to pain perception (Raij et al. 2004; Gross et al. 2007; Sarnthein and Jeanmonod 2008; Zhang et al. 2012). There has not been clear consensus on determining which rhythmic band has the most reliable correlation with different levels of elicited pain.

Additionally, to our knowledge, not many works have attempted to image the sources in the brain involved in pain at the cortical level using EEG (Moont et al. 2011), though a number of fMRI studies have been published (Boly et al. 2007; Ploner et al. 2010; Wager et al. 2013). Many studies based on both chronic pain and stimulated pain paradigm have shown several key cortical areas that are consistently responding to pain processing: anterior cingulate cortex (ACC), prefrontal cortex (PFC), insular cortex (IC), primary somatosensory cortex (S1) and secondary somatosensory cortex (S2) (Craig et al. 1996; Tracey and Mantyh 2007; Zhuo 2008; Wager et al. 2013). However, temporal dynamics among nodes of the network responsive to tonic painful stimuli have not yet been previously examined.

In order to study the temporal dynamics on a network level in response to different levels of stimuli, causal connectivity analysis can be performed. Directed connectivity measures based on the concept of Granger causality (Granger 1969) has been proposed (Kaminski and Blinowska 1991; Goebel et al. 2003; Babiloni et al. 2005) to discern the causal relationship among different time series. The directed transfer function (DTF) has been used to quantify the directionality and strength of the connectivity profile among different brain regions (Kaminski and Blinowska, 1991). DTF has been successfully applied in the field of epilepsy research to identify sources and sinks that may play important roles in generating seizures and other epileptic activities (Ding et al., 2007; Lu et al., 2012b; Wilke et al., 2010). The direction can be estimated, if by including the time series of the driver node (or source) in predicting the time series of the recipient node (or sink), it decreases the variance of the error. This intuitively means that the source plays an important role in determining the value of the sink and thus establishes the Granger causality between the nodes (Babiloni et al. 2005; He et al. 2011a, 2011b). This is on the basis that one node contains information about the future of the other while the reverse is not the case.

The goal of the present study was to investigate the effects of sustained thermal pain on the rhythmic brain activities of healthy subjects, measured by high-density 64-channel EEG. In this study, we systematically examine the dominant frequency ranges and brain regions that are most responsive to tonic painful stimuli, and investigate the neural correlates of the perceived pain using the scalp EEG. We further explored changes in temporal dynamics, at a network level, among major cortical regions that respond to painful stimuli and compared the connectivity patterns with and without stimulation and

at different temperatures.

4.2 Materials and Methods

4.2.1 Subjects

Twenty one (seven female, mean age $\pm$ SD: 25 $\pm$ 3.7) healthy volunteers were recruited for the experiment. None of the subjects had any neurological or psychiatric disease history. None of the subjects had any ongoing chronic pain. The study was approved by the Institutional Review Board of the University of Minnesota and was conducted according to the Declaration of Helsinki. The stimulus intensity applied was kept within each subject's individual tolerance level.

4.2.2 Experiment Paradigm

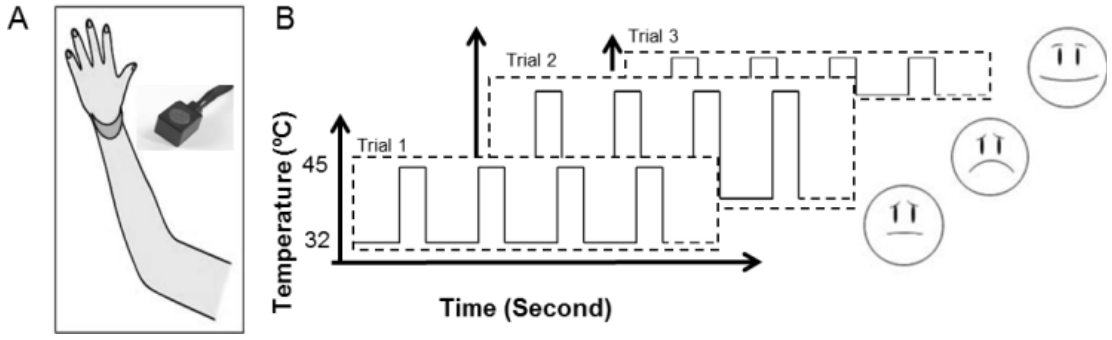

Figure. 4.1 Experiment Design

A. Stimulation setup. The thermode was placed at the dorsum of the subject's wrist. B. Stimulation paradigm. Thermal stimulation was applied continuously for 30 seconds in each trial with an inter-trial interval of 60 seconds for ten trials. Subjects were asked to describe and rate the pain received at the end of each 10-trial session.

Each subject experienced a sustained painful stimulus using a thermal stimulator (CHEPs, Medoc Ltd, Ramat Yishai, Israel) with the thermode placed on the dorsum of their left or right wrist (Fig. 4.1). The thermode delivers heat to the skin through direct contact. The size of the thermode is 2.7cm in diameter. Depending on individual

tolerance, the temperature of the thermode was kept at a range from 40 to 47 degrees Celsius for 30 seconds during the stimulus-on condition. Then the temperature dropped to and stayed at 32 °C for 60 seconds during the stimulus-off condition. Each recording session had 10 epochs of 30 seconds 'on' and 60 seconds 'off'. The thermode was moved slightly after each recording session to avoid sensitization or habituation on the same stimulation site. EEG signal was collected with a 64-channel system (Neuroscan Synamps 2, Compumedics Inc, Charlotte, USA).

4.2.3 Subjective Numerical Pain Ratings

Subjects were asked to rate the level of pain on a 0-10 scale, where 0 was defined as 'no pain' and 10 as 'the worst pain imaginable'. The rating was obtained at the end of each recording. The subjects were asked to describe if the pain sensation changed throughout the recording period.

4.2.4 Data Analysis

Raw EEG was recorded at 1000 Hz and down-sampled to 256 Hz, and the EEG data were then high-pass filtered at 1 Hz. 60Hz power line noise was removed with a notch filter. Continuous EEG data (25 seconds in length) were segmented from both the 30-second stimulation-on and stimulation-off portions in each epoch. The 25 second segments were selected during each trial and belonged to time intervals that started 4.5 seconds after the start of stimulation (for stimulation-on segments) or the end of it (for stimulation-off segments). This was done to avoid any artifacts caused by transient effects of rapid heating or cooling. Ten pairs of segmented data of stimulation-on and stimulation-off were concatenated sequentially in their original sequence.

The concatenated data were subsequently submitted to extended Infomax independent component analysis (ICA) (Delorme and Makeig 2004; Yang et al. 2011b, 2012). ICA is a widely used data-driven technique to separate spatio-temporal signals into spatial components that are independent from each other through the selected time segment. The temporal, spectral and spatial characteristics of the components were used to identify and remove artifacts in the electrophysiological recordings such as eye movements, muscle movements, etc. Components corresponding to eye blinks are noise-ridden and thus were excluded from further analysis (Makeig et al. 2002; Debener et al. 2005, 2006; Yang et al. 2011b, 2012). After removing artifacts, the remaining components were recombined to obtain noise-free electrophysiological signals.

4.2.5 Frequency analysis

Time-frequency information was obtained using spectrogram to capture the temporal changes in power in each of the following frequency bands: delta (1-4Hz), theta (4-8 Hz), alpha (8-13Hz), beta (13-30 Hz), Gamma (30-125 Hz) and total (1-125 Hz). Two different calculations of power change were performed in the study to quantify the power spectral changes in the EEG data and ICs. The first type of power change was based on the EEG sensor data and it was calculated from all recorded EEG channels. The second type of power change was calculated using all of the non-noisy ICs obtained from the previous ICA decomposition step. In order to compute global frequency changes, electrodes were grouped into four main regions: frontal, left parietal, right parietal and occipital regions (illustrated in Fig. 4.3B).

4.2.6 Canonical correlation analysis of frequency contribution

In order to find the region that is most tightly modulated by the stimulation, a goodness of fit (GOF) index was developed to quantify the correlation between the actual stimulation time course and the estimated stimulation time course, which was obtained by analyzing the power fluctuations of the spectrogram. Each step of this analysis is illustrated in Fig. 4.2. Spectral analysis was performed on the concatenated EEG of each electrode as described earlier (Fig. 4.2, Step 1). The time course of the power fluctuation in each rhythmic band was used to construct a matrix X to fit the stimulus time course Y (Fig. 4.2, Step 2). Mathematically, β was estimated such that:

$$Y = \vec{\beta} \times X + \varepsilon, \tag{4.1}$$

where X is the power matrix. Y is the time course of the stimulus which varies between 0 and 1, with 0 being the stimulation-off state and 1 being the stimulation-on state.

The weighting matrix $\vec{\beta}$, was computed using an inverse algorithm described in (Tadel et al. 2011). The modeled stimulus time course Y' was then obtained from

$$Y' = \vec{\beta} \times X, \tag{4.2}$$

at each electrode (Fig. 4.2, step 3). The correlation between the modeled time course Y' and the time course of the actual stimulus Y was calculated to quantify the goodness of fit (GOF). The goal was to find a set of β so that the GOF can be maximized. A high GOF index indicates that the stimulation paradigm can be more accurately perceived from the recorded EEG data, and thus locations with high GOF index are considered to be more responsive to the stimulus.

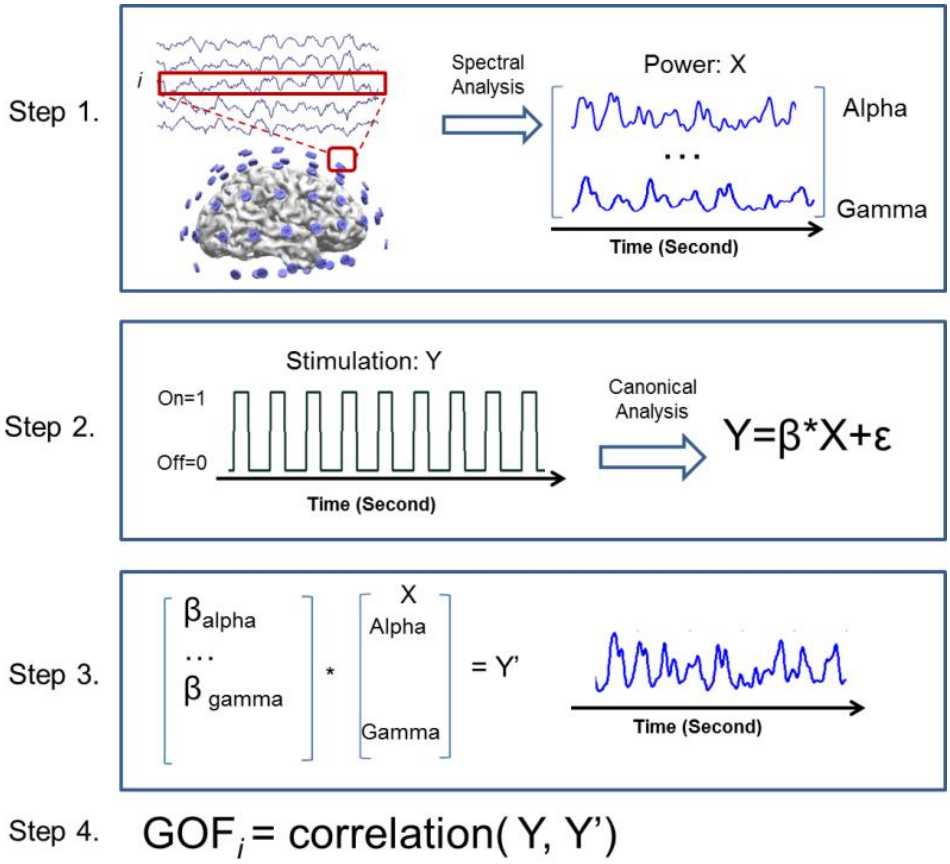

Figure. 4.2 Steps in GOF calculation

Step 1, the time course of each power band was computed at each electrode. Step 2, canonical analysis was performed to compute the weighting matrix β so that the correlation between resulted Y' (in Step 3) and stimulation time course Y was maximized. Step 3, calculate the expected stimulation time course Y' based on the β matrix obtained in Step 2. Step 4, compute the GOF value, or correlation, between Y' and Y at each electrode. GOF: goodness of fit.

4.2.7 Statistical analysis

Statistical analyses were performed using R statistical computing software (R Core Team 2013). Power changes in the alpha band were used as the fixed effect in relation to which the correlation between the temperature of stimulation and the pain scales reported by subjects were calculated. It is important to note that individual subjects were used as random effect in the analysis of variance (ANOVA), in order to account for subject-specific variability in stimulation responses.

4.2.8 Localization and imaging of pain from EEG

Brain sources representing activation due to pain were localized and imaged by solving the EEG inverse problem (He et al. 2011b; He and Ding 2013). The boundary element method (BEM) (He et al. 1987; Hamalainen and Sarvas 1989; Fuchs et al. 1998) was used to establish the relation between scalp potential and underlying neural activity. In the BEM model, the head volume conductor was separated into three conductive layers (the brain, the skull and the skin layers) with conductivity of 0.33 S/m, 0.0165 S/m and 0.33 S/m, respectively (Oostenveld and Oostendorp 2002; Lai et al. 2005; Zhang et al. 2006a). Low Resolution Electromagnetic Tomography (LORETA) (Pascual-Marqui et al., 1994) was used to calculate the three-dimensional current density source .

4.2.9 Granger Causality Analysis

In an effort to further investigate the network level effect of the painful stimulation, we performed Granger causality analysis on a time course extracted from five ROIs based on previous literature (Tracey and Mantyh 2007; Wager et al. 2013). The ROIs were in the anterior cingulate cortex (ACC), left primary sensory cortex, right primary sensory cortex, left insula cortex, and right insula cortex. An epoch of 5 seconds before and 5 seconds after the stimulation onset was extracted. Ten epochs of stimulation-on and 10 epochs of stimulation-off during each session were used for the subsequent source localization over the selected epochs, from each subject. Time series' of the source waveforms corresponding to the five ROIs were selected. It has been reported these anatomical locations are closely related to pain processing (Tracey and Mantyh 2007; Wager et al. 2013). The five time series were subjected to the DTF

computation, similar to the procedure previously described in the literature (Babiloni et al., 2005; Ding et al., 2007; He et al, 2011a; Kaminski and Blinowska, 1991; Lu et al., 2012; Wilke et al., 2010). Non-parametric permutation tests were conducted to test the significance of the obtained directional DTF values. The phase of the original input signals were shuffled 5000 times to form surrogate data. The threshold was set at $p< 0.01$ to consider a DTF value as significant for the permutation test (Wilke et al. 2008, 2011b). After the thresholding, a t-test was performed to examine whether there is any statistical difference between the stimulation-on and stimulation-off condition.

4.3 Results

4.3.1 Subjective Pain Rating

The correlation between subjective pain rating and the stimulation temperature was 0.67 for stimulating the left hand and 0.64 for stimulating the right hand. The majority of subjects reported that for each temperature the first one or two epochs were most painful and afterwards the intensity became stable. The numeric rating was based on the overall experience.

4.3.2 Global Power Change

To test if there are any pain induced changes at any specific location or in any specific frequency range, percentage power change in each frequency band was calculated at each electrode. The most severe pain that was experienced by each subject occurred when the highest temperatures were stimulated, although the actual tolerable highest temperatures differed among subjects. A group-averaged topoplot was computed when the stimulation was on the left wrist at the highest temperature (Fig. 4.3A).

Electrodes were grouped into four main regions: frontal, left parietal, right parietal and occipital regions (Fig. 4.3B). There was a global desynchronization observed in the lower frequency bands (1-13 Hz) in all four regions (Fig. 4.3C). Alpha band was observed to have the most pronounced reduction in power by the stimulation of pain sensation. Changes in power in beta and gamma bands are not statistically significant. The reduction in alpha power was mainly concentrated in the contralateral somatosensory area near electrode C4 (Fig. 4.3A). The maximal decrease in the alpha power was 27%.

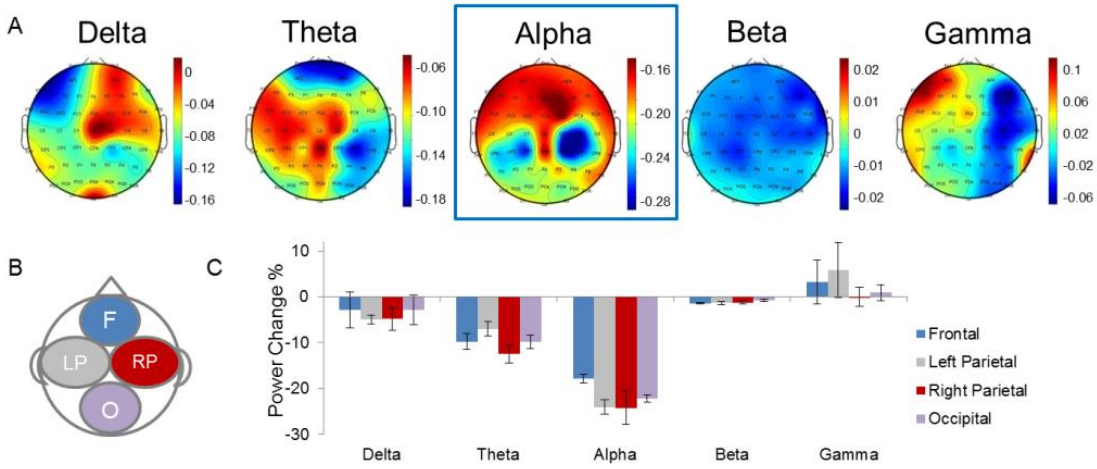

Figure. 4.3 Percentage power changes caused by presence of thermal stimulation

Group results of maximum temperature for each subject. Panel A shows the topoplot of changes in power in a particular frequency at each electrode. Global desynchronization was observed in the lower frequency band 1-30 Hz across all scalp electrodes. The colorbars are set to individual minimum and maximum value. The heights of the bars represent the maximum absolute change. Panel B shows how the electrodes were divided into four groups of frontal, left parietal, right parietal and occipital. Panel C shows the average changes in power in each frequency range in each brain region. Alpha band shows the most power deduction in the contralateral side of the somatosensory region.

4.3.3 Goodness of Fit

In order to quantify the relative contribution of the different frequency bands to the painful stimulation, we used a canonical correlation analysis to model stimulation with the time course of each frequency band as described in the method section. The

resulted group level goodness of fit (GOF) between actual stimulation and modeled expected stimulation is presented as a topoplot. Fig. 4.4A shows when stimulation was on the left, the highest correlation is in the contralateral somatosensory region on the right. Among all frequency bands, alpha has the most contribution. To allow group level

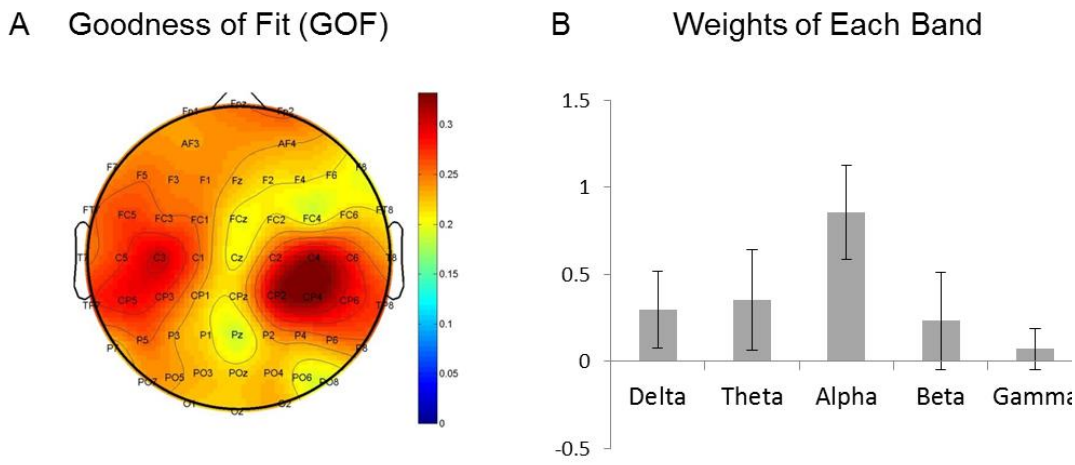

Figure. 4.4 Goodness of Fig results and frequency contributions

A. Goodness of Fit (GOF) for each electrode when the stimulation was on the left hand. Contralateral somatosensory region near C4 and CP4 have the maximum GOF value, namely 0.34. B. Group average of normalized β weighting of each power band at the maximum GOF region, i.e. CP4 electrode. Alpha band has the largest weight followed by theta and delta.

analysis, the weights for each frequency band were normalized by the total power of the weights, i.e. $\beta_\alpha^{normalized} = \frac{\beta_\alpha}{\sqrt{\beta_\alpha{}^2+\beta_\beta{}^2+\beta_\gamma{}^2+\beta_\delta{}^2+\beta_\theta{}^2}}$, where β_α, β_β, etc. are the calculated weights corresponding to frequency bands alpha, beta, etc. (Fig. 4B). Beta and theta bands have smaller contributions than alpha band. The weights of beta and theta band are 0.2 and 0.3 respectively.

4.3.4 EEG Correlation with Temperature and Subjective Pain Rating

Since alpha power at the sensorimotor region was found to be most responsive to

the thermal stimulation, it was further investigated if it had any predictive values for the thermal pain. A group level linear regression analysis was performed treating subjects as random effects to account for individual variance. When the stimulation was on the left, the reduction of alpha power in the contralateral region (electrodes C2, C4, CP2, CP4) was found to be correlated to the subjective pain rating (Fig. 4.5A). The changes were also shown to be correlated with the actual temperatures the subject was experiencing (Fig. 4.5B). However, there did not exist such a linear correlation relationship when the other frequency bands were regressed to the pain ratings (Fig. 4.5C) or stimulation temperature (Fig. 4.5D).

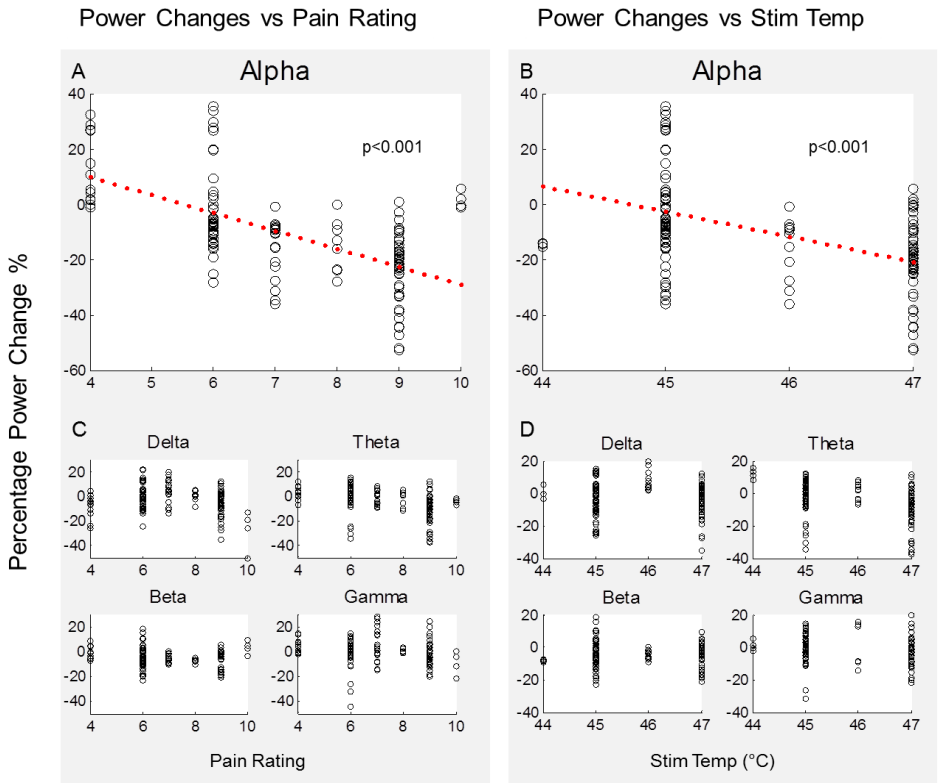

Figure. 4.5 Linear regression between percentage power changes and pain rating or stimulation intensity

A and B: alpha power changes versus subjective pain ratings and stimulation temperatures. Red dotted line is the fitted linear regression $p<0.001$. C and D: power changes in other frequency bands versus subjective pain ratings and stimulation temperatures. No statistically significant linear relationship was

4.3.5 Source Localization

Neurological sources that were most responsive to stimulation were estimated using the spatial map of selected ICs. We assigned numerical values to the binary stimulation condition so that when the stimulation is off, the value is 0, and when the stimulation is on, the value is 1. The selected component (Fig. 4.6A) showed a tight coupling between the power fluctuation and the stimulation status throughout the stimulation process. The correlation coefficient was -0.45 between the power change and the stimulation condition (Fig. 4.6B). EEG source localization results were also obtained by using both the distributed current density model and dipole source localization. Results from the two source imaging models were projected to the structural MRI of the Montreal Neurological institute (MNI) brain (Collins et al. 1994). Both the peak of the current density (orange gradient color) and the fitted single dipole (blue pin) (He et al. 1987; He and Musha 1992) were located at the right post-central gyrus in the parietal lobe (Fig. 4.6C). The threshold for cortical current density was set at 80% of the source maximum. Other alpha power-rich components were also checked for their response to the stimulation paradigm but were not found to be significantly correlated to the stimulation status (Fig. 4.6D and 4.6E).

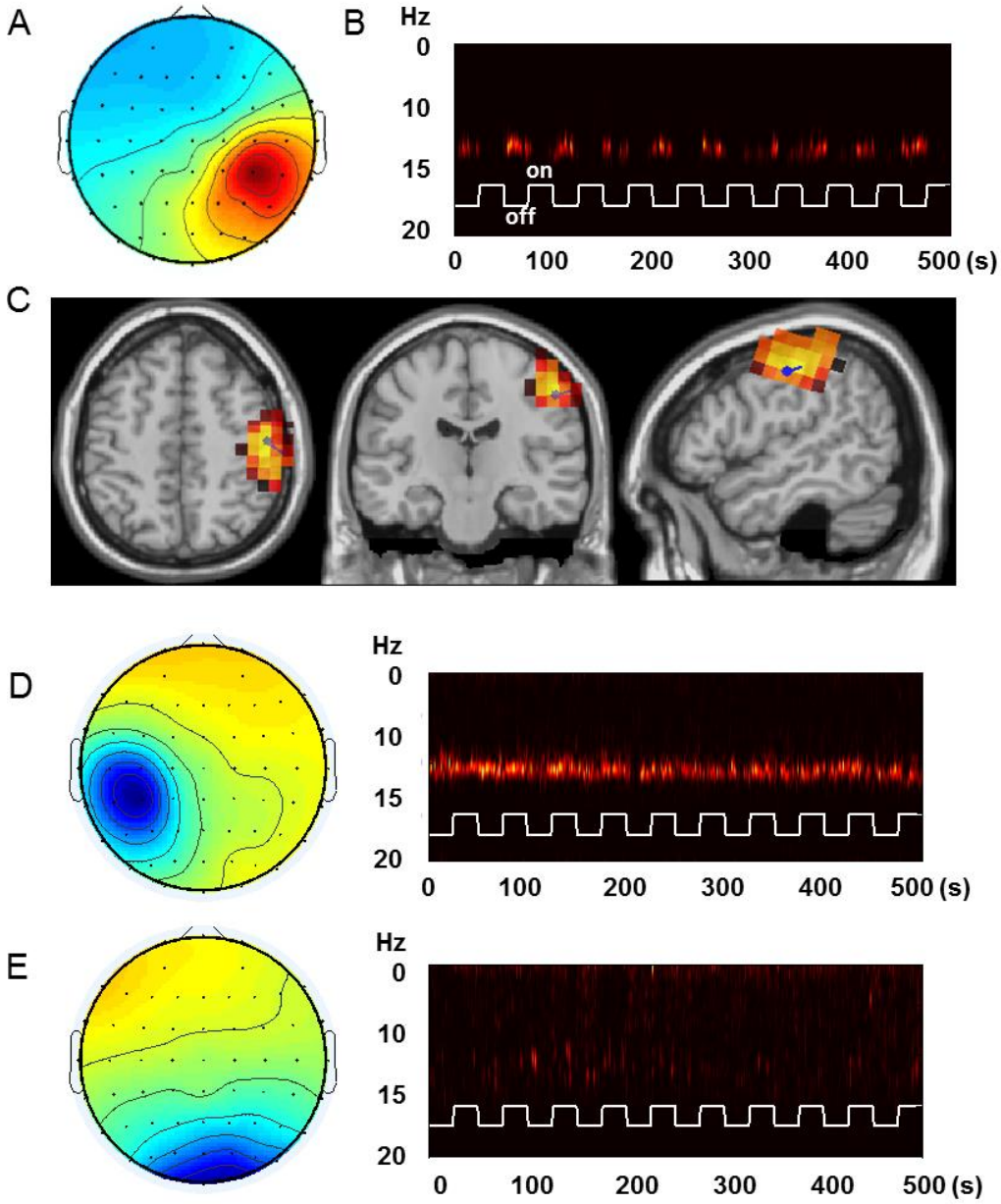

Figure 4.6 Inverse estimation of neurological sources that were related to pain perception

A and B. the topoplot and the spectral changes of the independent component that is most tightly modulated by stimulation status, i.e. 'on' versus 'off', indicated by the white line. The correlation value between the time course of the power changes and the stimulation is -0.6. C. localization results using both distributed cortical current density and dipole fitting. Both results were projected to the anatomical MR image of the MNI brain. Both the peak of the cortical current density (in orange gradient color) and the fitted single dipole (blue pin) were located at the SI area corresponds to contralateral wrist. The threshold for cortical current density was set at 80%. D and E: additional alpha-power dominant components on the ipsilateral side (D) and in the occipital lobe (E). The alpha power of these two components was not strongly coupled to the stimulation status.

4.3.6 Stimulation on the Right

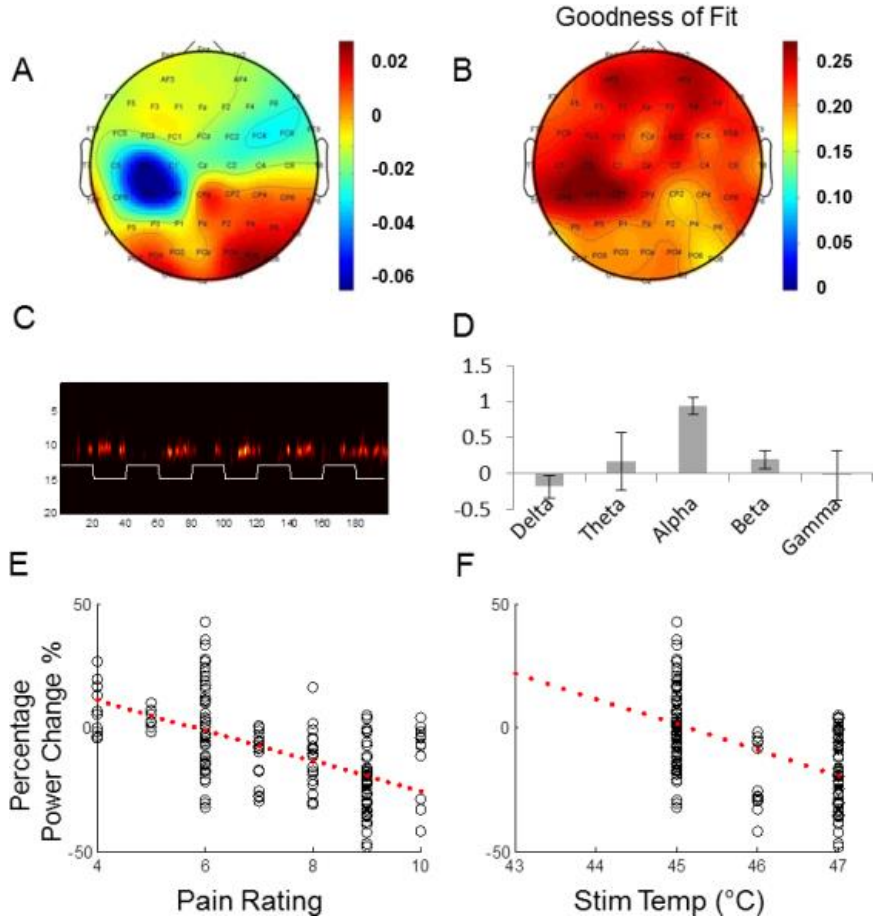

Figure. 4.7 Results when the stimulation was delivered on the right hand

A. alpha power in the left parietal region was most reduced by the presence of stimulus. B. the contralateral somatosensory region is most responsive to stimulation as quantified by GOF index. C. the independent component that was most coupled to the stimulation status. D. the relative contribution of each spectral band. Alpha band has the highest weight. E. and F. correlation between changes in alpha power and subjective pain rating as well as stimulation temperature.

To assess if there is any difference in perception on right vs left hand stimulation, we also conducted the same analysis when the stimulation was applied on the right hand (Fig. 4.7). The findings were similar but of the contralateral side, i.e., left hemisphere. Alpha power on the contralateral somatosensory region, in the left hemisphere, was found

to be most responsive to the thermal stimuli (Fig. 4.7A). The best fitted area was found to be in the left somatosensory region (Fig. 4.7B), reflected by the high GOF index near electrode C3 and CP3. An independent component was identified to be tightly modulated by the presence of painful stimulus, as seen in the time-frequency plot (Fig. 4.7C). Through the canonical correlation analysis, the alpha band appeared to have the highest weight in all power spectra in response to the stimulation (Fig. 4.7D). A linear relationship was found between changes in alpha power and the subjective pain ratings (Fig. 4.7E) and stimulation temperature (Fig. 4.7F). Overall, a big discrepancy between stimulation on the left- vs right-hand side was not observed.

4.3.7 Granger Causality Analysis

The strengths of Granger causality connectivity values were compared between stimulation-on versus stimulation-off at different temperatures (Fig. 4.8) when the stimulation was applied on the right side. At the highest stimulation temperature (Fig. 4.8, top row), where the pain ratings were between 7 and 10, there were more connectivity differences between the two stimulation statuses compared the temperatures that elicited no pain sensation (Fig. 4.8, bottom row). Stimulus induced changes in connectivity, in terms of both pattern and strength. At high degree as well as intermediate degree of pain (Fig. 4.8, middle row), there were connections originated from the contralateral side of the sensory region, i.e. left sensory cortex, and projected to other areas, most commonly to the contralateral (left) insula. Such difference in connectivity observed is the strongest in theta band, followed by alpha and delta, but not in the beta or gamma bands.

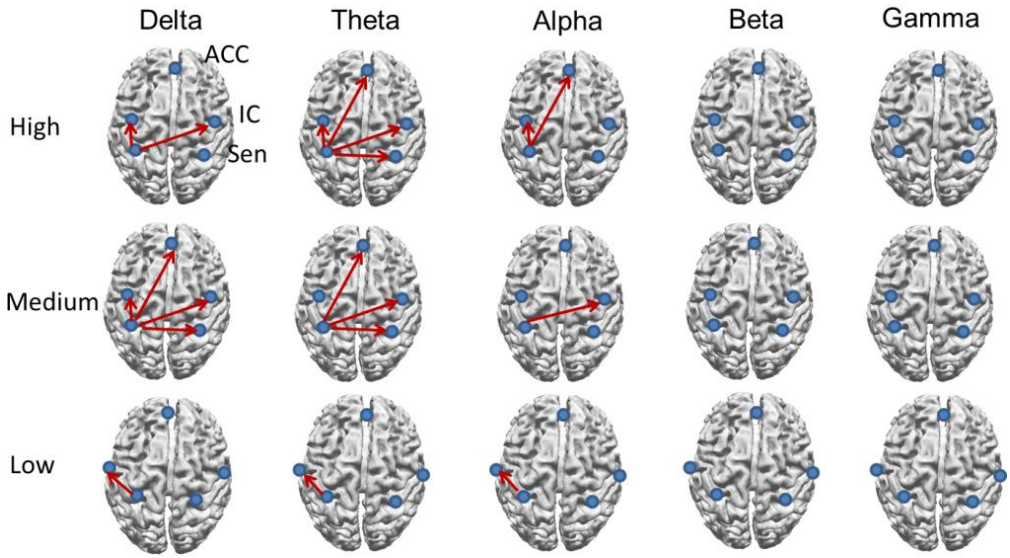

Figure. 4.8 Granger causality analysis at different temperatures with stimulation site on the right

Top row: Difference in connectivity between stimulation on versus stimulation off at the highest degree of pain for each subject. Middle row: Difference in connectivity between stimulation on versus stimulation off at the medium degree of pain. Bottom row: Difference in connectivity between stimulation on versus stimulation off at the lowest degree of pain.

4.4 Discussion

In this study, we have evaluated the temporal, spectral and spatial changes in the cortical activity of a group of healthy human subjects in response to tonic elicited pain. The major finding of our study was a decrease in lower frequency power throughout all of the electrodes over the scalp, most prominently in the alpha band when the pain index increased. The maximal decrease in alpha power was found to be concentrated in the contralateral somatosensory region. The degree of power decrease was correlated to both the stimulation temperature and the subjective pain rating.

Functional imaging of brain networks associated with pain processing is of vital importance to better understand the mechanisms of brain function in response to pain and consequently help develop new pain-relief therapies. Pain response in the brain is a

complex process which involves multiple cortical brain regions such as the primary and secondary somatosensory cortices, the anterior cingulated cortex, and the insular cortex (Bromm 2001). Recent advancement in neuroimaging techniques suggests the possibility of mapping the brain structure and networks that are involved in pain processing (Chen 2001; Ploner et al. 2002; Stern et al. 2006; Roberts et al. 2008). Our results reveal that contralateral somatosensory regions (SI, SII) were most responsive to painful stimuli. This is consistent with the consensus that SI and SII are part of the pain network (Zhuo 2008). These regions represent the sensory aspect of painful experience and can be thought of as pain gateways. Additionally EEG recordings in patients with high levels of chronic pain reveals increased activity in theta and low beta bands within the medial prefrontal cortex (mPFC), which includes the anterior cingulate cortex (ACC) and insula cortex (IC) (Stern et al. 2006). These regions are known to be related to the emotional aspect of pain processing (Craig et al. 1996; Tracey and Mantyh 2007; Zhuo 2008; Wager et al. 2013). Therefore, we extracted the temporal changes in these regions in the source space by solving for the underlying sources within the brain using the EEG inverse solution. By applying Granger causality analysis, we were able to observe that the presence of a painful stimulus can induce changes in the temporal dynamics among these nodes of the pain perception in contrast to the effects of innocuous stimulus (Fig. 4.8).

4.4.1 Comparison with transient stimulation findings

The evolution of pain using phased painful stimuli have been thoroughly examined and reported previously (Kakigi et al. 2005; Domnick et al. 2009; Huang et al. 2013). The specific finding of our work of contralateral somatosensory rhythm modulation was similar to studies with transient stimuli that lasted less than 40 ms, where

there is also a decrease in alpha power (Ploner et al. 2006; Hu et al. 2013). Cortical response to exogenous painful stimuli is well characterized using measures such as peak-to-peak amplitude of the N2-P2 evoked potential (Kakigi et al. 2005; Nir et al. 2012; Huang et al. 2013). In the present study, we focused on the neural responses to sustained rather than transient stimuli. This is because clinical pain often lasts longer than milliseconds, even for pain from acute injury (Huber et al. 2006; Nir et al. 2012). We recognized that tonic stimulations on the order of minutes are not able to completely capture the psychological impact of chronic pain on patients, but it could potentially shed some light in pain-coping strategies that may aid our understanding of chronic pain. For example, the difference in connectivity patterns at high levels of pain versus non-painful warmth sensations may provide insights in how information flows among brain regions from sensory input (somatosensory cortex) to the insula cortex and anterior cingulate cortex. Weights of different frequency bands can potentially be used in the future for estimating pain level, but further research on a larger population is warranted to improve specificity of the measure.

4.4.2 Comparison with other tonic stimulations

Reductions in alpha band were seen in previous works on tonic stimulation using both heat and cold-presser tests (Backonja et al. 1991; Chen and Rappelsberger 1994; Ferracuti et al. 1994; Chang et al. 2002b; Huber et al. 2006; Egsgaard et al. 2008; Nir et al. 2012). Among these, the research by Nir is one of the most recent works. Similar to our experimental setup, they collected continuous EEG while subjects received 5 minute long stimulations at three different temperatures. They reported that a decrease in lower alpha band (7-10 Hz) power in bilateral temporal regions is correlated with levels of pain

(Nir et al. 2012). In contrast to their approach, we did extensive EEG source localization and connectivity analysis to further explore the underlying mechanisms of tonic pain stimulation. Application of tonic chemical stimuli, such as injection of capsaicin or a hypertonic saline also showed a reduction in alpha power and an increase in beta power (Chang et al. 2004). We did not see an augmentation of beta activity but our finding that alpha frequency is the most responsive frequency to tonic painful stimuli is consistent with these findings previously reported.

4.4.3 Roles of different rhythmic bands

In this study, the frequency band that is the most correlated to the stimulations' presence is alpha. Theta and delta bands also showed decrease in power, but these changes were not statistically significant when tested for their predictive power in the different pain intensity analysis (Fig. 4.5). There have been mixed results in terms of theta power changes as a result of external painful stimulation. An increase of theta power in ipsilateral frontal electrodes during painfully cold stimulation has been reported by a few groups (Backonja et al. 1991; Ferracuti et al. 1994; Chang et al. 2002b). But at the same time, a diminished theta activity (Huber et al. 2006) has been reported, which is similar to our findings. Beta power changes seem to lack consensus as well (Backonja et al. 1991; Ferracuti et al. 1994; Chang et al. 2002b; Huber et al. 2006). We did not observe significant changes in the beta band using measures explored here.

In contrast with our findings, what we found about theta frequency's role in facilitating changes in connectivity has not been reported before. Several previous studies reported theta dominance in resting EEG/MEG in patients with neurogenic pain or other

pathologies, including tinnitus and Parkinson's disease versus control (Llinás et al. 1999; Sarnthein et al. 2003, 2006). It has been suggested that thalamocortical dysrhythmia may be the cause or result of several neurological symptoms (Llinás et al. 1999; Sarnthein et al. 2006). We did not study a pathological condition here. But in the current experimental setting, theta rhythm seems to be carrying the information from sensory input to ACC and insula. This may suggest the relationship between theta rhythm and pain perception.

4.4.4 Individual Differences

Data on individual personality or trait differences that may affect subjective differences in pain perception were not explicitly collected or correlated with pain rating in contrast to what was done by Coghill and colleagues (Coghill et al. 2003). Instead, individual differences were treated as random effects to account for some of the variances and to achieve a higher statistical power. This is because the primary goal of this study was to find a set of metrics that most commonly occur in the general population. The importance of inter-subject variance should be emphasized in the effort of objectively quantifying pain, since pain is a subjective experience. A set of customized parameters such as propensity to anxiety, history of pain or trauma, general pain tolerance or sensitivity may be taken into account in future studies of this type for more objective measures of pain.

4.4.5 Salient pain

One debate about neural imaging of pain, as a result of external stimuli, is whether the phenomena observed are results of pain or merely saliency. This work is not

an attempt to separate the two. In fact, we do not feel the need to separate the two. Modulation of spontaneous rhythmic activities by external stimulation has been previously reported in studies of non-noxious stimuli (Pfurtscheller and Lopes da Silva 1999; Yuan et al. 2010). A decrease in alpha power was previously found as a cortical response in other cognitive tasks such as reading sentences (Luo et al. 2010), complex decision making (Davis et al. 2011), object recognition (Freunberger et al. 2008) and arithmetic tasks (Miwakeichi et al. 2004). Anticipatory alpha rhythms that preceded the actual stimulus was found to be reduced in a painful CO_2 laser stimulation (Babiloni et al. 2006, 2008). Our results showed that pain stimuli suppressed the contralateral alpha rhythm, which is consistent with these previous findings.

It is true that pain may not be the exclusive cause of such rhythmic modulation. But previous studies with similar tonic thermal stimulation settings investigated this issue with competing auditory stimulations (Chang et al. 2002a; Huber et al. 2006) or with manipulation of attention (Huber et al. 2006). Chang's group found that unpleasant auditory stimulation and intramuscular injection of hypertonic saline induced similar degrees of arousal and unpleasantness. However, muscle pain induced a significant decrease of alpha activity compared to the baseline, but aversive auditory stimulation did not produce any significant changes in alpha activity compared to baseline as measured by EEG. Huber's work further tested the specificity of EEG in measuring human pain by directing subjects' attention to or away from the pain they were experiencing and found there was no significant difference in EEG activity between different levels of attention. These results indicate that specific EEG patterns are associated with human pain processing. However, their findings, where stimulation temperature was only provoking

warmth sensation but not pain (at 41.1 ±1.6°C), were different from ours. They found no difference in EEG changes between tonic heat pain as opposed to tonic non-painful heat stimulation, whereas we saw a linear trend between stimulation intensity and EEG decrease in delta, theta and, most predominantly, alpha band. This is in agreement with the fMRI findings in the second study by Wager's group recently published (Wager et al. 2013). They found that the fMRI responses increased with subjective pain rating on a continuum across painful and non-painful events.

The anatomical areas involved in pain and saliency frequently overlap specifically in the dorsal ACC (dACC) and fronto-insula (FI) (Seeley et al. 2007; Sridharan et al. 2008). Furthermore, salient responses often change with stimulation intensity just as elicited pain does. But according to recent works by Wager and colleagues, by using the similar stimulation paradigm, they were able to find pain-specific fMRI markers that include the ROIs in our connectivity analysis, including the somatosensory cortex, insula and ACC, among other regions (Wager et al. 2013).

4.4.6 Study limitations

As the connectivity analysis was based on the source space time course from EEG inverse estimations, there are a few cautionary notes that are worth mentioning. First of all, areas such as the periaqueductal gray matter, amygdala, hypothalamus and cerebellum were not included in the present study. We focused on the relationships among the anterior cingulate cortex, bilateral insula and the bilateral somatosensory cortex, because these structures were reported most widely as being involved in pain processing in the literature (Tracey and Mantyh 2007; Zhuo 2008; Wager et al. 2013).

Another note on our model is that because of the volume conduction effect, there may be a potential of cross-talk among closely located nodes of the brain volume which causes the EEG signal arising from different locations to smear and mix together which can lead to spurious connectivity. A few methods, including nulling beamforming (Cheung et al. 2010; Hui et al. 2010), have been developed to address this issue. However, based on our results, this may seem unlikely because the nodes selected are relatively far apart. Lastly, other causality measures, such as using phase slope of the cross-spectra (Nolte et al. 2008), effective connectivity methods (DCM) (Friston 2009; Murta et al. 2012) and structural equation models (SEM) were not explored here. But findings here may be useful in formulating the models in DCM in the future.

Granger causality measures reported here can be implemented in functional MRI, as it has excellent spatial resolution. However, fMRI has limited temporal resolution due to hemodynamic effects; but it has been shown recently that by using a faster sampling rate, on the order of 250- 500 ms repetition time (TR), it is possible to detect a multivariate network using Granger causality in several simulation studies (Deshpande et al. 2010a, 2010b; Rogers et al. 2010). With advancement in MRI acquisition techniques using multiband approaches, TR can be shortened to 400ms (Feinberg et al. 2010; Uğurbil et al. 2013). At this rate, we may be able to extract causal information using fMRI time courses in future studies.

In summary, we found that the spontaneous rhythms in all frequency bands except gamma band were suppressed globally at the presence of tonic painful thermal stimulation. The greatest changes were observed in the alpha power on the contralateral side of the somatosensory region. The degree of suppression may reflect the levels of

applied painful stimulation. There was also increased connectivity among major brain regions responsive to pain that were revealed through causality analysis. Although the current finding is based on the study of sustained pain from external stimuli in healthy subjects, it would help broaden our understanding of cortical response to patients with chronic pain.

Chapter 5 Functional Neuroimaging of Pain in Sickle Cell Disease

5.1 Introduction

Sickle cell disease (SCD) is an inherited blood disorder that results in chronic pain and a decrease of life expectancy. This disorder causes red blood cells (RBC) to deform into sickled shapes that cause recurrent ischemia-reperfusion injury which leads to organ damage, pain, and impaired oxygenation (Rees et al. 2010) There are many complications associated with SCD, but the most common reason for hospitalization is pain. Pain for SCD is unique because it can start in infancy and progressively increase throughout the life of the patient, causing chronic pain. Frequent episodes of acute pain, where patients feel intense pain that can last for days, can also occur due to vasoocclusive crises caused by venule occlusion from sickled RBC (Platt et al. 1991). Both neuropathic pain and nociceptive chronic pain pathways have been implicated in SCD (Wang et al. 2010b).One major challenge in the treatment of pain from sickle cell disease (SCD) is the current lack of an objective measure of pain. Imaging methods, such as EEG and fMRI, can be utilized in order to better understand the mechanisms of pain in SCD and offer the potential to develop objective methods to assess pain.

Functional brain imaging methods have found that during resting state, or the absence of a task, that the brain is active and forms specific patterns of activity called resting state networks (RSN). Certain RSN have been identified using functional magnetic resonance imaging (fMRI), including the default mode network (DMN), salience, sensory motor, and attention (Farmer et al. 2012). The DMN is active during

wakeful rest and may be related to introspection and self-referential thought (Raichle et al. 2001; Greicius et al. 2004). The regions of the DMN include the lateral and inferior parietal lobes, medial prefrontal cortex (mPFC), and posterior cingulate cortex (PCC). DMN is a prevalent network dynamic that appears in the absence of overt behavior and is thought to be responsible for a host of visceral mental activities. Altered DMN activity was first observed in Alzheimer's disease (Greicius et al. 2004) and more recently in a number of other neurological disorders, including epilepsy (Gotman et al. 2005) and chronic pain (Buckner et al. 2005, 2008). Temporomandibular disorder chronic pain patients have exhibited hyper-connectivity between the mPFC and other DMN regions due to pain rumination (Kucyi et al. 2013, 2014). The functional connectivity between the DMN and the insular cortex (IC) is increased for chronic lower back pain patients (Kong et al. 2010; Loggia et al. 2013). These abnormalities in functional connectivity suggest that chronic pain conditions alter resting state activity. In this work, we hypothesize that in SCD patients, the default-mode-network (DMN) is less active in comparison to healthy subjects. We hypothesize that the level of DMN in patients with SCD is altered by the condition and may serve as a potential biomarker for correlating with pain in these patients.

5.2 Method

5.2.1 Healthy subjects

We recorded 17 healthy volunteers (11 of them were female. Mean age was 28.6 ± 10.6 years). All subjects met the MR safety criteria and gave their written informed consent. None of the subject reported any previous neurological or psychiatric disorder,

psychoactive medication or history of drug abuse. The study was approved by the Institutional Review Boards (IRB) of the University of Minnesota respectively.

5.2.2 SCD patients

14 patients with SCD (8 of them were female. Mean age was 24.9 ± 6.7 years) were recruited by physicians at Fair View Hospital and Minnesota Children's Hospital. They participated in this study with written consent according to a protocol approved by the Institutional Review Board of the University of Minnesota.

5.2.3 MRI recording

We used 3 T Siemens Magnetom Trio scanner (Germany) with 16 channel head coil. Each subject was instructed to lie quietly in the scanner for two scans, each lasting for six minutes. Additionally, individual anatomical MRI data were collected which were consisted of 176 contiguous sagittal slices with 1 mm slice thickness (matrix size: 256 * 256; FOV: 256 mm * 256 mm; TR/TE=20 ms/3.3 ms) on a 3T MRI system (Siemens Trio, Siemens, Erlangen, Germany). Whole-brain functional images with BOLD contrast were acquired using gradient echo planar imaging sequence (32 axial 3-mm thick interleaved slices with 0.3-mm gap; TR/TE = 2000 ms/30 ms; flip angle = 90°; matrix size: 64 * 64; FOV: 192 mm * 192 mm).

5.2.4 FMRI preprocessing

All fMRI data were pre-processed for slice scan time correction, 3-D motion correction and temporal filtering using both BrainVoyager QX software (Brain Innovation, Maastricht, Netherlands) and Matlab (SPM8, Ashburner 2010). All brains

were aligned to the anterior-posterior commissural line and normalized by transformation into Talarirach space. FMRI data were then spatially coregistered to the structural MRI.

5.2.5 Seed based analysis

A seed region of interest (ROI) was selected by referencing Talairach Client's (Lancaster et al., 2000, 1997) archive of Talairach labels. Seeds were placed in central locations of the four main default mode nodes: medial prefrontal cortex, left- /right-lateral and inferior cortex, and the posterior cingulate cortex. Seeds were also placed in selected areas corresponds to pain processing of insula cortex. The time courses of both seed coordinates was regressed against all brain voxel time courses using BrainVoyager to create two brain maps of r-values for each fMRI scan. A p-value threshold less than 0.05 with correction via Bonferroni multiple comparisons was used to identify which voxels were significantly correlated with the seed location. All images were smoothed using a 2.0 mm full width at half maximum (FWHM) Gaussian kernel within BrainVoyager. The resulting voxels were clustered and counted to record a total volume of significantly correlated connectivity for each fMRI scan. For the group level analysis, connectivity maps were created with the same threshold levels and smoothing parameters described above. Only voxels with correlation less than the p-value of 0.05 corrected using the Bonferroni method, are reported as significant.

5.2.6 Independent Component Analysis of fMRI data

Independent component analysis (ICA) in the spatial domain was performed using Brain Voyager QX. Detailed methodological principles of ICA decomposition implemented in Brain Voyager QX were previously described (Formisano *et al*., 2004;

De Martino *et al*., 2007). Thirty components were computed and the voxel intensities of each IC maps were converted to z-scores. The spatial maps were color coded to reflect the absolute value and sign. It should be noted that the sign of each voxel value does not correspond to BOLD activation or deactivation. A positive value represents that the time course of the particular voxel is positively correlated with the time course of the IC. A higher z-score represents a higher correlation coefficient. As pointed out previously, the z-values have no statistical significance, as no hypothesis was tested (McKeown *et al*., 1998; De Martino *et al*., 2007).

5.2.7 Template-based selection of IC

A similar concept was previously described by Grecius et al (Greicius et al. 2004). Briefly, a template of the default mode network was obtained by averaging default mode activities in 10 healthy subjects. Cross correlation between the spatial pattern of each IC and the template representing the default mode network was computed in patients and in all healthy controls.

5.3 Results

5.3.1 Decreased DMN using ICA

Fig. 5.1 compares the default-mode network as detected by the ICA approach in patients versus controls. In healthy controls (Fig. 5.1A and C), significant clusters were found in PCC, bilateral inferior parietal cortex and medial prefrontal cortex. In contrast, in SCD patients no activation of DMN related IC was observed (Fig. 5.1B and D).

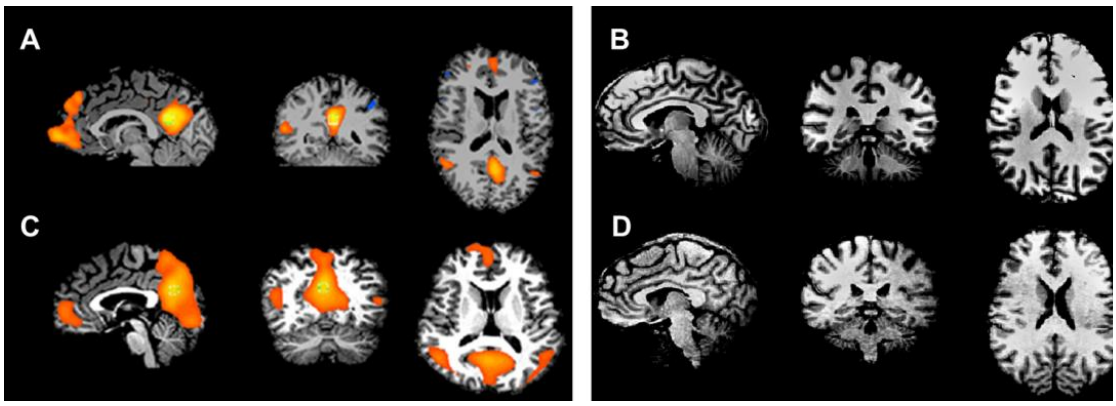

Figure. 5.1 DMN activity using template-based ICA

A. DMN in a single healthy control B. DMN in SCD a single patient. C. DMN in group level healthy controls. D. DMN in group level SCD patients.

5.3.2 Decreased DMN using fMRI connectivity analysis

Using seed-based connectivity analysis Fig. 5.2 compares the default-mode network in patients versus controls. In healthy controls (Fig. 5.2A and C), significant clusters were found in PCC, bilateral inferior parietal cortex and medial prefrontal cortex. In contrast, in SCD patients no activation of DMN related IC was observed (Fig. 5.2B and D).

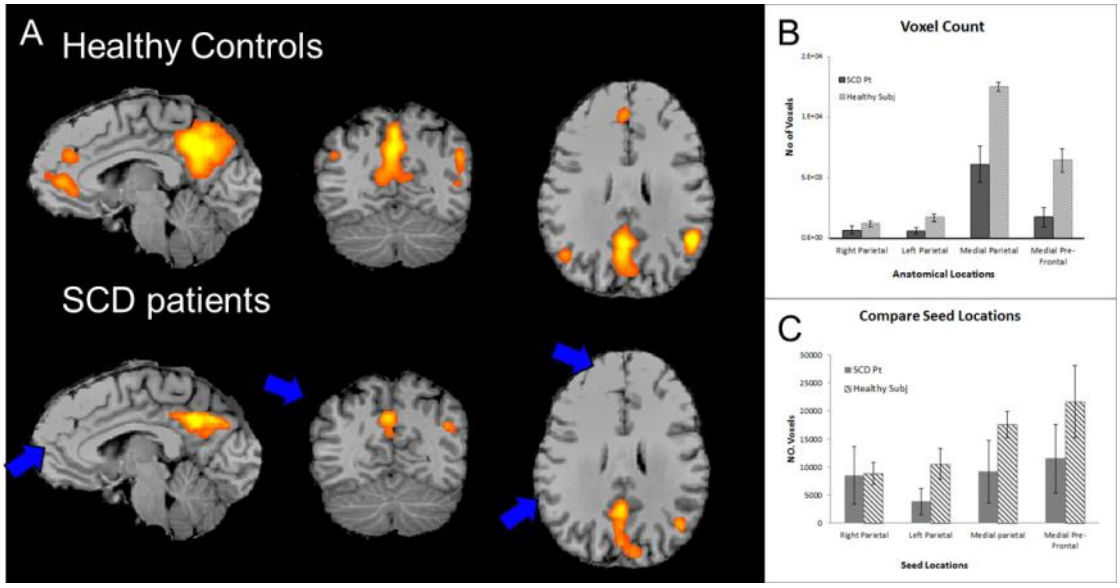

Figure. 5.2 DMN activity using seed-based connectivity analysis

A. DMN in a single healthy control B. DMN in SCD a single patient. C. DMN in group level healthy controls. D. DMN in group level SCD

5.2.3 Connectivity in insula cortex

Fig. 5.4 compares the difference in bilateral insular functional connectivity between SCD patients and healthy controls. The connectivity between the left and right insula appears to be stronger in SCD patients versus controls, especially when the seed is placed in the left insula (Fig. 5.4 A and B, bottom row).

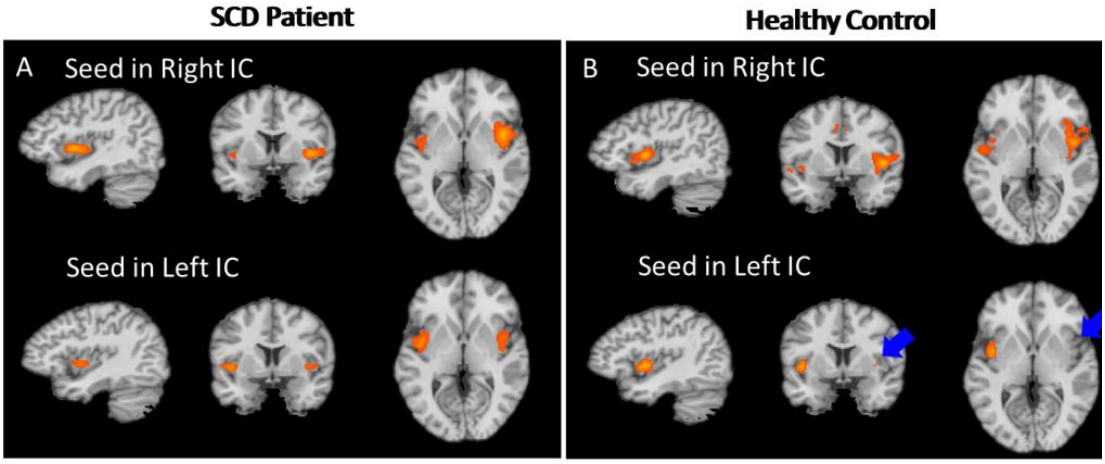

Figure. 5.3 Difference in connectivity between bilateral insula

A. Seed based results in the patient group. B. Seed based results in the healthy control group. Bilateral connectivity is strengthened in the patient group compared with controls. IC: insular cortex

5.4 Discussion

5.4.1 Decreased DMN in other pain and compare results

Our findings in DMN are in agreement with other studies of chronic back pain using fMRI (Baliki et al. 2008). In Baliki's work, a visual attention task was used and DMN in patients displayed a reduced deactivation compared with controls. In our study, we used resting state fMRI with two analysis methods using blind source separation of ICA and seed-based connectivity analysis. Chronic pain in SCD patients are suitable to be studied from the angle of DMN as the spontaneous painful sensation may produce salient percepts in the absence of exogenous input (Foss et al. 2006; Baliki et al. 2008).

5.4.2 Decreased DMN integrity in other disease

Altered connectivity of DMN during resting state is a prevalent phenomenon among mental disorders and ageing population (Greicius et al. 2004; Damoiseaux et al. 2008; Broyd et al. 2009). In healthy aging population, it has been shown that connectivity

between the right hippocampus and other regions of the DMN including the dorsal MPFC, ACC, middle temporal gyrus and right PCC is reduced (Damoiseaux et al. 2008). In Alzheimer's disease, where DMN connectivity is widely investigated,

5.4.3 Other pain areas

Acute pain studies on healthy controls have implicated multiple regions that are active to brief noxious stimuli. The most consistent regions across studies include the primary somatosensory cortex (S1), secondary somatosensory cortex (S2), anterior cingulate cortex (ACC), insular cortex (IC), prefrontal cortex (PFC), thalamus (Th), basal ganglia, and cerebellum (Apkarian et al. 2005; Apkarian, Hashmi, and Baliki 2011; Shao et al. 2012; Lee and Tracey 2013). The areas of S1, S2, and Th are related to sensory-discriminative pain processing, while ACC and IC are linked to affective-emotive pain processing (Moisset and Bouhassira 2007). Chronic pain has similarities and differences to acute pain activation regions. Chronic pain alters the brain structure and causes reduction in gray matter (Farmer, Baliki, and Apkarian 2012; Ceko et al. 2013; Maeda et al. 2013). Activity in the PFC was different between heat allodynia and normal heat pain, indicating neuropathic pain may induce physiological changes in the forebrain (Casey, Lorenz, and Minoshima 2003). Experimental pain applied to healthy controls and clinical chronic pain patients revealed that patients more frequently involve the PFC, IC and ACC compared to controls to process pain, where controls mainly involve S1, S2, and Th (Apkarian et al. 2005; Moisset and Bouhassira 2007; Lee and Tracey 2013). Our study demonstrated that SCD patients had activity in the IC during wakeful rest.

Functional neuroimaging studies have documented IC activation is associated with different functional roles including modulation of affective-emotional processing, cognitive and affective processes during learning, and aversive pain processing (Paulus and Stein 2006). The anterior IC has also been implicated to be sensitive to salient events (Menon and Uddin 2010). Emotional processing of sadness, happiness, anger, fear, empathy, and compassion all activate the IC (Damasio et al. 2000; Lamm and Singer 2010). The IC activation observed in SCD patients could be caused by any of these reasons; however, it is unlikely that the salience network was active. The salience network organizes neural responses to significantly intense stimuli, and none were presented in this study (Chiong et al. 2013). Emotional processing could have activated IC in SCD patients because mild to severe depression is frequently (44%) seen in SCD patients (Hasan et al. 2003). The insular cortex is an important structure involved in depression (Sprengelmeyer et al. 2011). Chronic pain is another candidate for IC activation. Fibromyalgia patients had greater connectivity between the DMN and IC compared to healthy controls (Napadow et al. 2010). Chronic back pain patients had this same trend and showed that IC activity also reflected the duration of spontaneous pain (Loggia et al. 2013; Baliki et al. 2006). IC activation observed in our study is most likely linked to DMN as well since subjects were in resting state, indicating chronic pain is the most likely reason for the IC activity.

5.4.5 Methodological limitations and future studies

Our current method is based on fMRI with fine spatial resolution but limited temporal resolution. Our results do not provide mechanistic explanation of this decreased DMN in SCD patients. We postulate that this phenomenon is pain specific because it has

also been observed in other chronic pain conditions (Baliki et al. 2008). In order to have a more mechanistic understanding of how DMN is decreasing in activity and how it is linked to neurophysiological manifestations, we would include concurrent EEG in our future study. EEG with its high temporal resolution, and direct measurement of underlying neurological activity, it can be correlated with fMRI. There have been some previous attempts in deploying simultaneous EEG and fMRI to study DMN in healthy subjects. However such studies often yield disparate results.

One confounding factor in our finding that may influence its specificity to pain is the role of medication. It is possible that medications for pain management are causing the altered connectivity of DMN. Observations from other type of chronic pain cannot help parse this out.

Chapter 6 Conclusions and Perspectives

6.1 Conclusions

Functional neuroimaging offers a great opportunity to noninvasively study the underlying activities in the normal as well as diseased brain. In this dissertation, we have investigated utilizing EEG source imaging and functional MRI in the diagnosis and management of epilepsy and pain.

One important application of functional neuroimaging techniques in detecting and localizing pathological activities lies in pre-surgical evaluations of patients suffering from intractable epilepsy. In one of the studies presented here, we have proposed an ICA-based automated method to lateralize and localize hemodynamic foci in focal epilepsy patients for presurgical evaluation. Focal activities identified by our method were in concordance with surgical resection in the majority of cases studied. Our findings suggest the possibility of noninvasively and accurately localizing epileptic foci using fMRI alone in presurgical planning. This was a feasibility study to demonstrate the value of the proposed method. Additional features can be incorporated in the algorithm to improve reliability and performance. A larger patient population needs to be studied to test the broad applicability of this method. This proposed method can be easily implemented in the current presurgical workup to provide additional information for guiding the surgical resection.

Unlike for patients with focal epilepsy, surgical resection is not a viable treatment option for patients suffering from generalized epilepsy. Furthermore, the underlying

mechanism of generating wide spread epileptic activity remains poorly understood. Therefore in order to provide benefits to these patients, there is a pressing need to improve our understanding of the neural network and mechanism of action in order to develop novel therapeutic approaches such as deep brain stimulation. In the second study presented, by combining the complementary strengths of EEG and fMRI, we showed consistent results concerning the genesis and propagation of GSWDs. EEG-informed fMRI revealed multiple brain regions that may be involved in GSWDs. By means of seed-based fMRI, we tested the specific network level activity and found temporal correlation between cortical and bithalamic BOLD activities. According to the Granger Causality analysis the mediodorsal nuclei of the thalamus serve as the main driver throughout the initiation and the propagation of the GSWDs. Once validated, this work can provide insight in understanding the enigmatic etiology of generalized epilepsy and offer guidance in treatments. This work suggests the thalamus, especially the mediodorsal nuclei, may serve as potential targets for deep brain stimulation to treat patients with drug-resistant generalized epilepsy.

Another field of application of such noninvasive imaging techniques is to provide better understanding of how the brain processes pain and ultimately to provide an objective measure of pain. For the study of exogenously elicited pain, by using scalp EEG we found that the spontaneous rhythms in all frequency bands except gamma band were suppressed globally at the presence of tonic painful thermal stimulation. The greatest changes were observed in the alpha power on the contralateral side to the stimulus in the somatosensory area. Additionally, the results suggested that the degree of suppression may reflect the level of applied painful stimulation. There was also increased

connectivity among major brain regions that responsive to pain, which was revealed through causality analysis. Although the current finding is based on the study of sustained pain from external stimuli in healthy subjects, it would help broaden our understanding of cortical response to patients with chronic pain.

In addition to external pain, we also studied patients with sickle cell disease, as they often suffer from chronic or acute pain as a result of the disease. We found that through fMRI based functional connectivity analyses, the resting state neural network in patients deviated from those of the healthy controls with both positive and negative effects. The default mode network, which is a ubiquitous resting state activity believed to be responsible for a host of cognitive functions such as memory consolidation and introspection, is reduced in patients with SCD compared to controls. On the other hand, insula cortex, which is a key node in the pain network, showed a marked increase in bilateral synchrony in patients with SCD as opposed to healthy controls.

In summary, the present dissertation research developed and evaluated the spatiotemporal imaging approaches for the non-invasive mapping of network activities in the diseased and normal brain. Evaluations were conducted in both patient and healthy control groups in order to test the clinical applicability of such noninvasive imaging tools. Regarding epilepsy, two investigations have been conducted to study the localization of hemodynamic foci in focal epilepsy patients and the widespread GSWDs of generalized epilepsy patients. The spatial resolution has been further improved by adding the component of fMRI through an EEG-fMRI integrated imaging framework. For the application in pain study, two investigations were conducted to study changes in network level activity due to external pain in healthy subjects and spontaneous pain in patients

with SCD. All of the results that were obtained suggest the importance of noninvasive spatiotemporal neuroimaging approaches for solving clinical problems and for investigating neuroscience questions. Furthermore, an improved understanding of neurological diseases and their mechanisms would help us to develop and deliver curative treatments of neurological diseases.

6.2 Perspectives

In addition to the development and progress obtained in the present dissertation research, there are remaining challenges, which also represent opportunities for future improvement of techniques and clinical applications.

6.2.1 Prospective clinical studies in focal epilepsy patients

We have demonstrated the feasibility and accuracy of the fMRI-based noninvasive, localization approach for the presurgical evaluation of patients with focal epilepsy through comparison against invasive procedures in a retrospective study. However, before applying a new neuroimaging method to clinical routines, prospective studies of large groups of patients are crucial in order to design a protocol that is most suitable for clinical applications. It will be important, in these prospective studies, to include the noninvasive seizure imaging protocol into the routine evaluation of epilepsy patients. The results of fMRI localization need to be presented in the pre-surgical conference, during which neurologists and neurosurgeons determine surgical plans based on the information obtained through various pre-surgical diagnostic resources. Surgical plans, including both the plan to implant intracranial electrodes as well as the plan to resect brain tissue, shall be determined in two ways. The first plan is determined based on

conventional procedures without fMRI localization results. The second plan is determined with the fMRI localization results. If the outcomes of the two plans are the same, this would indicate that fMRI localization is consistent with conventional procedures, and could potentially be used to reduce or eliminate the need for separate iEEG in the future. Alternatively, the outcome of the plan including fMRI localization results could suggest more or less iEEG coverage or resection, which would indicate that fMRI localization, provides additional useful information to the conventional procedures. In optimal cases, when fMRI localization conforms to anatomical MRI and other noninvasive neurological tests, patients could proceed directly to resection without the need of another surgery to implant iEEG. The difference between the outcomes of the two plans will show the extent to which such a noninvasive fMRI localization protocol can change the conventional clinical practices of the surgical treatment of epilepsy. The yield and accuracy of the resulting iEEG recording and the success rate of surgery will be important measures to determine the significance and the added value of such a new protocol.

6.2.2 Deep Brain Stimulation in Generalized Epilepsy Patients

In the study of patients with generalized epilepsy, we demonstrated the reciprocal relationship between thalamus, especially the mediodorsal nuclei of the thalamus and the medial frontal cortex. Our causal analysis suggested that the thalamus seems to be the driving force in initiating GSWDs. In order to validate these findings, depth electrodes should be implanted in these areas to provide direct evidence. Effects of stimulation delivered at either location can be measured by other intracranial electrodes or scalp EEG to determine whether thalamus is indeed responsible for generating GSWDs. Furthermore,

the mediodorsal nuclei of the thalamus could be tested as a potential DBS target similar to studies conducted in the anterior nuclei of the thalamus in the SANTE trial.

6.2.3 EEG-fMRI Study of Pain

The two present studies on pain were based on EEG or fMRI individually. Using EEG in healthy subjects receiving elicited external painful stimulation, we found changes in resting state rhythmic oscillations as well as patterns of connectivity among nodes responsible for pain processing. In patients with sickle cell disease, we used fMRI to find changes in connectivity patterns compared with controls. However, in order to bridge the gap between neural electrophysiological phenomena as measured by EEG and metabolic based activity as shown in fMRI, we need to perform both EEG and fMRI concurrently, especially given the benefits discussed in the epilepsy application. Therefore, the next step would be to study both healthy controls and patients suffering chronic pain using the two modalities simultaneously. With this method, we can probe into the neural correlates of default mode network and insula cortex activity, which currently remains unclear. Additionally, machine learning techniques can be applied to such concurrent electrophysiological and hemodynamic imaging to derive biomarkers of pain, which could aid the development of an objective measure of pain and new therapeutic approaches for pain in the near future.

Reference

Aghakhani Y. fMRI activation during spike and wave discharges in idiopathic generalized epilepsy. Brain. 2004 Feb 26;127(5):1127–44.

Aragri A, Scarabino T, Seifritz E, Comani S, Cirillo S, Tedeschi G, et al. How does spatial extent of fMRI datasets affect independent component analysis decomposition? Hum Brain Mapp. 2006 Sep 1;27(9):736–46.

Archer JS, Abbott DF, Waites AB, Jackson GD. fMRI "deactivation" of the posterior cingulate during generalized spike and wave. NeuroImage. 2003 Dec;20(4):1915–22.

Arendt-Nielsen L, Chen ACN. Lasers and other thermal stimulators for activation of skin nociceptors in humans. Neurophysiol Clin Neurophysiol. 2003 Dec;33(6):259–68.

Arthurs OJ, Boniface S. How well do we understand the neural origins of the fMRI BOLD signal? TRENDS Neurosci. 2002;25(1):27–31.

Ashburner J, Barnes G, Chen C-C, Daunizeau J, Flandin G, Friston K, et al. SPM8 manual

Assaf BA, Ebersole JS. Continuous Source Imaging of Scalp Ictal Rhythms in Temporal Lobe Epilepsy. Epilepsia. 1997 Oct 1;38(10):1114–23.

Babiloni C, Brancucci A, Percio CD, Capotosto P, Arendt-Nielsen L, Chen ACN, et al. Anticipatory Electroencephalography Alpha Rhythm Predicts Subjective Perception of Pain Intensity. J Pain. 2006 Oct;7(10):709–17.

Babiloni C, Capotosto P, Brancucci A, Del Percio C, Petrini L, Buttiglione M, et al. Cortical alpha rhythms are related to the anticipation of sensorimotor interaction between painful stimuli and movements: a high-resolution EEG study. J Pain. 2008;9(10):902–11.

Babiloni F, Cincotti F, Babiloni C, Carducci F, Mattia D, Astolfi L, et al. Estimation of the cortical functional connectivity with the multimodal integration of high-resolution EEG and fMRI data by directed transfer function. NeuroImage. 2005 Jan 1;24(1):118–31.

Backonja M, Howland EW, Wang J, Smith J, Salinsky M, Cleeland CS. Tonic changes in alpha power during immersion of the hand in cold water. Electroencephalogr Clin Neurophysiol. 1991;79(3):192–203.

Baillet S, Mosher JC, Leahy RM. Electromagnetic brain mapping. IEEE Signal Process Mag. 2001 Nov;18(6):14–30.

Bai X, Vestal M, Berman R, Negishi M, Spann M, Vega C, et al. Dynamic Time Course of Typical Childhood Absence Seizures: EEG, Behavior, and Functional Magnetic Resonance Imaging. J Neurosci. 2010 Apr 28;30(17):5884–93.

Baliki MN, Geha PY, Apkarian AV, Chialvo DR. Beyond Feeling: Chronic Pain Hurts the Brain, Disrupting the Default-Mode Network Dynamics. J Neurosci. 2008 Feb 6;28(6):1398–403.

Bandettini PA, Wong EC, Hinks RS, Tikofsky RS, Hyde JS. Time course EPI of human brain function during task activation. Magn Reson Med. 1992 Jun 1;25(2):390–7.

Baumgartner C, Pataraia E. Revisiting the role of magnetoencephalography in epilepsy: Curr Opin Neurol. 2006 Apr;19(2):181–6.

Beckmann CF, DeLuca M, Devlin JT, Smith SM. Investigations into resting-state connectivity using independent component analysis. Philos Trans R Soc B Biol Sci. 2005 May 29;360(1457):1001–13.

Bell AJ, Sejnowski TJ. An Information-Maximization Approach to Blind Separation and Blind Deconvolution. Neural Comput. 1995 Nov 1;7(6):1129–59.

Bénar C-G, Gross DW, Wang Y, Petre V, Pike B, Dubeau F, et al. The BOLD Response to Interictal Epileptiform Discharges. NeuroImage. 2002 Nov;17(3):1182–92.

Bénar C-G, Grova C, Kobayashi E, Bagshaw AP, Aghakhani Y, Dubeau F, et al. EEG–fMRI of epileptic spikes: Concordance with EEG source localization and intracranial EEG. NeuroImage. 2006 May 1;30(4):1161–70.

Berger PDH. Über das Elektrenkephalogramm des Menschen. Arch Für Psychiatr Nervenkrankh. 1929 Dec 1;87(1):527–70.

Bernhardt BC, Rozen DA, Worsley KJ, Evans AC, Bernasconi N, Bernasconi A. Thalamo–cortical network pathology in idiopathic generalized epilepsy: Insights from MRI-based morphometric correlation analysis. NeuroImage. 2009 Jun;46(2):373–81.

Blumenfeld H. From molecules to networks: cortical/subcortical interactions in the pathophysiology of idiopathic generalized epilepsy. Epilepsia. 2003;44(s2):7–15.

Blumenfeld H. Cellular and Network Mechanisms of Spike-Wave Seizures. Epilepsia. 2005 Nov 1;46:21–33.

Blumenfeld H, Varghese GI, Purcaro MJ, Motelow JE, Enev M, McNally KA, et al. Cortical and subcortical networks in human secondarily generalized tonic–clonic seizures. Brain. 2009 Apr 1;132(4):999–1012.

Boly M, Balteau E, Schnakers C, Degueldre C, Moonen G, Luxen A, et al. Baseline brain activity fluctuations predict somatosensory perception in humans. Proc Natl Acad Sci. 2007;104(29):12187–92.

Boon P, D'Havé M, Vanrumste B, Van Hoey G, Vonck K, Van Walleghem P, et al. Ictal source localization in presurgical patients with refractory epilepsy. J Clin Neurophysiol Off Publ Am Electroencephalogr Soc. 2002 Oct;19(5):461–8.

Breivik H, Collett B, Ventafridda V, Cohen R, Gallacher D. Survey of chronic pain in Europe: Prevalence, impact on daily life, and treatment. Eur J Pain. 2006 May 1;10(4):287–287.

Brodbeck V, Spinelli L, Lascano AM, Wissmeier M, Vargas M-I, Vulliemoz S, et al. Electroencephalographic source imaging: a prospective study of 152 operated epileptic patients. Brain. 2011 Oct 1;134(10):2887–97.

Bromm B. Brain Images of Pain. Physiology. 2001 Oct 1;16(5):244–9.

Bromm B. The involvement of the posterior cingulate gyrus in phasic pain processing of humans. Neurosci Lett. 2004 May 6;361(1–3):245–9.

Bromm B, Chen ACN. Brain electrical source analysis of laser evoked potentials in response to painful trigeminal nerve stimulation. Electroencephalogr Clin Neurophysiol. 1995 Jul;95(1):14–26.

Broyd SJ, Demanuele C, Debener S, Helps SK, James CJ, Sonuga-Barke EJS. Default-mode brain dysfunction in mental disorders: A systematic review. Neurosci Biobehav Rev. 2009 Mar;33(3):279–96.

Buckner RL, Andrews-Hanna JR, Schacter DL. The Brain's Default Network. Ann N Y Acad Sci. 2008 Mar 1;1124(1):1–38.

Buckner RL, Snyder AZ, Shannon BJ, LaRossa G, Sachs R, Fotenos AF, et al. Molecular, Structural, and Functional Characterization of Alzheimer's Disease: Evidence for a Relationship between Default Activity, Amyloid, and Memory. J Neurosci. 2005 Aug 24;25(34):7709–17.

Calhoun V d., Adali T, Pearlson G d., Pekar J j. Spatial and temporal independent component analysis of functional MRI data containing a pair of task-related waveforms. Hum Brain Mapp. 2001 May 1;13(1):43–53.

Calhoun VD, Adali T, Stevens MC, Kiehl KA, Pekar JJ. Semi-blind ICA of fMRI: A method for utilizing hypothesis-derived time courses in a spatial ICA analysis. NeuroImage. 2005 Apr 1;25(2):527–38.

Chang P, Arendt-Nielsen L, Chen AC. Differential cerebral responses to aversive auditory arousal versus muscle pain: specific EEG patterns are associated with human pain processing. Exp Brain Res. 2002a Dec 1;147(3):387–93.

Chang PF, Arendt-Nielsen L, Chen AC. Dynamic changes and spatial correlation of EEG activities during cold pressor test in man. Brain Res Bull. 2002b;57(5):667–75.

Chang PF, Arendt-Nielsen L, Graven-Nielsen T, Svensson P, Chen ACN. Comparative EEG activation to skin pain and muscle pain induced by capsaicin injection. Int J Psychophysiol. 2004 Jan;51(2):117–26.

Chen ACN. New perspectives in EEG/MEG brain mapping and PET/fMRI neuroimaging of human pain. Int J Psychophysiol. 2001 Oct;42(2):147–59.

Chen ACN, Niddam DM, Arendt-Nielsen L. Contact heat evoked potentials as a valid means to study nociceptive pathways in human subjects. Neurosci Lett. 2001 Dec 18;316(2):79–82.

Chen ACN, Rappelsberger P. Brain and Human pain: Topographic EEG amplitude and coherence mapping. Brain Topogr. 1994 Dec 1;7(2):129–40.

Cheung BLP, Riedner BA, Tononi G, Van Veen B. Estimation of Cortical Connectivity From EEG Using State-Space Models. IEEE Trans Biomed Eng. 2010 Sep;57(9):2122–34.

Christmann C, Koeppe C, Braus DF, Ruf M, Flor H. A simultaneous EEG–fMRI study of painful electric stimulation. NeuroImage. 2007 Feb;34(4):1428–37.

Coghill RC, McHaffie JG, Yen Y-F. Neural correlates of interindividual differences in the subjective experience of pain. Proc Natl Acad Sci. 2003;100(14):8538–42.

Collins DL, Neelin P, Peters TM, Evans AC. Automatic 3D Intersubject Registration of MR Volumetric Data... : Journal of Computer Assisted Tomography. 1994

Cordes D, Haughton VM, Arfanakis K, Carew JD, Turski PA, Moritz CH, et al. Frequencies Contributing to Functional Connectivity in the Cerebral Cortex in "Resting-state" Data. Am J Neuroradiol. 2001 Aug 1;22(7):1326–33.

Craig AD, Reiman EM, Evans A, Bushnell MC. Functional imaging of an illusion of pain. Nature. 1996 Nov 21;384(6606):258–60.

Cullen TJ, Walker MA, Eastwood SL, Esiri MM, Harrison PJ, Crow TJ. Anomalies of asymmetry of pyramidal cell density and structure in dorsolateral prefrontal cortex in schizophrenia. Br J Psychiatry. 2006;188(1):26–31.

Dale AM, Sereno MI. Improved Localizadon of Cortical Activity by Combining EEG and MEG with MRI Cortical Surface Reconstruction: A Linear Approach. J Cogn Neurosci. 1993 Apr 1;5(2):162–76.

Damoiseaux JS, Beckmann CF, Arigita EJS, Barkhof F, Scheltens P, Stam CJ, et al. Reduced resting-state brain activity in the "default network" in normal aging. Cereb Cortex. 2008 Aug 1;18(8):1856–64.

Daunizeau J, Laufs H, Friston KJ. EEG–fMRI Information Fusion: Biophysics and Data Analysis. In: Mulert C, Lemieux L, editors. EEG - FMRI. Springer Berlin Heidelberg.

Daunizeau J, Vaudano AE, Lemieux L. Bayesian multi-modal model comparison: A case study on the generators of the spike and the wave in generalized spike–wave complexes. NeuroImage. 2010 Jan 1;49(1):656–67.

David O, Guillemain I, Saillet S, Reyt S, Deransart C, Segebarth C, et al. Identifying Neural Drivers with Functional MRI: An Electrophysiological Validation. PLoS Biol. 2008 Dec 23;6(12):e315.

Davis CE, Hauf JD, Wu DQ, Everhart DE. Brain function with complex decision making using electroencephalography. Int J Psychophysiol. 2011 Feb;79(2):175–83.

Davis KD, Wood ML, Crawley AP, Mikulis DJ. fMRI of human somatosensory and cingulate cortex during painful electrical nerve stimulation. Neuroreport. 1995 Dec 29;7(1):321–5.

Debener S, Ullsperger M, Siegel M, Engel AK. Single-trial EEG–fMRI reveals the dynamics of cognitive function. Trends Cogn Sci. 2006 Dec;10(12):558–63.

Debener S, Ullsperger M, Siegel M, Fiehler K, Cramon DY von, Engel AK. Trial-by-Trial Coupling of Concurrent Electroencephalogram and Functional Magnetic Resonance Imaging Identifies the Dynamics of Performance Monitoring. J Neurosci. 2005 Dec 14;25(50):11730–7.

deCharms RC, Maeda F, Glover GH, Ludlow D, Pauly JM, Soneji D, et al. Control over brain activation and pain learned by using real-time functional MRI. Proc Natl Acad Sci U S A. 2005 Dec 20;102(51):18626–31.

Delorme A, Makeig S. EEGLAB: an open source toolbox for analysis of single-trial EEG dynamics including independent component analysis. J Neurosci Methods. 2004 Mar 15;134(1):9–21.

Deshpande G, Sathian K, Hu X. Assessing and Compensating for Zero-Lag Correlation Effects in Time-Lagged Granger Causality Analysis of fMRI. IEEE Trans Biomed Eng. 2010a Jun;57(6):1446–56.

Deshpande G, Sathian K, Hu X. Effect of hemodynamic variability on Granger causality analysis of fMRI. NeuroImage. 2010b Sep;52(3):884–96.

Devinsky O, Morrell MJ, Vogt BA. Review Article. Brain. 1995 Feb 1;118(1):279–306.

Ding L, Worrell GA, Lagerlund TD, He B. Ictal source analysis: Localization and imaging of causal interactions in humans. NeuroImage. 2007 Jan 15;34(2):575–86.

Ding M, He B. Exploring Functional and Causal Connectivity in the Brain. In: He B, editor. Neural Eng [Internet]. Springer US; 2013 [cited 2015 Jan 9]. p. 545–64.

Domnick C, Hauck M, Casey KL, Engel AK, Lorenz J. C-fiber-related EEG-oscillations induced by laser radiant heat stimulation of capsaicin-treated skin. J Pain Res. 2009 Mar 17;2:49–56.

Drury, Henry TR. Ictal patterns in generalized epilepsy. J Clin Neurophysiol Off Publ Am Electroencephalogr Soc. 1993 Jul;10(3):268–80.

Egsgaard LL, Wang L, Arendt-Nielsen L. Volunteers with high versus low alpha EEG have different pain–EEG relationship: a human experimental study. Exp Brain Res. 2008 Nov 15;193(3):361–9.

Engel J. A Proposed Diagnostic Scheme for People with Epileptic Seizures and with Epilepsy: Report of the ILAE Task Force on Classification and Terminology. Epilepsia. 2001 Jun 1;42(6):796–803.

Engel J, Henry TR, Risinger MW, Mazziotta JC, Sutherling WW, Levesque MF, et al. Presurgical evaluation for partial epilepsy Relative contributions of chronic depth ‐ electrode recordings versus FDG ‐ PET and scalp ‐ sphenoidal ictal EEG. Neurology. 1990 Nov 1;40(11):1670–1670.

Engel J, Pedley TA, Aicardi J. Epilepsy: A Comprehensive Textbook. Lippincott Williams & Wilkins; 2008.

Farmer MA, Baliki MN, Apkarian AV. A dynamic network perspective of chronic pain. Neurosci Lett. 2012 Jun 29;520(2):197–203.

Feige B, Scheffler K, Esposito F, Salle FD, Hennig J, Seifritz E. Cortical and Subcortical Correlates of Electroencephalographic Alpha Rhythm Modulation. J Neurophysiol. 2005 May 1;93(5):2864–72.

Feinberg DA, Moeller S, Smith SM, Auerbach E, Ramanna S, Glasser MF, et al. Multiplexed Echo Planar Imaging for Sub-Second Whole Brain FMRI and Fast Diffusion Imaging. PLoS ONE. 2010 Dec 20;5(12):e15710.

Ferracuti S, Seri S, Mattia D, Cruccu G. Quantitative EEG modifications during the cold water pressor test: hemispheric and hand differences. Int J Psychophysiol. 1994;17(3):261–8.

Fisher R, Salanova V, Witt T, Worth R, Henry T, Gross R, et al. Electrical stimulation of the anterior nucleus of thalamus for treatment of refractory epilepsy. Epilepsia. 2010 May;51(5):899–908.

Formisano E, Esposito F, Di Salle F, Goebel R. Cortex-based independent component analysis of fMRI time series. Magn Reson Imaging. 2004 Dec;22(10):1493–504.

Foss JM, Apkarian AV, Chialvo DR. Dynamics of Pain: Fractal Dimension of Temporal Variability of Spontaneous Pain Differentiates Between Pain States. J Neurophysiol. 2006 Feb 1;95(2):730–6.

Fox MD, Snyder AZ, Vincent JL, Corbetta M, Essen DCV, Raichle ME. The human brain is intrinsically organized into dynamic, anticorrelated functional networks. Proc Natl Acad Sci U S A. 2005 Jul 5;102(27):9673–8.

Fransson P. Spontaneous low-frequency BOLD signal fluctuations: An fMRI investigation of the resting-state default mode of brain function hypothesis. Hum Brain Mapp. 2005 Sep 1;26(1):15–29.

Freunberger R, Klimesch W, Griesmayr B, Sauseng P, Gruber W. Alpha phase coupling reflects object recognition. NeuroImage. 2008 Aug 15;42(2):928–35.

Friston K. Causal Modelling and Brain Connectivity in Functional Magnetic Resonance Imaging. PLoS Biol. 2009 Feb 17;7(2):e1000033.

Fuchs M, Drenckhahn R, Wischmann H, Wagner M. An improved boundary element method for realistic volume-conductor modeling. IEEE Trans Biomed Eng. 1998 Aug;45(8):980–97.

Fukushima M, Yamashita O, Kanemura A, Ishii S, Kawato M, Sato M. A State-Space Modeling Approach for Localization of Focal Current Sources From MEG. IEEE Trans Biomed Eng. 2012 Jun;59(6):1561–71.

Gaskin DJ, Richard P. The Economic Costs of Pain in the United States. J Pain. 2012 Aug;13(8):715–24.

Goebel R, Roebroeck A, Kim D-S, Formisano E. Investigating directed cortical interactions in time-resolved fMRI data using vector autoregressive modeling and Granger causality mapping. Magn Reson Imaging. 2003 Dec;21(10):1251–61.

Goldman RI, Stern JM, Engel J, Cohen MS. Simultaneous EEG and fMRI of the alpha rhythm. Neuroreport. 2002 Dec 20;13(18):2487–92.

Gotman J, Grova C, Bagshaw A, Kobayashi E, Aghakhani Y, Dubeau F. Generalized epileptic discharges show thalamocortical activation and suspension of the default state of the brain. Proc Natl Acad Sci U S A. 2005;102(42):15236–40.

Gotman J, Kobayashi E, Bagshaw AP, Bénar C-G, Dubeau F. Combining EEG and fMRI: A multimodal tool for epilepsy research. J Magn Reson Imaging. 2006 Jun 1;23(6):906–20.

Granger CWJ. Investigating Causal Relations by Econometric Models and Cross-spectral Methods. Econometrica. 1969 Aug 1;37(3):424–38.

Greicius MD, Srivastava G, Reiss AL, Menon V. Default-mode network activity distinguishes Alzheimer's disease from healthy aging: Evidence from functional MRI. Proc Natl Acad Sci U S A. 2004 Mar 30;101(13):4637–42.

Greicius MD, Supekar K, Menon V, Dougherty RF. Resting-State Functional Connectivity Reflects Structural Connectivity in the Default Mode Network. Cereb Cortex. 2009 Jan 1;19(1):72–8.

Gross J, Schnitzler A, Timmermann L, Ploner M. Gamma Oscillations in Human Primary Somatosensory Cortex Reflect Pain Perception. PLoS Biol. 2007;5(5):e133.

Grouiller F, Thornton RC, Groening K, Spinelli L, Duncan JS, Schaller K, et al. With or without spikes: localization of focal epileptic activity by simultaneous electroencephalography and functional magnetic resonance imaging. Brain. 2011 Oct 1;134(10):2867–86.

Hämäläinen M, Hari R, Ilmoniemi RJ, Knuutila J, Lounasmaa OV. Magnetoencephalography—theory, instrumentation, and applications to noninvasive studies of the working human brain. Rev Mod Phys. 1993 Apr 1;65(2):413–97.

Hamalainen MS, Sarvas J. Realistic conductivity geometry model of the human head for interpretation of neuromagnetic data. IEEE Trans Biomed Eng. 1989 Feb;36(2):165–71.

Hamandi K, Salek-Haddadi A, Fish DR, Lemieux L. EEG/functional MRI in epilepsy: The Queen Square Experience. J Clin Neurophysiol Off Publ Am Electroencephalogr Soc. 2004 Aug;21(4):241–8.

Hamandi K, Salek-Haddadi A, Laufs H, Liston A, Friston K, Fish DR, et al. EEG–fMRI of idiopathic and secondarily generalized epilepsies. NeuroImage. 2006 Jul 15;31(4):1700–10.

He B, Dai Y, Astolfi L, Babiloni F, Yuan H, Yang L. eConnectome: A MATLAB toolbox for mapping and imaging of brain functional connectivity. J Neurosci Methods. 2011a Feb 15;195(2):261–9.

He B, Ding L. Electrophysiological Neuroimaging. Neural Eng. Springer Berlin Heidelberg; 2013. p. 499–544.

He B, Liu Z. Multimodal Functional Neuroimaging: Integrating Functional MRI and EEG/MEG. Biomed Eng IEEE Rev In. 2008;1:23–40.

He B, Musha T, Okamoto Y, Homma S, Nakajima Y, Sato T. Electric Dipole Tracing in the Brain by Means of the Boundary Element Method and Its Accuracy. IEEE Trans Biomed Eng. 1987 Jun;BME-34(6):406–14.

He B, Yang L, Wilke C, Yuan H. Electrophysiological Imaging of Brain Activity and Connectivity #x2014;Challenges and Opportunities. IEEE Trans Biomed Eng. 2011b Jul;58(7):1918–31.

He DB, Musha T. Equivalent dipole estimation of spontaneous EEG alpha activity: two-moving dipole approach. Med Biol Eng Comput. 1992 May 1;30(3):324–32.

Hesdorffer DC, Hauser WA, Annegers JF, Cascino G. Major depression is a risk factor for seizures in older adults. Ann Neurol. 2000 Feb 1;47(2):246–9.

Holmes MD, Tucker DM, Quiring JM, Hakimian S, Miller JW, Ojemann JG. Comparing Noninvasive Dense Array and Intracranial Electroencephalography for Localization of Seizures: Neurosurgery. 2010 Feb;66(2):354–62.

Homma S, Nakajima Y, Musha T, Okamoto Y, He B. Dipole-tracing method applied to human brain potentials. J Neurosci Methods. 1987 Oct;21(2–4):195–200.

Huang G, Xiao P, Hung YS, Iannetti GD, Zhang ZG, Hu L. A novel approach to predict subjective pain perception from single-trial laser-evoked potentials. NeuroImage. 2013;81:283–93.

Huber MT, Bartling J, Pachur D, Woikowsky-Biedau S v., Lautenbacher S. EEG responses to tonic heat pain. Exp Brain Res. 2006 Aug;173(1):14–24.

Hui HB, Pantazis D, Bressler SL, Leahy RM. Identifying true cortical interactions in MEG using the nulling beamformer. NeuroImage. 2010 Feb 15;49(4):3161–74.

Hu L, Peng W, Valentini E, Zhang Z, Hu Y. Functional Features of Nociceptive-Induced Suppression of Alpha Band Electroencephalographic Oscillations. J Pain. 2013 Jan;14(1):89–99.

Hyvarinen A. Fast and robust fixed-point algorithms for independent component analysis. IEEE Trans Neural Netw. 1999 May;10(3):626–34.

Jacobs J, LeVan P, Moeller F, Boor R, Stephani U, Gotman J, et al. Hemodynamic changes preceding the interictal EEG spike in patients with focal epilepsy investigated using simultaneous EEG-fMRI. NeuroImage. 2009 May 1;45(4):1220–31.

Jann K, Wiest R, Hauf M, Meyer K, Boesch C, Mathis J, et al. BOLD correlates of continuously fluctuating epileptic activity isolated by independent component analysis. NeuroImage. 2008 Aug;42(2):635–48.

Jiang H, Golay X, van Zijl PCM, Mori S. Origin and minimization of residual motion-related artifacts in navigator-corrected segmented diffusion-weighted EPI of the human brain. Magn Reson Med. 2002 Apr 1;47(4):818–22.

Johnson MD, Lim HH, Netoff TI, Connolly AT, Johnson N, Roy A, et al. Neuromodulation for Brain Disorders: Challenges and Opportunities. IEEE Trans Biomed Eng. 2013 Mar;60(3):610–24.

Jung K-Y, Kim J-M, Kim DW, Chung C-S. Independent component analysis of generalized spike-and-wave discharges: primary versus secondary bilateral synchrony. Clin Neurophysiol. 2005 Apr;116(4):913–9.

Kaiboriboon K, Lüders HO, Hamaneh M, Turnbull J, Lhatoo SD. EEG source imaging in epilepsy—practicalities and pitfalls. Nat Rev Neurol. 2012 Sep;8(9):498–507.

Kakigi R, Inui K, Tamura Y. Electrophysiological studies on human pain perception. Clin Neurophysiol. 2005 Apr;116(4):743–63.

Kaminski MJ, Blinowska KJ. A new method of the description of the information flow in the brain structures. Biol Cybern. 1991 Jul 1;65(3):203–10.

Kobayashi K, Yoshinaga H, Ohtsuka Y, Gotman J. Dipole Modeling of Epileptic Spikes Can Be Accurate or Misleading. Epilepsia. 2005 Mar 1;46(3):397–408.

Koessler L, Benar C, Maillard L, Badier J-M, Vignal JP, Bartolomei F, et al. Source localization of ictal epileptic activity investigated by high resolution EEG and validated by SEEG. NeuroImage. 2010 Jun;51(2):642–53.

Kong J, Loggia ML, Zyloney C, Tu P, LaViolette P, Gollub RL. Exploring the brain in pain: Activations, deactivations and their relation. PAIN. 2010 Feb;148(2):257–67.

Krettek JE, Price JL. The cortical projections of the mediodorsal nucleus and adjacent thalamic nuclei in the rat. J Comp Neurol. 1977 Jan 15;171(2):157–91.

Kringelbach ML, Jenkinson N, Green AL, Owen SL, Hansen PC, Cornelissen PL, et al. Deep brain stimulation for chronic pain investigated with magnetoencephalography. Neuroreport. 2007;18(3):223–8.

Kucyi A, Moayedi M, Weissman-Fogel I, Goldberg MB, Freeman BV, Tenenbaum HC, et al. Enhanced Medial Prefrontal-Default Mode Network Functional Connectivity in Chronic Pain and Its Association with Pain Rumination. J Neurosci. 2014 Mar 12;34(11):3969–75.

Kucyi A, Salomons TV, Davis KD. Mind wandering away from pain dynamically engages antinociceptive and default mode brain networks. Proc Natl Acad Sci. 2013 Nov 12;110(46):18692–7.

Kwong KK, Belliveau JW, Chesler DA, Goldberg IE, Weisskoff RM, Poncelet BP, et al. Dynamic magnetic resonance imaging of human brain activity during primary sensory stimulation. Proc Natl Acad Sci. 1992 Jun 15;89(12):5675–9.

Lai Y, van Drongelen W, Ding L, Hecox KE, Towle VL, Frim DM, et al. Estimation of in vivo human brain-to-skull conductivity ratio from simultaneous extra- and intra-cranial electrical potential recordings. Clin Neurophysiol. 2005 Feb;116(2):456–65.

Lai Y, Zhang X, van Drongelen W, Korhman M, Hecox K, Ni Y, et al. Noninvasive cortical imaging of epileptiform activities from interictal spikes in pediatric patients. NeuroImage. 2011 Jan 1;54(1):244–52.

Lancaster JL, Rainey LH, Summerlin JL, Freitas CS, Fox PT, Evans AC, et al. Automated Labeling of the Human Brain. Hum Brain Mapp. 1997;5(4):238–42.

Lancaster JL, Woldorff MG, Parsons LM, Liotti M, Freitas CS, Rainey L, et al. Automated Talairach Atlas labels for functional brain mapping. Hum Brain Mapp. 2000;10(3):120–31.

Lantz G, Grave de Peralta R, Spinelli L, Seeck M, Michel CM. Epileptic source localization with high density EEG: how many electrodes are needed? Clin Neurophysiol. 2003 Jan;114(1):63–9.

Laufs H, Duncan JS. Electroencephalography/functional MRI in human epilepsy: what it currently can and cannot do: Curr Opin Neurol. 2007 Aug;20(4):417–23.

Lemieux L, Salek-Haddadi A, Josephs O, Allen P, Toms N, Scott C, et al. Event-Related fMRI with Simultaneous and Continuous EEG: Description of the Method and Initial Case Report. NeuroImage. 2001 Sep;14(3):780–7.

Leonard CM. The prefrontal cortex of the rat. I. cortical projection of the mediodorsal nucleus. II. efferent connections. Brain Res. 1969 Feb;12(2):321–43.

Leonardi M, Ustun TB. The Global Burden of Epilepsy. Epilepsia. 2002 Jul 1;43:21–5.

LeVan P, Gotman J. Independent component analysis as a model-free approach for the detection of BOLD changes related to epileptic spikes: A simulation study. Hum Brain Mapp. 2009 Jul;30(7):2021–31.

LeVan P, Tyvaert L, Gotman J. Modulation by EEG features of BOLD responses to interictal epileptiform discharges. NeuroImage. 2010 Mar;50(1):15–26.

Lin F-H, Hara K, Solo V, Vangel M, Belliveau JW, Stufflebeam SM, et al. Dynamic Granger–Geweke causality modeling with application to interictal spike propagation. Hum Brain Mapp. 2009;30(6):1877–86.

Liu AK, Belliveau JW, Dale AM. Spatiotemporal imaging of human brain activity using functional MRI constrained magnetoencephalography data: Monte Carlo simulations. Proc Natl Acad Sci. 1998;95(15):8945–50.

Liu Z, He B. fMRI–EEG integrated cortical source imaging by use of time-variant spatial constraints. NeuroImage. 2008 Feb;39(3):1198–214.

Liu Z, Kecman F, He B. Effects of fMRI–EEG mismatches in cortical current density estimation integrating fMRI and EEG: A simulation study. Clin Neurophysiol. 2006 Jul;117(7):1610–22.

Liu Z, de Zwart JA, van Gelderen P, Kuo L-W, Duyn JH. Statistical feature extraction for artifact removal from concurrent fMRI-EEG recordings. NeuroImage. 2012 Feb 1;59(3):2073–87.

Llinás RR, Ribary U, Jeanmonod D, Kronberg E, Mitra PP. Thalamocortical dysrhythmia: A neurological and neuropsychiatric syndrome characterized by magnetoencephalography. Proc Natl Acad Sci. 1999 Dec 21;96(26):15222–7.

Loggia ML, Kim J, Gollub RL, Vangel MG, Kirsch I, Kong J, et al. Default mode network connectivity encodes clinical pain: An arterial spin labeling study. PAIN®. 2013 Jan;154(1):24–33.

Logothetis NK. What we can do and what we cannot do with fMRI. Nature. 2008 Jun 12;453(7197):869–78.

Lopes R, Lina JM, Fahoum F, Gotman J. Detection of epileptic activity in fMRI without recording the EEG. NeuroImage. 2012 Apr;60(3):1867–79.

Lowe MJ, Mock BJ, Sorenson JA. Functional Connectivity in Single and Multislice Echoplanar Imaging Using Resting-State Fluctuations. NeuroImage. 1998 Feb;7(2):119–32.

Luo Y, Zhang Y, Feng X, Zhou X. Electroencephalogram oscillations differentiate semantic and prosodic processes during sentence reading. Neuroscience. 2010 Aug 25;169(2):654–64.

Lu Y, Yang L, Worrell GA, Brinkmann B, Nelson C, He B. Dynamic imaging of seizure activity in pediatric epilepsy patients. Clin Neurophysiol. 2012a Nov;123(11):2122–9.

Lu Y, Yang L, Worrell GA, He B. Seizure source imaging by means of FINE spatio-temporal dipole localization and directed transfer function in partial epilepsy patients. Clin Neurophysiol. 2012b Jul;123(7):1275–83.

Makeig S, Westerfield M, Jung T-P, Enghoff S, Townsend J, Courchesne E, et al. Dynamic Brain Sources of Visual Evoked Responses. Science. 2002 Jan 25;295(5555):690–4.

Marques JP, Rebola J, Figueiredo P, Pinto A, Sales F, Castelo-Branco M. ICA decomposition of EEG signal for fMRI processing in epilepsy. Hum Brain Mapp. 2009 Sep 15;30(9):2986–96.

De Martino F, Gentile F, Esposito F, Balsi M, Di Salle F, Goebel R, et al. Classification of fMRI independent components using IC-fingerprints and support vector machine classifiers. NeuroImage. 2007 Jan;34(1):177–94.

Marzetti L, Del Gratta C, Nolte G. Understanding brain connectivity from EEG data by identifying systems composed of interacting sources. NeuroImage. 2008 Aug 1;42(1):87–98.

McKeown MJ, Jung T-P, Makeig S, Brown G, Kindermann SS, Lee T-W, et al. Spatially independent activity patterns in functional MRI data during the Stroop color-naming task. Proc Natl Acad Sci. 1998 Feb 3;95(3):803–10.

McKeown MJ, Sejnowski TJ. Independent component analysis of fMRI data: examining the assumptions. Hum Brain Mapp. 1998;6(5-6):368–72.

Michel CM, Lantz G, Spinelli L, De Peralta RG, Landis T, Seeck M. 128-channel EEG source imaging in epilepsy: clinical yield and localization precision. J Clin Neurophysiol Off Publ Am Electroencephalogr Soc. 2004 Apr;21(2):71–83.

Mitra PP, Ogawa S, Hu X, Uğurbil K. The nature of spatiotemporal changes in cerebral hemodynamics as manifested in functional magnetic resonance imaging. Magn Reson Med. 1997 Apr 1;37(4):511–8.

Miwakeichi F, Martínez-Montes E, Valdés-Sosa PA, Nishiyama N, Mizuhara H, Yamaguchi Y. Decomposing EEG data into space–time–frequency components using Parallel Factor Analysis. NeuroImage. 2004 Jul;22(3):1035–45.

Moeller F, Maneshi M, Pittau F, Gholipour T, Bellec P, Dubeau F, et al. Functional connectivity in patients with idiopathic generalized epilepsy: Functional Connectivity in IGE Patients. Epilepsia. 2011 Mar;52(3):515–22.

Moeller F, Siebner HR, Wolff S, Muhle H, Boor R, Granert O, et al. Changes in activity of striato–thalamo–cortical network precede generalized spike wave discharges. NeuroImage. 2008 Feb;39(4):1839–49.

Montalenti E, Imperiale D, Rovera A, Bergamasco B, Benna P. Clinical features, EEG findings and diagnostic pitfalls in juvenile myoclonic epilepsy: a series of 63 patients. J Neurol Sci. 2001 Feb 15;184(1):65–70.

Moont R, Crispel Y, Lev R, Pud D, Yarnitsky D. Temporal changes in cortical activation during conditioned pain modulation (CPM), a LORETA study. PAIN. 2011 Jul;152(7):1469–77.

Murta T, Leal A, Garrido MI, Figueiredo P. Dynamic Causal Modelling of epileptic seizure propagation pathways: A combined EEG–fMRI study. NeuroImage. 2012 Sep;62(3):1634–42.

Negishi M, Martuzzi R, Novotny EJ, Spencer DD, Constable RT. Functional MRI connectivity as a predictor of the surgical outcome of epilepsy: Connectivity Study of Surgical Outcome. Epilepsia. 2011 Sep;52(9):1733–40.

Niazy RK, Beckmann CF, Iannetti GD, Brady JM, Smith SM. Removal of FMRI environment artifacts from EEG data using optimal basis sets. NeuroImage. 2005 Nov 15;28(3):720–37.

Nilsson L, Tomson T, Farahmand BY, Diwan V, Persson PG. Cause-Specific Mortality in Epilepsy: A Cohort Study of More Than 9,000 Patients Once Hospitalized for Epilepsy. Epilepsia. 1997 Oct 1;38(10):1062–8.

Nir R-R, Sinai A, Moont R, Harari E, Yarnitsky D. Tonic pain and continuous EEG: Prediction of subjective pain perception by alpha-1 power during stimulation and at rest. Clin Neurophysiol. 2012 Mar;123(3):605–12.

Nir R-R, Sinai A, Raz E, Sprecher E, Yarnitsky D. Pain assessment by continuous EEG: Association between subjective perception of tonic pain and peak frequency of alpha oscillations during stimulation and at rest. Brain Res. 2010 Jul 16;1344:77–86.

Nolte G, Ziehe A, Nikulin VV, Schlögl A, Krämer N, Brismar T, et al. Robustly Estimating the Flow Direction of Information in Complex Physical Systems. Phys Rev Lett. 2008 Jun 10;100(23):234101.

Ogawa S, Lee T-M. Magnetic resonance imaging of blood vessels at high fields: In vivo and in vitro measurements and image simulation. Magn Reson Med. 1990 Oct 1;16(1):9–18.

Ogawa S, Tank DW, Menon R, Ellermann JM, Kim SG, Merkle H, et al. Intrinsic signal changes accompanying sensory stimulation: functional brain mapping with magnetic resonance imaging. Proc Natl Acad Sci. 1992 Jul 1;89(13):5951–5.

O'Muircheartaigh J, Vollmar C, Barker GJ, Kumari V, Symms MR, Thompson P, et al. Abnormal thalamocortical structural and functional connectivity in juvenile myoclonic epilepsy. Brain. 2012 Dec 1;135(12):3635–44.

Oostenveld R, Oostendorp TF. Validating the boundary element method for forward and inverse EEG computations in the presence of a hole in the skull. Hum Brain Mapp. 2002 Nov 1;17(3):179–92.

Pascual-Marqui RD, Michel CM, Lehmann D. Low resolution electromagnetic tomography: a new method for localizing electrical activity in the brain. Int J Psychophysiol. 1994 Oct;18(1):49–65.

Paz JT, Davidson TJ, Frechette ES, Delord B, Parada I, Peng K, et al. Closed-loop optogenetic control of thalamus as a tool for interrupting seizures after cortical injury. Nat Neurosci. 2013 Jan;16(1):64–70.

Pfurtscheller G, Lopes da Silva FH. Event-related EEG/MEG synchronization and desynchronization: basic principles. Clin Neurophysiol. 1999 Nov 1;110(11):1842–57.

Pittau F, Dubeau F, Gotman J. Contribution of EEG/fMRI to the definition of the epileptic focus. Neurology. 2012;78(19):1479–87.

Platt OS, Thorington BD, Brambilla DJ, Milner PF, Rosse WF, Vichinsky E, et al. Pain in Sickle Cell Disease. N Engl J Med. 1991 Jul 4;325(1):11–6.

Ploner M, Gross J, Timmermann L, Pollok B, Schnitzler A. Oscillatory activity reflects the excitability of the human somatosensory system. NeuroImage. 2006 Sep;32(3):1231–6.

Ploner M, Gross J, Timmermann L, Schnitzler A. Cortical representation of first and second pain sensation in humans. Proc Natl Acad Sci. 2002;99(19):12444–8.

Ploner M, Lee MC, Wiech K, Bingel U, Tracey I. Prestimulus functional connectivity determines pain perception in humans. Proc Natl Acad Sci. 2010 Jan 5;107(1):355–60.

Plummer C, Wagner M, Fuchs M, Vogrin S, Litewka L, Farish S, et al. Clinical utility of distributed source modelling of interictal scalp EEG in focal epilepsy. Clin Neurophysiol. 2010 Oct;121(10):1726–39.

Price JL, Drevets WC. Neurocircuitry of Mood Disorders. Neuropsychopharmacology. 2009 Aug 19;35(1):192–216.

Qin P, Di H, Liu Y, Yu S, Gong Q, Duncan N, et al. Anterior cingulate activity and the self in disorders of consciousness. Hum Brain Mapp. 2010;31(12):1993–2002.

Raichle ME, MacLeod AM, Snyder AZ, Powers WJ, Gusnard DA, Shulman GL. A default mode of brain function. Proc Natl Acad Sci. 2001 Jan 16;98(2):676–82.

Raichle ME, Snyder AZ. A default mode of brain function: A brief history of an evolving idea. NeuroImage. 2007 Oct 1;37(4):1083–90.

Raij TT, Forss N, Stančák A, Hari R. Modulation of motor-cortex oscillatory activity by painful Aδ- and C-fiber stimuli. NeuroImage. 2004 Oct;23(2):569–73.

Ray JP, Price JL. The organization of the thalamocortical connections of the mediodorsal thalamic nucleus in the rat, related to the ventral forebrain–prefrontal cortex topography. J Comp Neurol. 1992;323(2):167–97.

Ray JP, Price JL. The organization of projections from the mediodorsal nucleus of the thalamus to orbital and medial prefrontal cortex in macaque monkeys. J Comp Neurol. 1993;337(1):1–31.

R Core Team. R: A language and environment for statistical computing. [Internet]. R Foundation for Statistical Computing, Vienna, Austria; 2013. Available from: http://www.R-project.org/

Rees DC, Williams TN, Gladwin MT. Sickle-cell disease. The Lancet. 2010 Dec 17;376(9757):2018–31.

Roberts K, Papadaki A, Gonçalves C, Tighe M, Atherton D, Shenoy R, et al. Contact heat evoked potentials using simultaneous EEG and fMRI and their correlation with evoked pain. BMC Anesthesiol. 2008 Dec 17;8(1):8.

Rodin EA, Rodin MK, Thompson JA. Source analysis of generalized spike-wave complexes. Brain Topogr. 1994 Dec 1;7(2):113–9.

Rodionov R, De Martino F, Laufs H, Carmichael DW, Formisano E, Walker M, et al. Independent component analysis of interictal fMRI in focal epilepsy: Comparison with general linear model-based EEG-correlated fMRI. NeuroImage. 2007 Nov;38(3):488–500.

Rogers BP, Katwal SB, Morgan VL, Asplund CL, Gore JC. Functional MRI and multivariate autoregressive models. Magn Reson Imaging. 2010 Oct;28(8):1058–65.

Russchen FT, Amaral DG, Price JL. The afferent input to the magnocellular division of the mediodorsal thalamic nucleus in the monkey, Macaca fascicularis. J Comp Neurol. 1987;256(2):175–210.

Sarnthein J, Jeanmonod D. High thalamocortical theta coherence in patients with neurogenic pain. NeuroImage. 2008 Feb;39(4):1910–7.

Sarnthein J, Morel A, von Stein A, Jeanmonod D. Thalamic theta field potentials and EEG: high thalamocortical coherence in patients with neurogenic pain, epilepsy and movement disorders. Thalamus Relat Syst. 2003 Aug;2(03):231–8.

Sarnthein J, Stern J, Aufenberg C, Rousson V, Jeanmonod D. Increased EEG power and slowed dominant frequency in patients with neurogenic pain. Brain. 2006 Jan 1;129(1):55–64.

Seeley WW, Menon V, Schatzberg AF, Keller J, Glover GH, Kenna H, et al. Dissociable Intrinsic Connectivity Networks for Salience Processing and Executive Control. J Neurosci. 2007 Feb 28;27(9):2349–56.

Seifritz E, Esposito F, Hennel F, Mustovic H, Neuhoff JG, Bilecen D, et al. Spatiotemporal Pattern of Neural Processing in the Human Auditory Cortex. Science. 2002 Sep 6;297(5587):1706–8.

Seneviratne U, Cook M, D'Souza W. The electroencephalogram of idiopathic generalized epilepsy. Epilepsia. 2012 Feb 1;53(2):234–48.

Sohrabpour A, Lu Y, Kankirawatana P, Blount J, Kim H, He B. Effect of EEG electrode number on epileptic source localization in pediatric patients. Clin Neurophysiol. Epub

Sridharan D, Levitin DJ, Menon V. A critical role for the right fronto-insular cortex in switching between central-executive and default-mode networks. Proc Natl Acad Sci. 2008 Aug 26;105(34):12569–74.

Stern J, Jeanmonod D, Sarnthein J. Persistent EEG overactivation in the cortical pain matrix of neurogenic pain patients. NeuroImage. 2006 Jun;31(2):721–31.

Tadel F, Baillet S, Mosher JC, Pantazis D, Leahy RM. Brainstorm: A User-friendly Application for MEG/EEG Analysis. Intell Neurosci. 2011 Jan;2011:8:1–8:13.

Thomas CG, Harshman RA, Menon RS. Noise Reduction in BOLD-Based fMRI Using Component Analysis. NeuroImage. 2002 Nov;17(3):1521–37.

Thornton RC, Rodionov R, Laufs H, Vulliemoz S, Vaudano A, Carmichael D, et al. Imaging haemodynamic changes related to seizures: Comparison of EEG-based general linear model, independent component analysis of fMRI and intracranial EEG. NeuroImage. 2010 Oct;53(1):196–205.

Tracey I, Mantyh PW. The Cerebral Signature for Pain Perception and Its Modulation. Neuron. 2007 Aug;55(3):377–91.

Uğurbil K, Xu J, Auerbach EJ, Moeller S, Vu AT, Duarte-Carvajalino JM, et al. Pushing spatial and temporal resolution for functional and diffusion MRI in the Human Connectome Project. NeuroImage. 2013 Oct 15;80:80–104.

Valeriani M, Le Pera D, Niddam D, Chen ACN, Arendt-Nielsen L. Dipolar modelling of the scalp evoked potentials to painful contact heat stimulation of the human skin. Neurosci Lett. 2002 Jan 18;318(1):44–8.

Van de Ven VG, Formisano E, Röder CH, Prvulovic D, Bittner RA, Dietz MG, et al. The spatiotemporal pattern of auditory cortical responses during verbal hallucinations. NeuroImage. 2005 Sep;27(3):644–55.

Voets NL, Beckmann CF, Cole DM, Hong S, Bernasconi A, Bernasconi N. Structural substrates for resting network disruption in temporal lobe epilepsy. Brain. 2012 Aug 1;135(8):2350–7.

Wager TD, Atlas LY, Lindquist MA, Roy M, Woo C-W, Kross E. An fMRI-Based Neurologic Signature of Physical Pain. N Engl J Med. 2013 Apr 11;368(15):1388–97.

Wang AL, Mouraux A, Liang M, Iannetti GD. Stimulus Novelty, and Not Neural Refractoriness, Explains the Repetition Suppression of Laser-Evoked Potentials. J Neurophysiol. 2010a Oct 1;104(4):2116–24.

Wang G, Worrell G, Yang L, Wilke C, He B. Interictal spike analysis of high-density EEG in patients with partial epilepsy. Clin Neurophysiol. 2011 Jun;122(6):1098–105.

Wang ZJ, Wilkie DJ, Molokie R. Neurobiological Mechanisms of Pain in Sickle Cell Disease. ASH Educ Program Book. 2010b Dec 4;2010(1):403–8.

Wang Z, Zhang Z, Jiao Q, Liao W, Chen G, Sun K, et al. Impairments of Thalamic Nuclei in Idiopathic Generalized Epilepsy Revealed by a Study Combining Morphological and Functional Connectivity MRI. Zang Y-F, editor. PLoS ONE. 2012 Jul 11;7(7):e39701.

Wennberg R, Cheyne D. On noninvasive source imaging of the human K-complex. Clin Neurophysiol. 2013 May 1;124(5):941–55.

Wilke C, Ding L, He B. Estimation of Time-Varying Connectivity Patterns Through the Use of an Adaptive Directed Transfer Function. IEEE Trans Biomed Eng. 2008 Nov;55(11):2557–64.

Wilke C, Van Drongelen W, Kohrman M, He B. Neocortical seizure foci localization by means of a directed transfer function method. Epilepsia. 2010;51(4):564–72.

Wilke C, Worrell G, He B. Graph analysis of epileptogenic networks in human partial epilepsy. Epilepsia. 2011a Jan 1;52(1):84–93.

Wilke C, Worrell G, He B. Graph analysis of epileptogenic networks in human partial epilepsy. Epilepsia. 2011b;52(1):84–93.

Worrell GA, Lagerlund TD, Sharbrough FW, Brinkmann BH, Busacker NE, Cicora KM, et al. Localization of the Epileptic Focus by Low-Resolution Electromagnetic Tomography in Patients with a Lesion Demonstrated by MRI. Brain Topogr. 2000 Jun 1;12(4):273–82.

Wu SC, Swindlehurst AL, Wang PT, Nenadic Z. Efficient Dipole Parameter Estimation in EEG Systems With Near-ML Performance. IEEE Trans Biomed Eng. 2012 May;59(5):1339–48.

Yang L, Wilke C, Brinkmann B, Worrell GA, He B. Dynamic imaging of ictal oscillations using non-invasive high-resolution EEG. NeuroImage. 2011a Jun;56(4):1908–17.

Yang L, Wilke C, Brinkmann B, Worrell GA, He B. Dynamic imaging of ictal oscillations using non-invasive high-resolution EEG. NeuroImage. 2011b Jun;56(4):1908–17.

Yang L, Worrell GA, Nelson C, Brinkmann B, He B. Spectral and spatial shifts of post-ictal slow waves in temporal lobe seizures. Brain. 2012 Oct 1;135(10):3134–43.

Yuan H, Liu T, Szarkowski R, Rios C, Ashe J, He B. Negative covariation between task-related responses in alpha/beta-band activity and BOLD in human sensorimotor cortex: An EEG and fMRI study of motor imagery and movements. NeuroImage. 2010 Feb;49(3):2596–606.

Zhang CH, Lu Y, Brinkmann B, Welker K, Worrell G, He B. Lateralization and localization of epilepsy related hemodynamic foci using presurgical fMRI. Clin Neurophysiol. 2015 Jan;126(1):27–38.

Zhang Y, Ding L, van Drongelen W, Hecox K, Frim DM, He B. A cortical potential imaging study from simultaneous extra- and intracranial electrical recordings by means of the finite element method. NeuroImage. 2006a Jul 15;31(4):1513–24.

Zhang Y, Drongelen W van, He B. Estimation of in vivo brain-to-skull conductivity ratio in humans. Appl Phys Lett. 2006b Nov 27;89(22):223903.

Zhang ZG, Hu L, Hung YS, Mouraux A, Iannetti GD. Gamma-Band Oscillations in the Primary Somatosensory Cortex--A Direct and Obligatory Correlate of Subjective Pain Intensity. J Neurosci. 2012 May 30;32(22):7429–38.

Zhang Z, Liao W, Chen H, Mantini D, Ding J-R, Xu Q, et al. Altered functional–structural coupling of large-scale brain networks in idiopathic generalized epilepsy. Brain. 2011 Oct 1;134(10):2912–28.

Zhang Z, Lu G, Zhong Y, Tan Q, Chen H, Liao W, et al. fMRI study of mesial temporal lobe epilepsy using amplitude of low-frequency fluctuation analysis. Hum Brain Mapp. 2010 Dec 1;31(12):1851–61.

Zhuo M. Cortical excitation and chronic pain. Trends Neurosci. 2008 Apr;31(4):199–207.

Zijlmans M, Huiskamp G, Hersevoort M, Seppenwoolde J-H, Huffelen AC van, Leijten FSS. EEG-fMRI in the preoperative work-up for epilepsy surgery. Brain. 2007 Sep 1;130(9):2343–53.